Application of the wind atlas method to extremes of wind climatology

Abild, J.

Publication date:
1994

Document Version
Publisher's PDF, also known as Version of record

RISØ

Risø-R-722(EN)

Application of the Wind Atlas Method to Extremes of Wind Climatology

J. Abild

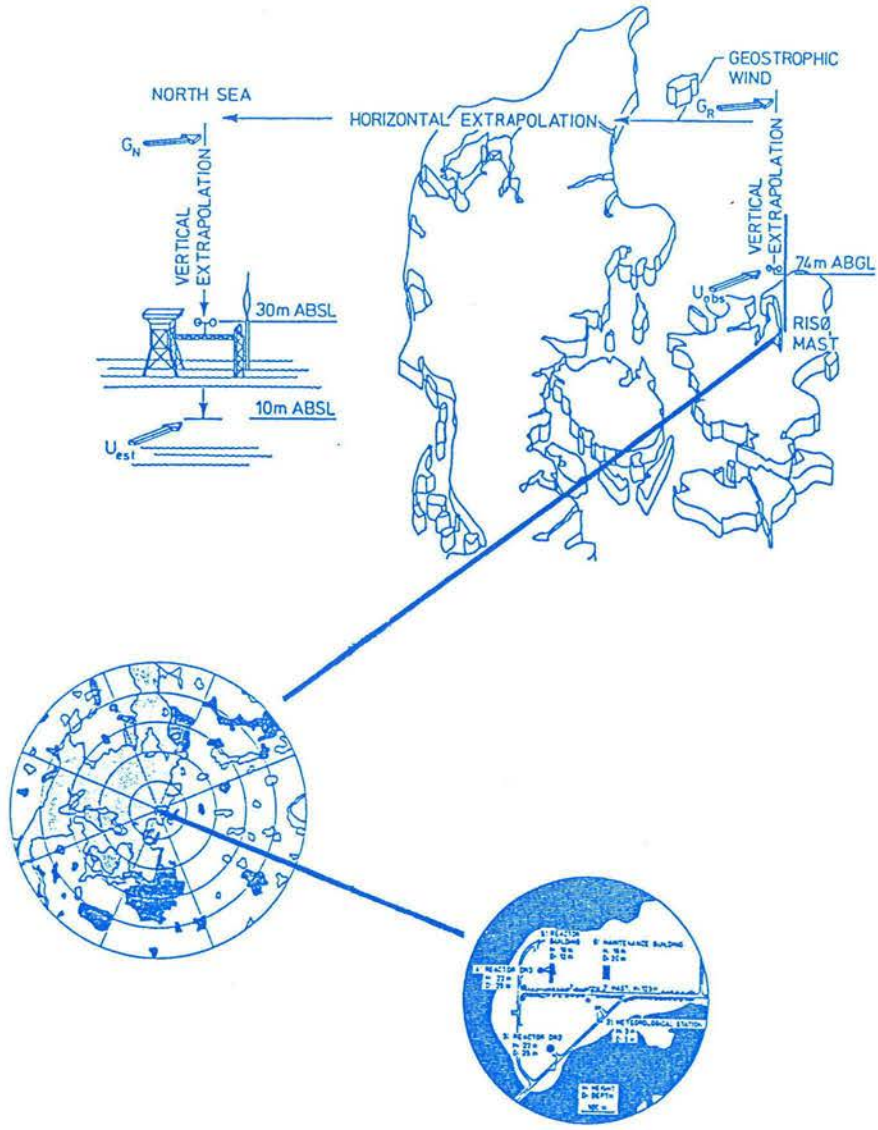

Risø National Laboratory, Roskilde, Denmark
January 1994

Application of the Wind Atlas Method to Extremes of Wind Climatology

Risø-R-722(EN)

J. Abild

Risø National Laboratory, Roskilde, Denmark
January 1994

Abstract A terrain description model is established for the Risø site through a WA^{S}P computation. Mean wind profiles for eight wind direction sectors are compared with the model boundary profiles. Wind data from the 72/76 m recording level of the Risø mast are updated, including identification of missing and erroneous data. The wind atlas procedure ("the double extrapolation method") is applied to extrapolate Risø data to open-water conditions 10 m above mean sea level. Three different extreme value distributions are applied to the extrapolated storm data – two of which are based on the annual maximum (AM) method, and one on the peak-over-threshold (POT) method. T-year estimates including standard error estimates are provided. Finally, a verification is performed by comparing extrapolated storm data with corresponding measured wind data from the Dan and Gorm fields in the North Sea. A high correlation is found for severe storms from the west. A significantly lower correlation is found for moderate and easterly storms.

ISBN 87-550-1438-0
ISSN 0106-2840

Grafisk Service · Risø · 1994

Contents

1 Introduction

"The worst storm in living memory" is a phrase often heard when a severe storm has raged itself out. However justified this statement might be, it is a well-known fact that exaggeration is an inherent delusion by humans; we only have to recall a familiar story by Hans Christian Andersen, our famous author.

Therefore, a description of historical extreme events such as storms should not be based solely on human recollection, but include as a minimum some estimates of the consequences of such events (I.G. Jensen, 1985) or even better, actual measurements.

From a historical point of view, measurements of climatological parameters such as wind speed are a fairly recent enterprise, only covering a period of approximately one hundred years. For the major part of this period data have been collected through visual observations, inflicting some subjectivity onto the data recording.

Instrumental measurements, leading to objective data material with an accurate graduation, have been made only in recent decades. In this respect the wind measurements recorded at the Risø mast perform a unique time series of a homogeneous quality. In spite of some changes in the instrumentation, the recordings are almost intact from the start in February 1958 till now.

Subsequent to an updating (including identification of missing and erroneous data) this data material is selected as historical data with the purpose of predicting future extreme storm events on the basis of statistical inference.

Selecting data material from an inland climatological station surrounded by a complex terrain creates the problem of how to incorporate a data correction which takes into account the changes of terrain, thereby making the subsequent statistical inference of a more general validity. This problem was one of the factors initiating the development of *Wind Atlas for Denmark* (1981). The objective of this study was to evaluate the wind resources with the purpose of locating sites for wind power plants in Denmark.

The main contribution to this work was an extrapolation procedure linking the observed wind speed and height at a specified terrain to the free wind (the geostrophic wind) at a height of approximately one kilometre.

A further development of this procedure led to a PC-program (WA^{S}P - Wind Atlas Analysis and Application Programme) for horizontal and vertical extrapolation of wind data (statistics) including a terrain description model.

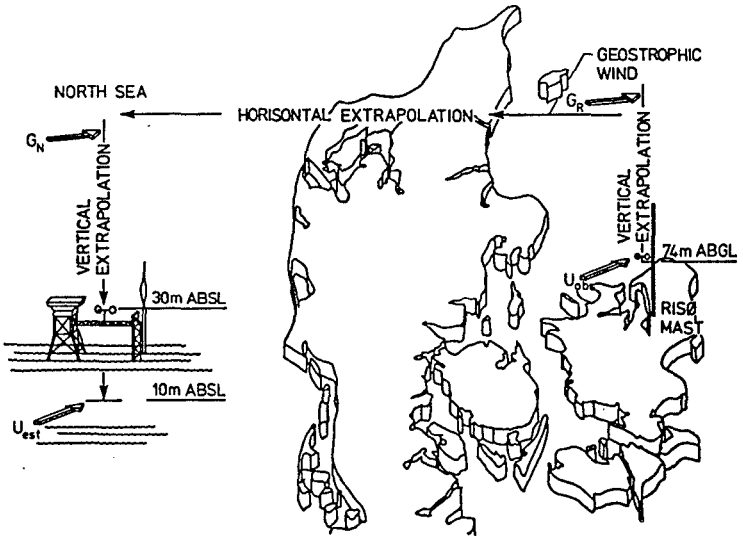

Figure 1: The principle of the double-vertical extrapolation procedure.

This model is applied to the terrain surrounding the Risø site.

Just recently a *European Wind Atlas* (1989) has been published, introducing a double vertical extrapolation model. Although the wind atlas methodology is primarily designed for mean wind extrapolation, it is, however, one of the primary objectives of the present study to use the methodology for extreme wind data and hopefully to verify its applicability.

In order not to unnecessarily complicate the extrapolation and thereby the verification, the "site of interest" was chosen to be *open waters 10 m above mean sea level.* The statistical treatment of extrapolated Risø data includes application of three extreme value distributions, two of which belong to the annual maximum method (AM) and one to the peak-over-threshold method (POT).

The data material is separated into eight wind direction sectors computing extreme T-year estimates including standard error on estimates for each sector. Finally, verification is performed by comparing the extrapolated storm data with measured wind data from the North Sea.

In section 2: Scope of the study, an introduction is given to the following sections.

Beaufort number	Description	Velocity equivalent at a standard height of 10 metres above open flat ground			Specifications for estimating speed over land
		Knots	Metres per second	Kilometres per hour	
0	Calm	< 1	0 – 0.2	< 1	Smoke rises vertically.
1	Light air	1 – 3	0.3 – 1.5	1 – 5	Direction of wind shown by smoke-drift but not by wind vanes.
2	Light breeze	4 – 6	1.6 – 3.3	6 – 11	Wind felt on face; leaves rustle; ordinary vanes moved by wind.
3	Gentle breeze	7 – 10	3.4 – 5.4	12 – 19	Leaves and small twigs in constant motion; wind extends light flag.
4	Moderate breeze	11 – 16	5.5 – 7.9	20 – 28	Raises dust and loose paper; small branches are moved.
5	Fresh breeze	17 – 21	8.0 – 10.7	29 – 38	Small trees in leaf begin to sway, crested wavelets form on inland waters.
6	Strong breeze	22 – 27	10.8 – 13.8	39 – 49	Large branches in motion; whistling heard in telegraph wires; umbrellas used with difficulty.
7	Near gale	28 – 33	13.9 – 17.1	50 – 61	Whole trees in motion; inconvenience felt when walking against the wind.
8	Gale	34 – 40	17.2 – 20.7	62 – 74	Breaks twigs off trees; generally impedes progress.
9	Strong gale	41 – 47	20.8 – 24.4	75 – 88	Slight structural damage occurs (chimney-pots and slates removed).
10	Storm	48 – 55	24.5 – 28.4	89 – 102	Seldom experienced inland; trees uprooted; considerable structural damage occurs.
11	Violent storm	56 – 63	28.5 – 32.6	103 – 117	Very rarely experienced; accompanied by widespread damage.
12	Hurricane	64 and over	32.7 and over	118 and over	

Figure 2: The Beaufort table for wind force and wind speed equivalents.

2 Concept of the study

This section outlines the methodology and concept of the present study, summarizing into a short form the contents of each section.

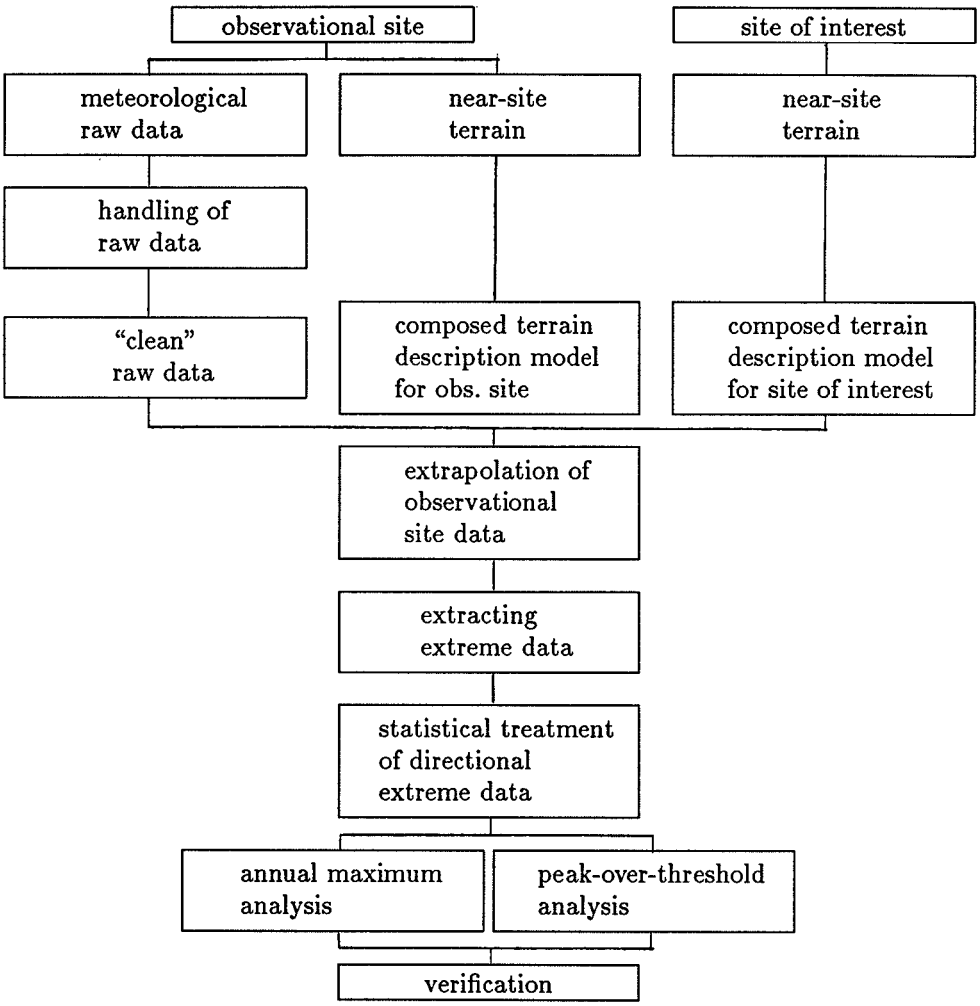

Figure 3: Schematic representation of the methodology applied.

Observational site:

The meteorological station at Risø situated on a small peninsula at the bottom of Roskilde Fjord, a location just north of Roskilde, a town on the island of Zealand, Denmark.

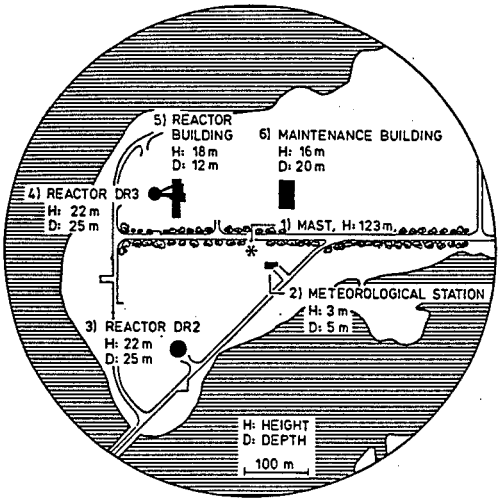

Near-site terrain:

A complex mixture of farmland with low wooded areas and small hills (the NE, E, and SE-sectors), towns and suburbs (S-sector), and mainly fjord in the NW and N-sectors.

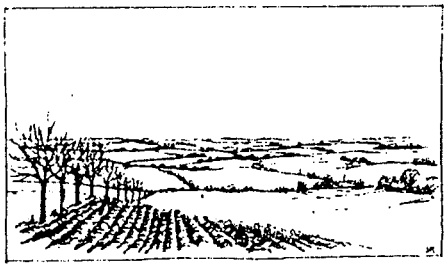

Meteorological raw data:

Thirty years of wind speed, direction and temperature recordings from the 7/11 m, 23/27 m, 39/43 m, 56 m, 72/76 m, and 117/123 m level of the meteorological mast.

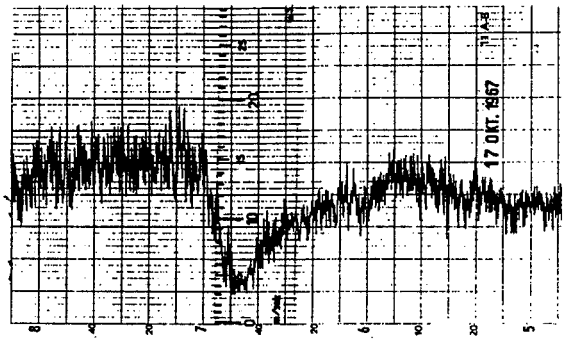

Handling of raw data

Identification of missing and erroneous data. Evaluation of storm period data. Selection of recording level for further analysis.

METEOROLOGICAL DATA FROM RISOE

A FEBRUARY 1973

DAS.TIME HR/MIN	WINDSPEED M/SEC. IN THE HEIGHTS 11M	27M	76M	117M	WINDDIRECTION IN THE HEIGHTS 11M	27M	76M	117M
8 00	5.7	7.5	9.5	10.9	255	250	270	269
10	5.0	6.7	9.1	10.8	257	249	272	266
20	4.8	6.7	9.5	10.9	259	254	275	269
30	4.2	7.0	9.9	11.2	266	255	278	271
40	3.7	6.2	9.3	10.5	266	255	277	272
50	3.6	5.9	8.8	10.4	264	254	278	271
9 00	4.1	6.5	9.1	10.3	262	253	278	273
10	4.3	6.9	9.4	10.5	267	256	279	273
20	4.7	7.6	9.5	10.9	273	259	279	*273
30	4.9	7.7	9.6	10.9	274	259	281	273
40	4.1	6.8	9.1	10.0	269	257	279	274
50	5.0	6.7	8.8	9.4	257	249	271	265
10 00	5.8	7.3	8.8	9.7	255	247	267	259
10	5.1	6.5	7.8	8.5	255	248	272	265
20	4.4	6.2	8.3	9.3	260	253	272	266
30	3.8	6.0	7.9	8.9	264	255	279	271
40	4.4	6.6	8.0	8.7	266	253	275	265
50	6.1	7.2	7.8	8.2	258	241	265	257
11 00	7.6	8.5	8.9	9.5	250	238	261	253
10	7.6	8.7	9.0	9.5	252	240	261	253
20	7.1	8.4	9.2	9.6	254	245	266	257
30	7.5	9.0	9.7	10.0	255	244	266	256
40	7.1	8.8	9.7	10.1	255	245	267	256
50	5.8	8.4	9.8	9.8	262	253	270	259
12 00	7.2	8.3	9.1	9.6	252	244	264	253
10	7.6	8.7	9.2	9.9	254	240	262	249
20	8.5	9.3	10.0	10.5	252	240	260	251
30	7.6	9.0	10.0	10.6	255	244	264	253
40	5.7	7.7	9.0	9.4	257	248	268	255
50	4.7	6.8	8.4	8.6	262	252	271	258
13 00	5.1	6.7	7.8	8.2	255	249	269	256
10	6.3	7.4	8.0	8.7	254	243	263	252
20	7.6	8.6	9.2	9.9	252	239	260	249
30	7.0	7.8	8.4	9.0	254	240	260	251
40	6.4	7.4	8.1	8.7	252	242	264	251
50	****	****	****	****	***	***	***	***

"Clean" raw data

Twenty-seven years of hourly corrected data from the 72/76-m recording level.

Composed terrain description model for the observational site

Description of the terrain close to the Risø mast, such as roughness changes, obstacles and orographic features.

Computation of the resulting wind speed increase/reduction at the various recording levels through the " Wind Atlas Analysis and Application Programme" (WAsP).

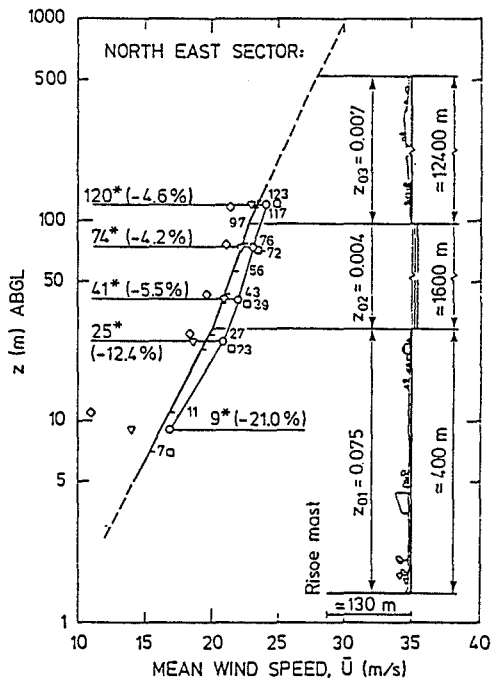

The composed terrain description model for the "site of interest"

Description of the site of interest: roughness changes, obstacles, and orographic features.

In the present study the site of interest is a North Sea location near the Gorm field implying homogeneous terrain.

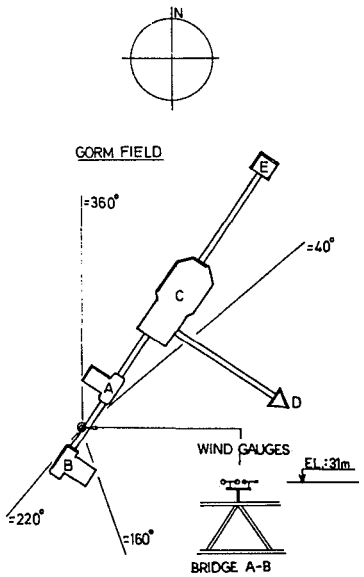

Extrapolation of observational-site data

Recognizing terrain features such as inhomogeneities in the surface roughness at the Risø site, a corrected surface friction velocity is related to the Risø wind speed data.

The geostrophic drag law is used to extrapolate the Risø wind speed data to geostrophic wind data ("free wind data"). Then applying the inverse procedure, the free wind speed data are extrapolated to the 10-m level at a specified location in the North Sea, taking into account the change of wind direction due to roughness changes from the Risø site to open-water conditions in the North Sea.

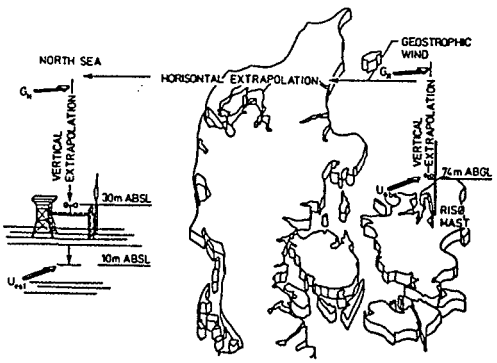

Extraction of extreme data

A storm selection filter is introduced for each wind direction sector of the extrapolated Risø data.

A sufficient amount of extreme data is extracted for further statistical analysis.

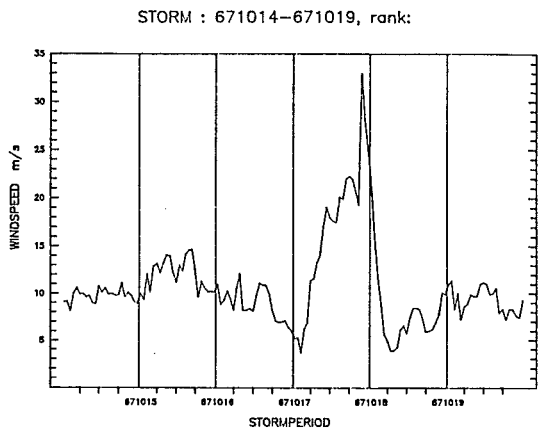

Statistical treatment of directional extreme data

Identifying the basic stochastic process. Statistical modelling of initial (marginal and conditional) distributions of wind speed and direction.

Performing goodness of fit tests.

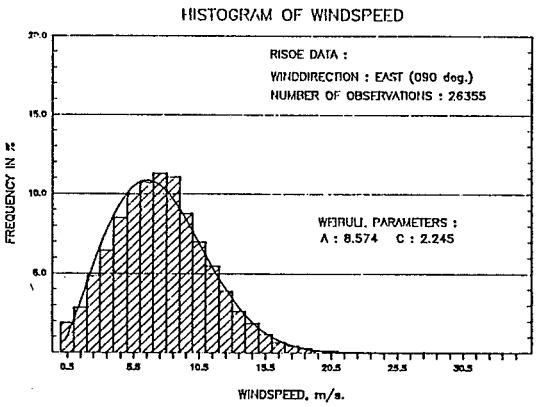

Annual maximum analysis

Extracting maximum directional/undirectional wind speed values from each year.

Estimating parameters in the selected extreme value distribution representing the annual maximum values.

Calculating extreme T-year events including standard error on estimates.

Performing goodness of fit tests.

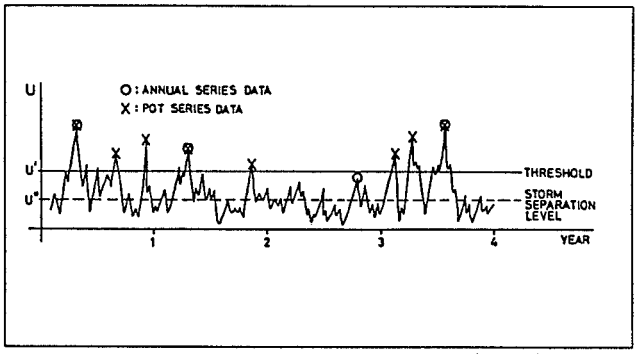

Peak-over-threshold analysis

Extracting undirectional/directional peak values above a specified threshold.

Selecting appropriate distributions for the number of events passing the threshold and for the peak exceedances.

Computing the compound probability distribution.

Estimate of parameters in the distribution.

Calculating extreme T-year events including standard error on estimates.

Performing goodness of fit tests.

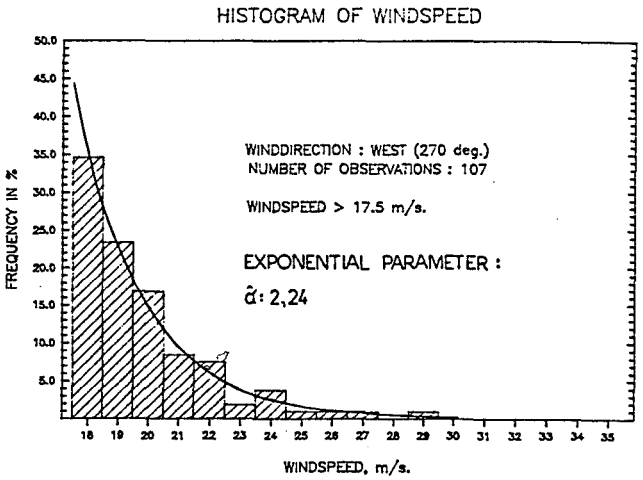

Verification

Handling of wind speed data from the Dan and Gorm fields.

Comparison between selected storm periods for extrapolated Risø and North Sea data.

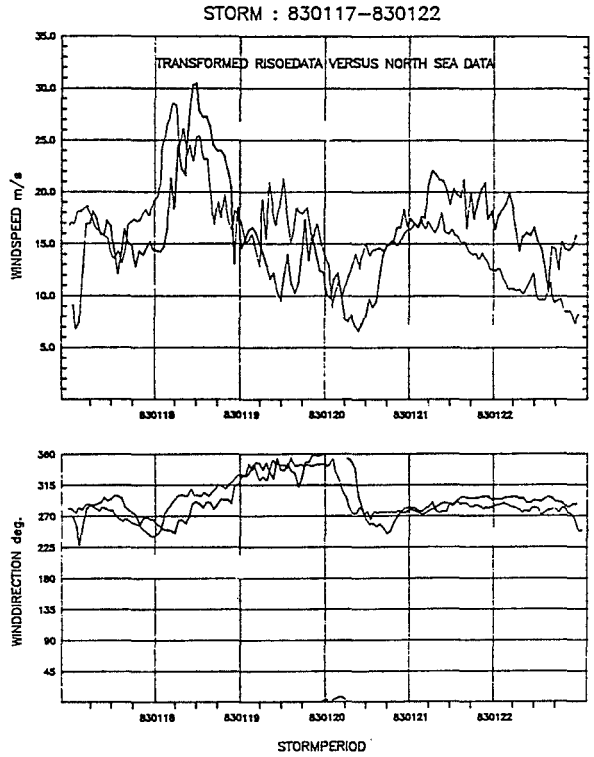

3 Terrain description model

In the process of extrapolating wind data from one site to another, an important task is the accurate description of the terrain around the site.

The principle of such a description is outlined in the Danish Wind Atlas (Petersen et al., 1981) but further developed in WAsP – Wind Atlas Analysis and Application Programme (Ib Troen et al., 1987), which is a PC-program for horizontal and vertical extrapolation of wind data (- statistics). A detailed description of this program is not within the scope of this study, but can be found both in an introductory note (Ib Troen et al., Oct. 1987) and in the actual User's Guide.[1]

The terrain description model consists of three different models, which will be dealt with in the following sections using the west sector at Risø as an illustrative example.

3.1 The roughness change model

One of the principal conditions of the wind atlas procedure is the extrapolation to homogeneous upstream conditions.

Homogeneous terrain of sufficiently large extension (up to 10 km) is seldom met in practice. Therefore, it is necessary to invoke a model that takes into account the influence of change in the roughness. It is generally recognized that a roughness change creates an internal boundary layer downstream from the change in terrain roughness. Within this boundary layer is a transition zone in which the wind speed depends on both the upstream and downstream roughness. In the lowest part of the internal boundary layer the wind speed will depend only on the downstream roughness.

The heights h_1 and h_2 can be calculated from the following equations (the Danish Wind Atlas, 1981):

$$h_1 = 0.7 \cdot 10^{-8}\, z_0^{0.3}\, l^3 \quad , z_0 = z_{01} \quad , \tag{1}$$

[1]The WAsP Programme and User's Guide are distributed solely by Dept. of Meteorology and Wind Energy, Risø National Laboratory, P.O. Box 49, DK-4000 Roskilde, Denmark, phone +45 42 371212, telex 43116 risoe dk, telefax +45 42 370115.

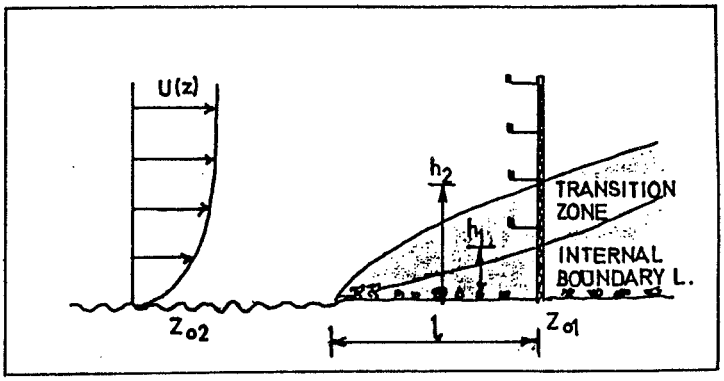

Figure 4: Sketch of internal boundary layer development after a change in surface conditions. Double-kink model.

$$h_2 = 0.7\, z_0 \left(\frac{l}{z_0}\right)^{0.8} \qquad z_0 = \max \begin{Bmatrix} z_{01} \\ z_{02} \end{Bmatrix} , \tag{2}$$

z_0 and l in metres.

For practical purposes (construction of boundary-layer profiles, etc.), a single-kink model can be advantageous (N.O. Jensen, 1981). The effect of the transition zone (double kink on the boundary-layer profile) is neglected here, giving rise to a (theoretical) error of only a few per cent on the wind speed estimate.

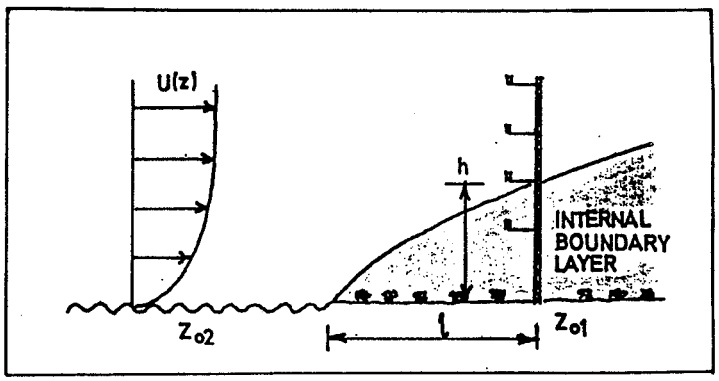

Figure 5: Sketch of internal boundary layer development after a change in surface conditions. Single-kink model.

The height, h can be calculated from the following equation (N.O. Jensen, 1981):

$$h \simeq 0.4\, z_0 \left(\frac{l}{z_0}\right)^{0.8} \qquad z_0 = \max \begin{cases} z_{01} \\ z_{02} \end{cases}, \tag{3}$$

z_0 and l in metres.

The actual roughness classification of the terrain surrounding a given site consists of the following procedures:

1. Selecting number of sections (8 or 11).
2. Division of each sector in accordance with major changes in upstream roughness. The horizontal extension should be at least 5 km, preferably more than 10 km. The maximum number (n) of roughness changes to be accounted for is: $n \leq 10$.
3. Correction in the "mean" roughness to account for changes in roughness within the division.
4. Calculation of roughness lengths from terrain characteristics including area weighting of roughness lengths (see Fig. 6 and Table 1).

The area weighted roughness lengths, z_0^R can be computed by the following equation:

$$z_0^R \simeq \text{inv.}\ln(A_1/A_{TOT} \cdot \ln z_{01} + A_2/A_{TOT} \cdot \ln z_{02} .....) \tag{4}$$

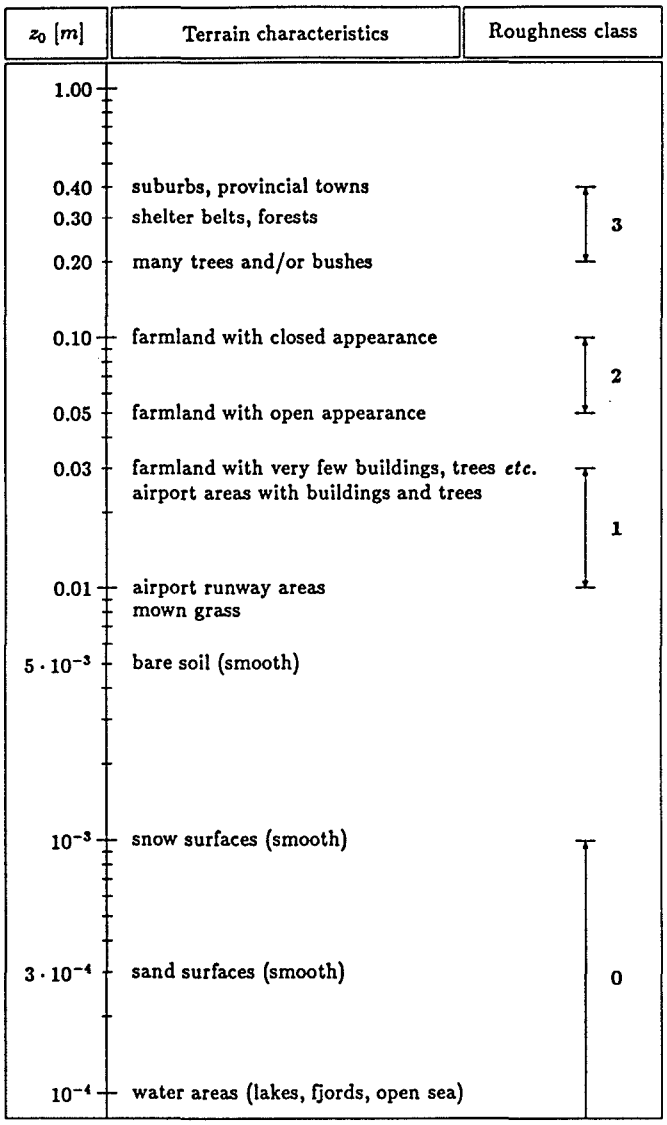

Figure 6: Roughness length, terrain characteristics, and roughness class.

Table 1:Area-weighted roughness length, z_0^R. The area is divided into quarters and each quarter is classified according to the EEC Wind Atlas roughness classification. z_0^R is given as a function of the number of quarters of each roughness class in the area.

Class:	0	1	2	3	z_0^R
z_0 [m]:	0.0002	0.03	0.10	0.40	[m]
	3	1			0.001
	3		1		0.002
	3			1	0.003
	2	2			0.004
	2	1	1		0.006
	2	1		1	0.010
	2		2		0.009
	2		1	1	0.015
	2			2	0.025
	1	3			0.011
	1	2	1		0.017
	1	2		1	0.027
	1	1	2		0.024
	1	1	1	1	0.038
	1	1		2	0.059
	1		3		0.033
	1		2	1	0.052
	1		1	2	0.079
	1			3	0.117
		3	1		0.042
		3		1	0.064
		2	2		0.056
		2	1	1	0.086
		2		2	0.127
		1	3		0.077
		1	2	1	0.113
		1	1	2	0.163
		1		3	0.232
			3	1	0.146
			2	2	0.209
			1	3	0.292

3.1.1 Application of the roughness change model

The meteorological station at Risø is situated in a very complex and inhomogeneous terrain on the island of Zealand, approximately 30 km west of Copenhagen. The mast is situated on a small peninsula at the bottom of Roskilde Fjord just north of Roskilde. Apart from the fjord, the nearby environment is farmland with low, wooded areas and low hills. The largest hill is Masterhøj, 46 m; it is situated about three kilometres SSE of the station. The terrain implies that the upstream condition for most of the sectors is a land-water-land trajectory which on a large scale is followed by even more water/land changes. The land trajectory is composed of a complex mixture of farmland, forests, and provincial towns which necessitates a subjective division of the terrain surrounding the mast.

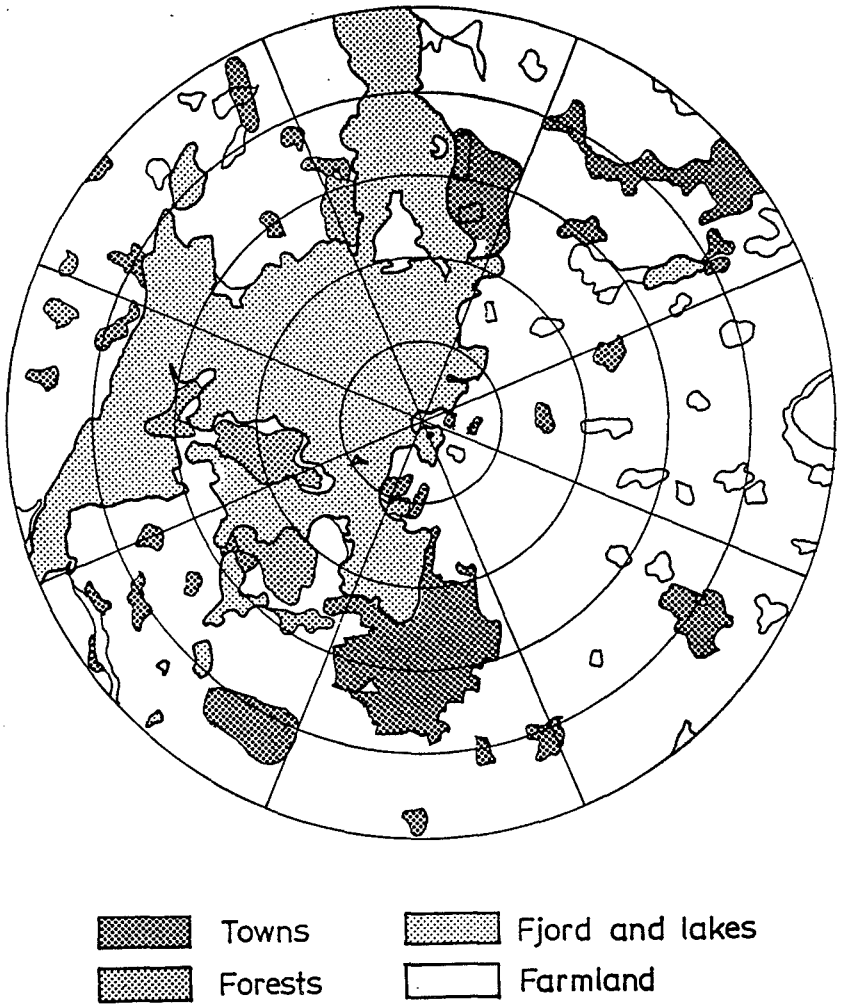

Figure 7: The terrain around the Risø site out to a distance of 10 km. Eight sector divisions are provided in accordance with the Danish Wind Atlas.

It should be borne in mind that near-surface wind speed ($z < 100$ m) is influenced primarily by changes of roughness within a distance of approximately two kilometres from the site of interest. This indicates that special attention should be drawn to the description of the terrain close to the site. Up to a distance of, say 20 km from the site, major changes of the terrain roughness should however be included in the description when aiming at the establishment of a link between the geostrophic and the surface wind speed. A computation of the west sector is used to illustrate the procedure of the roughness change model.

(The west sector)
A detailed terrain description covering a distance of 10 km from the site has been performed as follows: circle rings with a 1-km spacing have been drawn on a 1:400.000 map. The total area between any two circle rings (A_{TOT}) is divided into sub-areas (A_1, A_2 ... A_N) with a specific terrain charactistic (z_{01}, z_{02} ..... z_{0N}). The area-weighted roughness length z_0^R is hereafter calculated by Eq. (4). This procedure seems practical in the case of very complex terrain.

Table 2: Computation of terrain roughness in the west sector. The area-weighted roughness is calculated according to Eq. (4). Note that the description is more detailed close to the site.

Terrain	Distance (km)									
	0 – 0.3	0.3 – 2	2 – 3	3 – 4	4 – 5	5 – 6	6 – 7	7 – 8	8 – 9	9 – 10
A_{TOT} x 10^{-3} m^2	35	1535	1964	2749	3534	4320	5105	5891	6677	7461
Lake $z_{01} = 0.001$ A_1/A_{TOT}	–	1.0	0.975	0.546	0.607	0.509	0.744	0.594	0.180	0.141
Bog $z_{02} = 0.03$ A_2/A_{TOT}	–	–	0.018	0.146	0.085	0.134	0.039	0.034	0.037	0.008
Farmland $z_{03} = 0.05$ A_3/A_{TOT}	–	–	–	0.018	0.011	0.294	0.138	0.272	0.724	0.769
Forest $z_{04} = 0,3$ A_4/A_{TOT}	–	–	0.008	0.291	0.297	0.063	0.074	0.005	0.013	0.038
Towns $z_{05} = 0.4$ A_5/A_{TOT}	1.0	–	–	–	–	–	0.004	0.095	0.045	0.044
Area–weighted roughness z_0^R	0.4	0.001	0.001	0.009	0.008	0.007	0.003	0.006	0.027	0.034
Mean area–weighted roughness $\bar{z}_0^R$	0.4	0.001		0.007					0.031	

Table 3: Roughness description of the terrain surrounding the Risø site.

	Sector							
Rougness class	0 (N)	45 (NE)	90 (E)	135 (SE)	180 (S)	225 (SW)	270 (W)	315 (NW)
z_{01}	0.300	0.075	0.050	0.030	0.030	0.025	0.400	0.400
Dist. (m) x_1	250	400	700	100	100	300	300	300
z_{02}	0.001	0.004	0.260	0.002	0.001	0.004	0.001	0.001
Dist. (m) x_2	4000	2000	1000	700	950	4000	3000	5000
z_{03}	0.013	0.051	0.059	0.054	0.050	0.034	0.007	0.018
Dist. (m) x_3	7000	14000	14000	7000	1500	7000	8000	8000
z_{04}	0.026	0.1	0.1	0.089	0.141	0.055	0.031	0.053
Dist. (m) x_4	14000	↓	18000	9000	2500	11000	10000	17000
z_{05}	0.050		0.200	0.058	0.027	0.100	0.060	0.010
Dist. (m) x_5	↓		21000	20000	5000	↓	15000	20000
z_{06}			0.400	0.001	0.230		0.010	0.001
Dist. (m) x_6			32000	↓	8000		20000	↓
z_{07}			0.001		0.060		0.050	
Dist. (m) x_7			↓		↓		↓	

In accordance with major changes of the upstream roughness, sector divisions are made by seeking out major changes in the area-weighted roughness. A mean area-weighted roughness ($\bar{z}_0^R$) in a division is computed by taking the sample mean of all area-weighted roughnesses within the division. The result for the west sector can be found in Table 2.

To complete the analysis for the west sector, major changes out to approximately 20 km from the site have been included in the roughness description.

The resulting roughness description of all the terrain surrounding the site can be found in Table 3.

3.2 The shelter model

As previously mentioned, the terrain near the site should be treated in more detail with special attention to the obstacles which might cause sheltering effects. To provide an obstacle description, the WASP program computes the shelter reduction (R_1) at the height of interest.

For more comprehensive information on the subject of sheltering obstacles, the interested reader is referred to Martin Jensen (1959). For the purpose of physical modelling, obstacles are considered as "boxes" with a rectangular cross section having certain physical characteristics which determine the shelter effect:

1. the distance from the obstacle to the site
2. the height of obstacle compared to the height of the point of interest
3. the length and depth of the obstacle
4. the obstacle porosity.

As a general rule, the porosity can be set equal to zero for buildings and to approximately 0.5 for trees. For windbreaks, the following characteristics may be applied:

Table 4: Porosity of windbreaks.

Appearance	Porosity
Solid (wall)	0
Very dense	≤ 0.35
Dense	0.35 – 0.50
Open	≥ 0.50

In a practical application, the problem arises whether a terrain feature should be regarded as a roughness element or as an obstacle. It is recommended that all terrain features (up to a number of 50) that might cause sheltering effects should be included in the shelter model and accordingly excluded from the roughness change model.

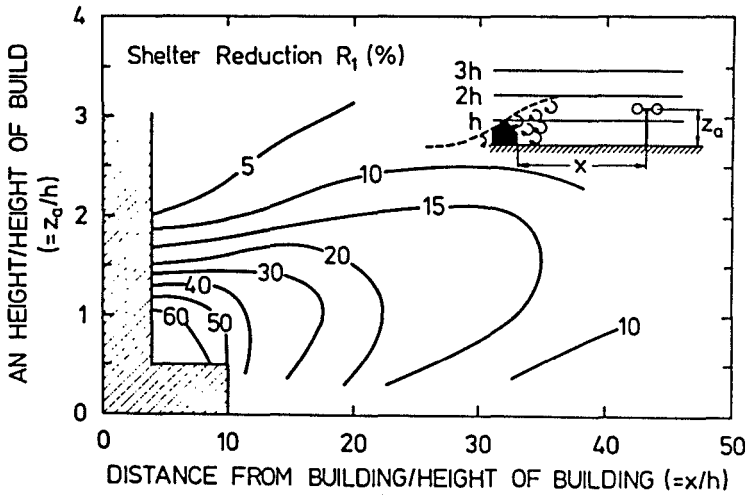

Figure 8: Reduction of wind speed due to shelter from a two-dimensional obstacle.

3.2.1 Application of the shelter model.

The procedure of obstacle description is illustrated in Fig. 9.

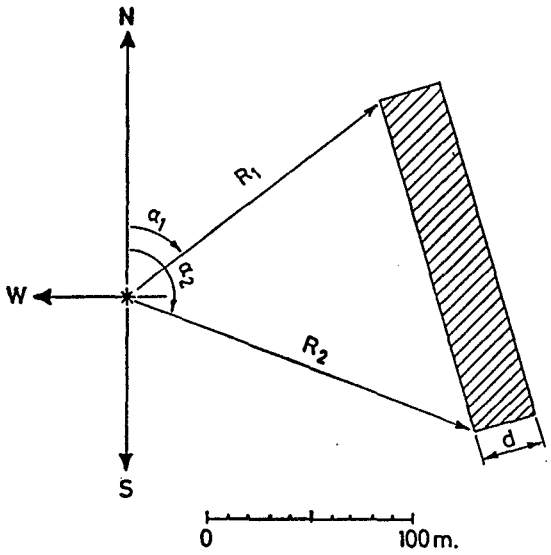

*	site position
α_1	angle from N to first corner [*deg*]
R_1	radial distance to first corner [*m*]
α_2	angle from N to second corner [*deg*]
R_2	radial distance to second corner [*m*]
d	depth of obstacle [*m*]
h	height of obstacle [*m*]
type	building, row of trees, dense thin estimated porosity

Figure 9: The figure shows how to provide shelter information.

The shelter model at the Risø site includes six obstacles as can been seen from Fig. 10.

Table 5 illustrates the wind-speed shelter reduction in the various sectors at 9 and 74 m height.

It is clearly recognized that the shelter effect decreases rapidly with height and that only the wind shelter from the NE has any significant influence on the wind speed at 74 m height.
The present height of the windbreak is approximately 12 m which causes a significant reduction of the wind speed at low levels . Bearing in mind the period of the study (about 30 years) and the extension of the windbreak, it is considered more reasonable to include the windbreak in the roughness change model; the same argument applies to other growths close to the site.

Table 5: Shelter reduction at the Risø site at 9 and 74 m height.

Sector	Shelter reduction in percentage	
	9 m	74 m
0	1.0	0.1
45	24.7	5.8
90	4.7	2.9
135	3.9	1.9
180	0.3	0.2
225	12.5	0.2
270	0.9	0.0
315	21.2	0.2

Finally, it should be noted that any reduction or increase of the wind speed caused by, e.g. nearby anemometers or tower wake, can be entered directly into the input option of the roughness change model, see Appendix A.

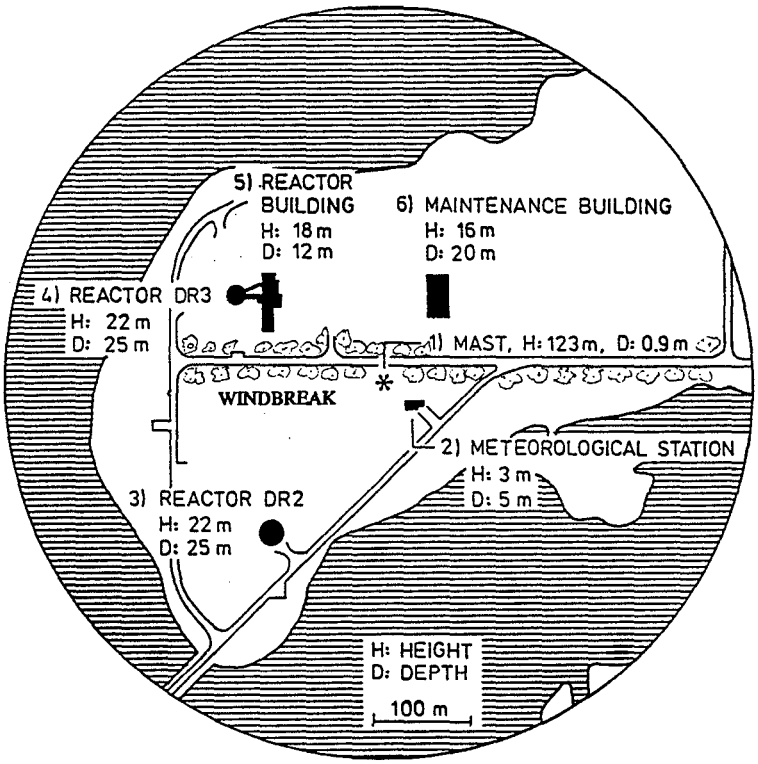

Figure 10: Obstacle identification at the Risø site.

3.3 The orographic model

In regions with small-scale smooth hills and valleys the wind may be treated as a potential flow with modifications from turbulence and wind shear. WA^{S}P utilizes the BZ-model (Troen, 1987) to calculate the wind velocity perturbations induced by orographic features. The model is related to the Jackson and Hunt theory for two-dimensional flow over hills and escarpments (Jackson and Hunt, 1975; Taylor et al., 1983). In accordance with this theory, the velocity perturbation $\Delta u(x,z)$ is given by:

$$\Delta u(x,z) = \sigma(x,z)\frac{H}{L}\frac{\ln\left(\frac{L}{z_0}\right)}{\ln\left(\frac{\delta}{z_0}\right)} \tag{5}$$

where

$\sigma(x,z)$: is a function that depends on the integrated slope of the terrain feature

H: is the height of the hill or escarpment

L: is the *length scale* of the hill or escarpment

δ: is the height of the "inner" region (resembling the height of the internal boundary layer at a distance L downwind from a roughness change (see section 3.1 page 17)) and is a function of L/z_0.

The problem of finding a solution to $\sigma(x,z)$ and δ for different orographic features is dealt with in papers by Jackson (1979) and N.O. Jensen (1978) and (1983) and in a review in WMO/TD No. 15, 1984 by N.O. Jensen et al.

At a hill crest or escarpment the fractional speed-up ratio at the height δ above ground is closely given by:

$$\Delta U(\delta) \simeq 2\frac{H}{L} \quad L >> H \tag{6}$$

where $\Delta U(\delta)$ is defined as the difference in wind speed at height δ between the crest wind speed ($U_2(\delta)$) and upstream wind speed ($U_1(\delta)$) relative to the upstream wind speed, ($U_1(\delta)$) (see Fig. 11). The approximate value of the height δ can be found from

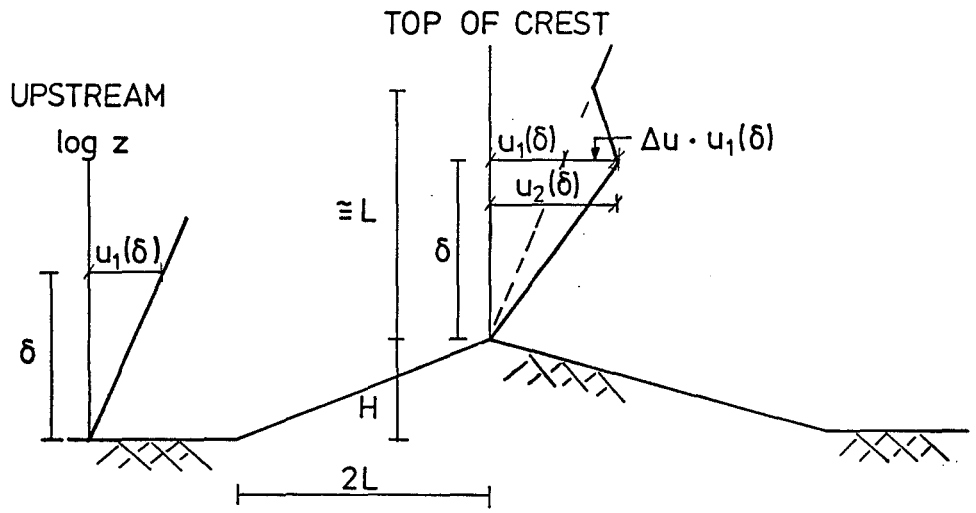

Figure 11: Idealized wind profiles that illustrate the speed-up of flow passing the hill crest. Under neutral conditions the height of the upper profile kink may be assumed equal to L.

$$\delta \simeq 0.5\, z_0 \left(\frac{L}{z_0}\right)^{0.8} \quad . \tag{7}$$

Thence, the crest wind speed ($U_2(\delta)$) at height δ can be calculated from the upstream wind speed ($U_1(\delta)$) by the following equation:

$$U_2(\delta) \simeq U_1(\delta)\left(1 + 2\,\frac{H}{L}\right) \quad . \tag{8}$$

Note that for practical application the theory is valid only for gently sloping hills and escarpments and that the solutions (5–8) are symmetric regardless of asymmetric features in the orography.

If the terrain comprises orographic terrain features like steep slopes or cliffs, separation might occur in which case the model will not give realistic results. The problem might be dealt with by including such features in the obstacle model if the consequence is a sheltering effect. Other corrections might be entered through the input option of the roughness change model.

3.3.1 Application of the orographic model.

The orographic model is based on a digital height-contour map for the terrain around the site. The standard limit is a maximum of 10,000 points in 200 contour maps which, in view of the horizontal length scale of velocity perturbations of approximately 10 terrain heights, is more than sufficient in the present case. WASP employs a high-resolution zooming polar grid emphasizing near-site terrain features.

Based on a digitized standard topographical map from the Danish Geodetic Institute, a domain-sized 6100 × 7700 m around the site has been extracted as a basis for the digital height contour map. The spacing between the height contours is 5 m. On request, the WASP program can produce extra contour lines between the height contours by means of a linear interpolation.

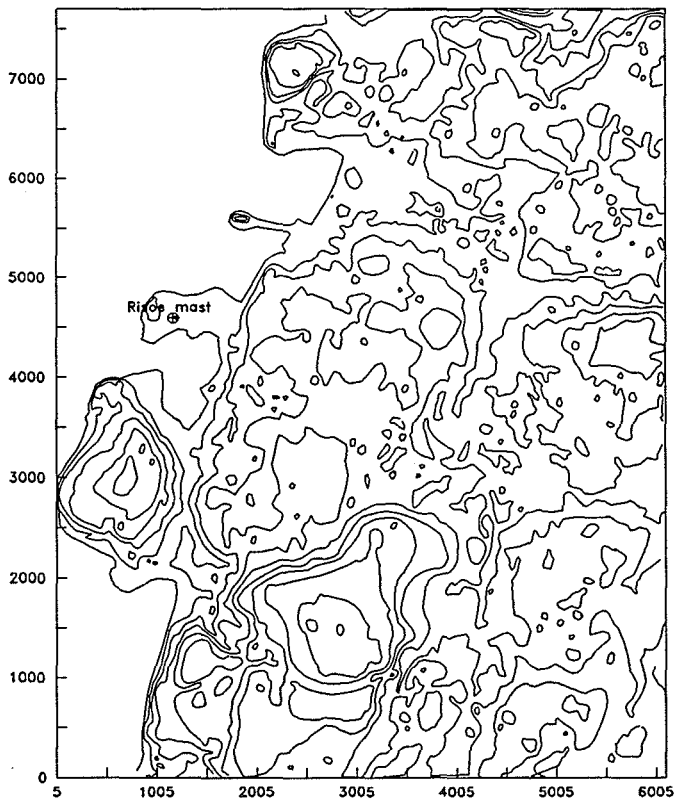

Figure 12: Domain of the orographic model around the Risø site. The scaling is stated in metres, contour lines are 5-m height contours.

Table 6: Relation between domain and grid size at the centre of the model.

Domain size [km]	5	10	2	50	100
Grid size [m]	1.3	2.7	5.3	13.3	26.6

Cartesian coordinates for the Risø mast is $(x, y, z) = (1{,}200,\ 4{,}600,\ 6.5)$ relative to the coordinate system. Through the "hill" option in the orographic model, a test was carried out as to the influence on wind speed due to velocity perturbation from the Veddelev hill (height approx. 30 m) about 1500 m south of the site.

Regarding the potential flow regime, this hill has no significant influence on the wind velocity at the site (less than 0.5% at all heights).

The main influence on the velocity perturbation comes from orographic features of the small peninsula. This is in good agreement with former analysis (Jensen et al., 1978) and shows that a domain of less size than the one chosen with a higher degree of resolution would have been appropriate in the present study. In Table 7 is shown the reduction and increase of the wind speed at heights of 9 and 74 m, respectively, due to orographic features.

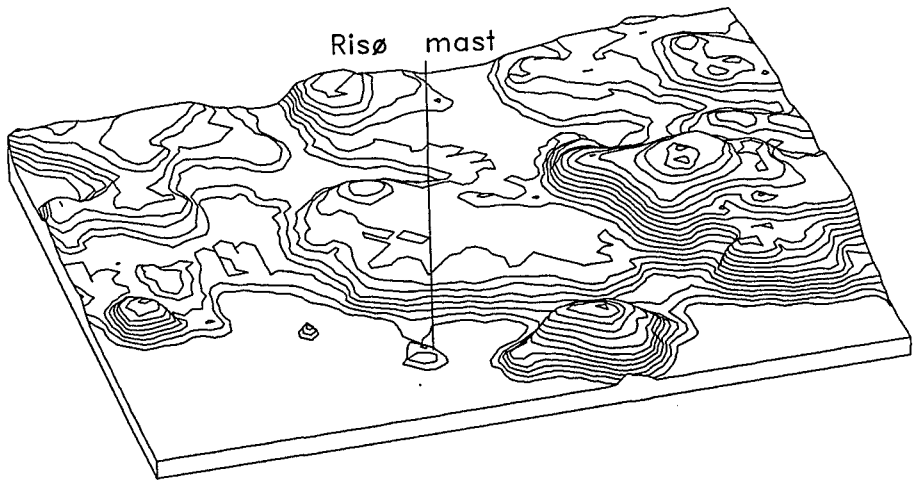

Figure 13: Perspective of the domain seen from northwest with a tilting of 30°.

Table 7: Orographic reduction/increase of wind speed at heights of 9 and 74 m, respectively, at the Risø site.

Sector	Reduction (-) / Increase (+) in wind speed (%)	
	9 m	74 m
0	+ 6.3	+ 2.8
45	+ 3.7	+ 1.6
90	- 1.3	- 0.7
35	+ 1.4	+ 0.5
180	+ 6.0	+ 2.7
225	+ 3.6	+ 1.6
270	- 1.1	- 0.7
315	+ 1.9	+ 0.6

3.4 Composed terrain model

To compose the three terrain models is not merely a question of superposition. A high degree of interaction exists between them, especially between the roughness change and the orographic model.

Before going into a discussion regarding the accuracy of the terrain model, it is appropriate to present the output from the WASP computation.

On making use of Eq. (3), it is now possible to construct boundary layer profiles for each sector on the basis of the roughness change model. In order to verify this model, the mean wind velocity has been computed at different anemometer heights on the Risø mast (period: 1958 – 1986 except the years 1973 and 1974). To secure near-neutral conditions wind speeds only above 10 m/s have been used.

The computed mean wind velocities are made to fit the constructed boundary layer profiles at the 74–m level by multiplying with an appropriate factor. As a supplement and with the same factor as used above, a similar procedure is applied for a 10-year period (1958 – 1967) and for a 5-year period (1982 – 1986) to examine any changes as to time in the wind velocity profile.

Corrections are performed to the "long–term" mean wind velocity caused by sheltering and orographic effects. This is done for all eight sectors. In Fig 14 the resulting wind speed profile is drawn for the west sector. In Appendix A the same wind speed profiles are found for other wind direction sectors.

Table 8: Result of the composed terrain model (the wind atlas analysis model) in terms of statistical parameters in the Weibull distribution*, i.e. the model of wind speed distribution at the 74–m height at the Risø site.

DK/00 DANISH WINDATLAS 21/ 6/88 16:04

risoemast* Height: 74.0 m a.g.l.

Sect	Rch	Input		Obstacle	Orography			A	k	%	E%
0:	4	0.0%	0°	-0.1%	2.8%	0°	:	6.8	1.83	6.6	4.0
45:	3	0.0%	0°	-5.8%	1.6%	-1°	:	6.4	1.96	9.2	4.2
90:	6	0.0%	0°	-2.9%	-0.7%	0°	:	7.1	2.36	12.3	6.6
135:	5	0.0%	0°	-1.9%	0.5%	1°	:	7.6	2.14	12.0	8.4
180:	6	0.0%	0°	-0.2%	2.7%	0°	:	8.7	2.08	15.8	17.3
225:	4	0.0%	0°	-0.2%	1.6%	-1°	:	9.4	2.07	17.8	24.3
270:	6	0.0%	0°	0.0%	-0.7%	0°	:	9.7	2.01	18.2	28.6
315:	5	0.0%	0°	-0.2%	0.6%	1°	:	7.3	1.70	8.1	6.6
M= 7.3 m/s E= 474. W/m²								8.2	1.92		

*The two-parameter Weibull distribution is

$$f(u;k,A) = \frac{k}{A}\left(\frac{u}{A}\right)^{k-1} \exp\left\{-\left(\frac{u}{A}\right)^{k}\right\} \quad .$$

Note that the 9, 25, 41, 74, and 120–m levels are not actual measuring heights. Actual anemometer heights are indicated by □ before 1973, and by ▽ after 1973. The corrected profile is indicated by o. Speed-up is indicated by a percentage marked with +, and accordingly reductions are indicated by a percentage marked with –.

3.5 Concluding remarks

As stated in earlier terrain analyses from the Risø site (Panofsky, et al., 1972) and as identified in the roughness change model, roughness changes are clearly recognized in the measured wind velocity profiles. For some of these profiles the roughness changes seem to be accentuated.

In spite of the choice of a minimum wind speed of 10 m/s suggesting a near–neutral condition, a plausible explanation of this phenomenon might be a combination of thermal and roughness effects as the wind flow passes land–water–land trajectories close to the site. In connection with the Øresund experiments, results by J.C. Doran et al. (1987) indicate that this can have a significant influence on the boundary layer profile, especially at low heights (< 100 m).

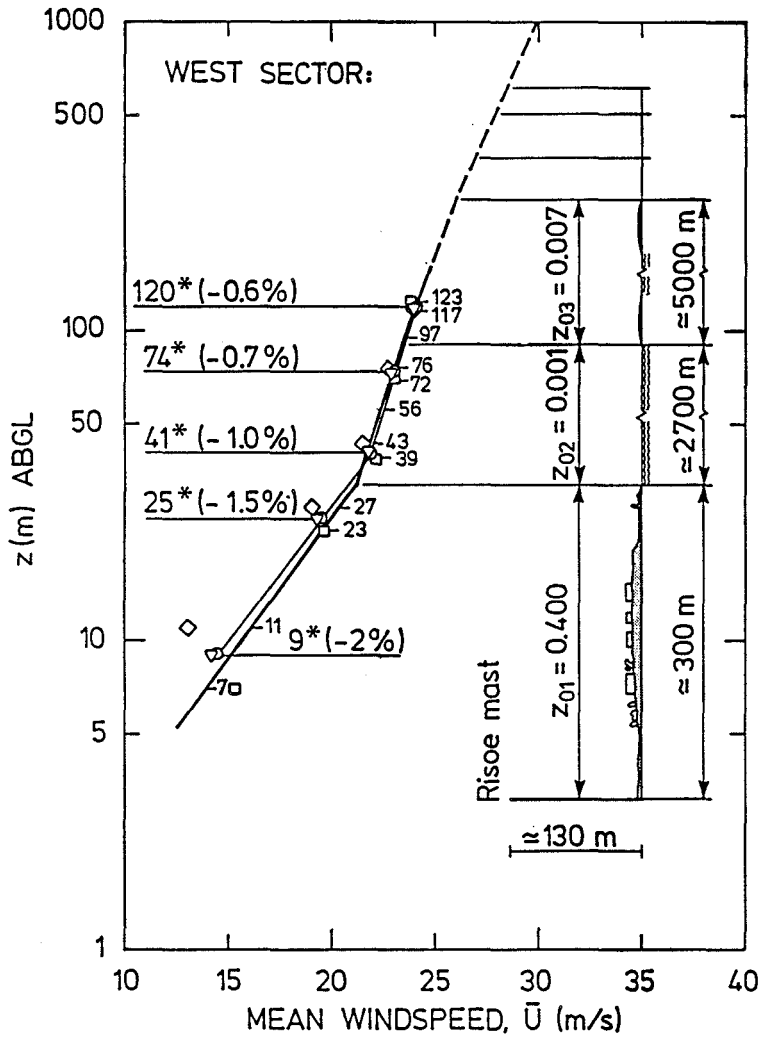

Figure 14: Comparison of the model boundary profile with the measured mean wind velocity profile ($u > 10$ m/s) for the west sector. Regarding the other sectors, see Appendix A .

∇: long-term measured mean wind velocity profile, period: 1958–1986
o: long-term corrected mean wind velocity profile, period: 1958–1986
$\diamond$: short-term measured mean wind velocity profile, period 1982–1986
$\square$: short-term measured mean wind velocity profile, period 1958–1967.

In addition to this, a combination of roughness and orographic changes in the near-site terrain might cause sheltering effects that are not recognized by the model.

It is clearly seen from the profiles, however, that the corrections due to shelter or orographic effects give a significant improvement of the model at low heights, but this is not evident at high levels (> 25 m). Finally, it should be noted that in terms of fractional wind speed the discrepancy between the model and the measured profile is of order less than 5%.

Only a trial will show whether the model can maintain the same degree of accuracy when it comes to large-scale descriptions of the terrain.

4 Description of the data sampling and reduction procedures

As a part of the activities of the Danish Atomic Energy Programme, the meteorological mast at Risø was erected in the early summer of 1957 to get data on the meteorological conditions in the lower layers of the atmosphere. The mast, approximately 125 m high, was erected on a small hill 6.5 m above sea level on the Risø peninsula in the angle formed by the two roads Centralvej and Molevej.

Throughout the years, the instrumentation and data sampling procedures have undergone some changes culminating in 1970 with the mounting of new booms for the instrumentation.

In spite of these changes the time series is almost intact during the period from February 1958 until now, creating an exceptional possibility of a long-term analysis of wind data of a homogeneous quality. The following sections deal with the data sampling, giving a historical review of the changes in instrumentation and sampling procedures. Furthermore, they contain a description of the data reduction method applied in the present study which includes identification of missing and erroneous data.

4.1 Historical review of climatological measurements at Risø

Five major changes have taken place in the instrumentation during the lifetime of the Risø mast.

First instrumentation

June 1957 – November 1959
Four Wilh. Lambrecht cup anemometers No. 1467 (counter-clockwise turning) were mounted on the tower to measure the wind velocity at the 23-m, 39-m, 72-m, and 96-m height.

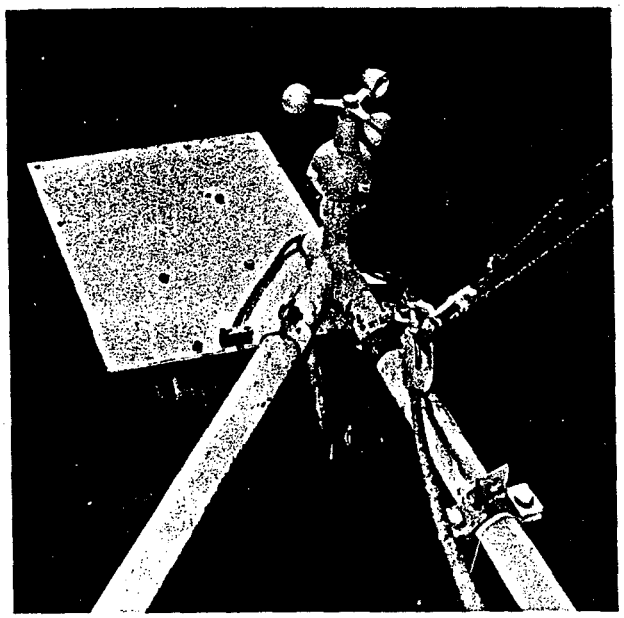

Figure 15: A cup anemometer (Wilh. Lambrecht No. 1467) mounted on a triangular boom to the Risø mast.

Furthermore, three cup anemometers combined with vanes (Wilh. Lambrecht No. 1464) were placed at the 7-m, 56-m, and 123-m height.

Ventilated PT-100 thermometers were mounted at the 6-m, 22-m, 39-m, 55-m, 71-m, and 95-m level. A turbulence recorder was placed at the 56-m height.

Observations were continuously recorded by seven Siemens ink recorders of the moving-coil type.

Data reading procedure for wind speed – and direction:
From 1 February 1958 data were evaluated from the recordings with 10-min intervals. Each reading represented a 10-min average of the period beginning five minutes before the hour. Mean wind speed values were obtained by the "equal area" method to the nearest half meter per second. Likewise, the wind direction was determined to the nearest 10 degree.

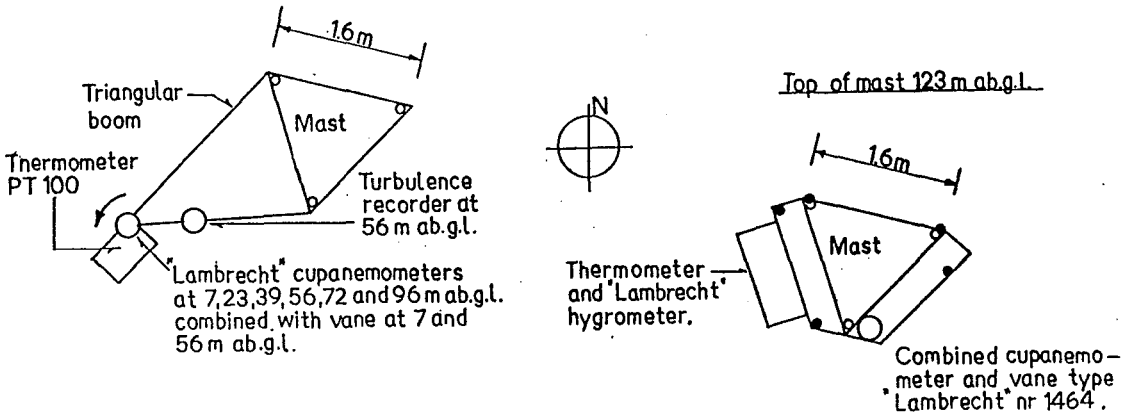

Figure 16: Cross section of the Risø mast showing the placing of the first instrumentation (June 1957 – November 1959).

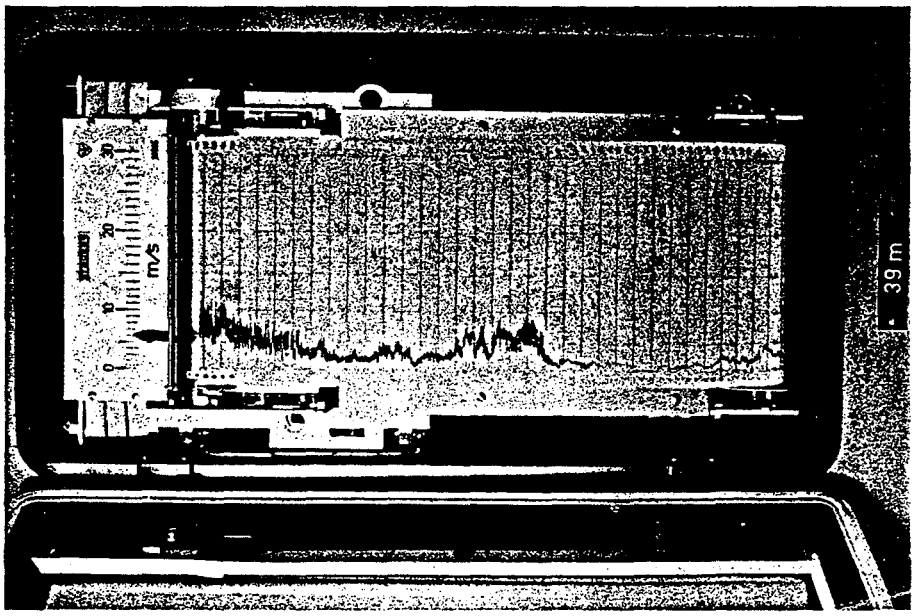

Figure 17: The Siemens wind velocity recorder.

Second instrumentation

November 1959 – February 1970
All cup anemometers were exchanged with the more sturdy Testmann three-cup type (Type 876, clockwise turning, Fig. 18).

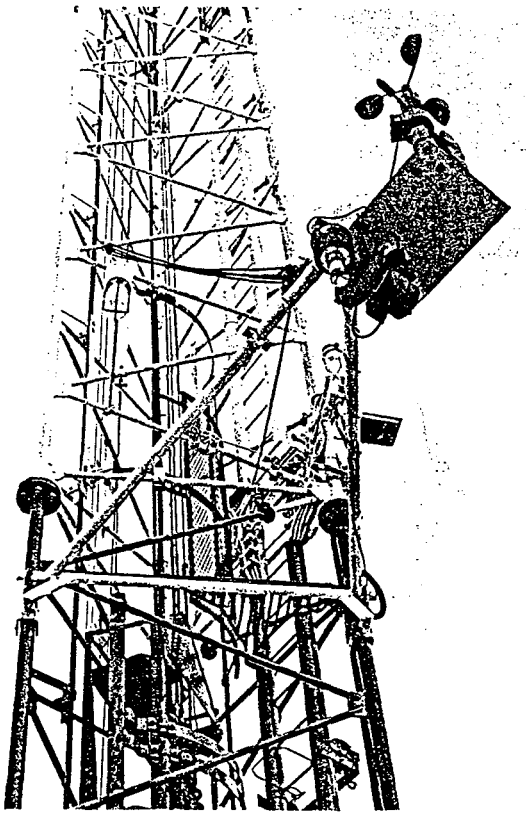

Figure 18: The combined Testman cup anemometer mounted on the triangular boom to the Risø mast.

The data-reading procedure continued in the same way as previously until May 1964, when a new automatic recording system was taken into use.

Consequently, each reading represented approximately 17-min averages starting 10 minutes before the hour and ending approximately 7 minutes after the hour. Wind speed values were read in 0.1 meter per second. No change took place in the reading of wind direction, and the Siemens ink recorders were still running.

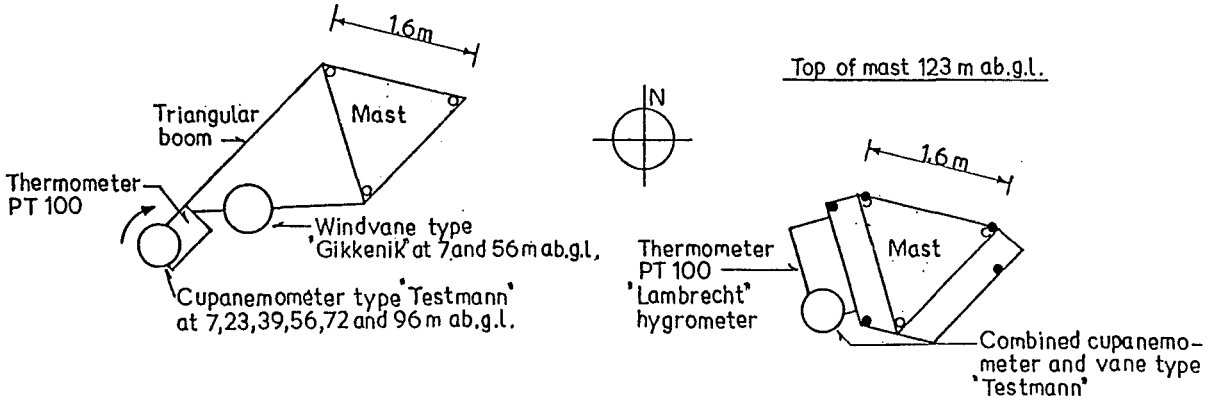

Figure 19: Cross section of the Risø mast showing the placement of the second instrumentation (November 1959 – February 1970).

In September 1967 this new recording system was abandoned and the old system with 10-min average readings from the Siemens moving coil system was resumed. From January 1968 readings of wind speeds were temporarily made from the 72-m level together with wind directions from the 123-m level.

Third instrumentation

February 1970 – January 1973
New rolling booms were installed between February and May 1970. In this period the wind speed recording and reading were performed from the 123-m level. From mid-May a temporary instrumentation was taken into use at the 27-m and 76-m level (Testman type 801). There was no change in the reading procedure (10-min averages around each full hour), but only the 76-m level was read. Between February 1972 and July 1972 the meteorology station was rebuilt.

Fourth instrumentation

January 1973 – June 1984
New Testmann cup anemometers (clockwise turning – type Risø 70) were mounted on the new rolling booms at the 11-m, 27-m, 76-m, and 117-m height. Medio 1974 directional instrumentation was mounted at all levels including a cup anemometer at the 43-m level.

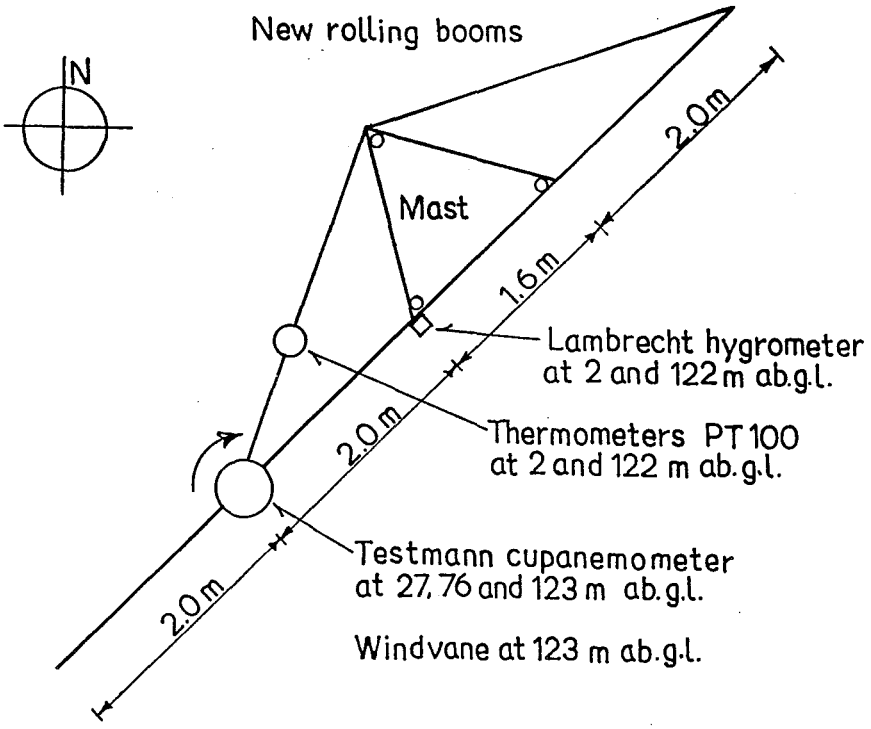

Figure 20: Cross section of the Risø mast showing the temporary instrumentation between May 1970 and June 1974.

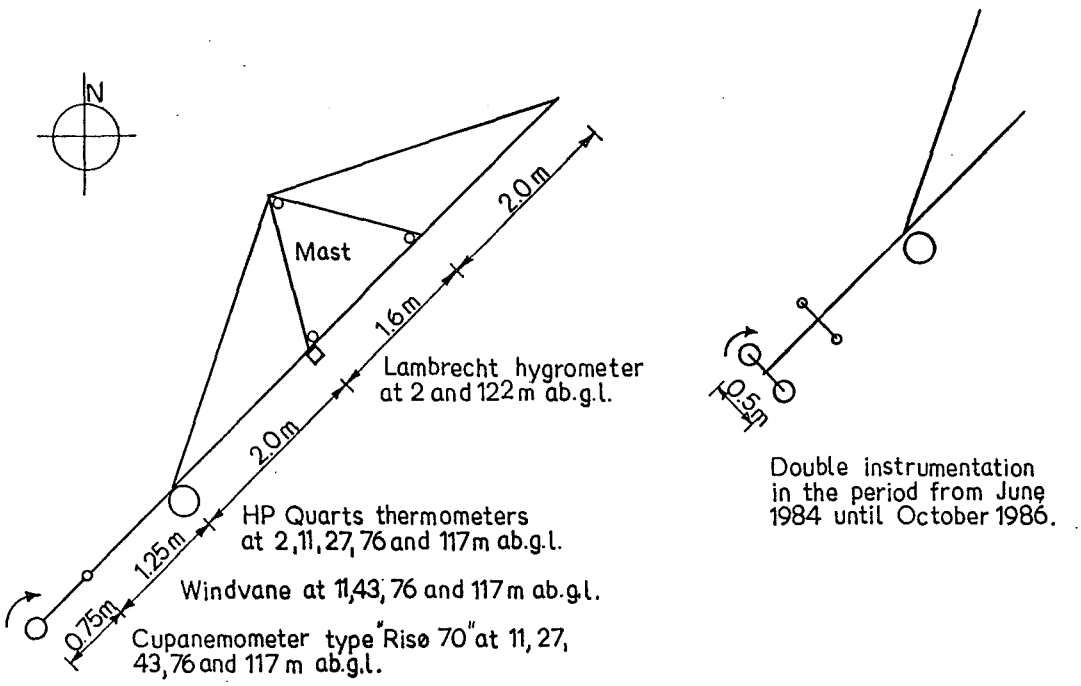

Figure 21: Cross section of the Risø mast showing the placement of the fourth instrumentation (January 1973 – June 1987).

Due to some initial difficulties with the new equipment, the readings from 1973 and 1974 are erroneous to a large extent. Contrary to other periods, the data from this period have not been corrected through readings from the moving-coil recording system.

Fifth instrumentation

June 1984 –
Implementation of a new data recording system (ADAM) including a temporary double system of cup anemometers (and readings) in order to calibrate the new system.

A new 12-point moving coil recorder was taken into use supplemented with a new software package for data sampling and calibration. Regarding data storage a new procedure is still being considered. The old recording system was dismounted in October 1986.

4.2 Data storage

Meteorological data from the Risø mast are stored on two different user-owned packs at the local Risø computer centre. The major time series covering the period between February 1958 and October 1986, including software for updating and correcting the meteorological data, are found on KLIMAPACK. Annual time series from 1976 until 1986 (continuous 10-min averages, i.e. six registrations per hour) can be found on METFYSPACK. Most data files are stored under the user code: LEIFMET. File attributes for data files:

MAXRECSIZE	=	30
BLOCKSIZE	=	720
AREASIZE	=	120
SECURITYTYPE	=	PUBLIC

Table 9: Directory of major meteorological data files on KLIMAPACK.

File		Period	No. of Records
(LEIFMET)	PACK5867NEW	Feb 1958 – Dec 1967	87648
(LEIFMET)	PACK6872NEW	Jan 1968 – Dec 1972	43848
(LEIFMET)	PACK7375NEW	Jan 1973 – Dec 1975	26280
(LEIFMET)	PACK7681NEW	Jan 1976 – Dec 1981	52632
(LEIFMET)	PACK8286NEW	Jan 1982 – Oct 1986	43834
(LEIFMET)	JABSTRIK/58T086	Feb 1958 – Oct 1986	254232

The meteorological data, the major of which has been manually inspected, are stored in six major files on KLIMAPACK (see Table 9). Each record on these files is clearly identified by year, month, day, and hour with a capacity of 30 channels per record, containing hourly meteorological data (see Table 10). If, on the basis of the manual inspection, data are found to be erroneous or simply missing they are exchanged with data of unrealistic, high absolute value.

Data from 1973 and 1974 should not be used until a qualified updating has taken place.

Table 10: Contents of the meteorological KLIMAPACK data files.

File	(LEIFMET) PACK5867 NEW	(LEIFMET) PACK6872 NEW	(LEIFMET) PACK7375 NEW	(LEIFMET) PACK7681 NEW	(LEIFMET) PACK8286 NEW	(LEIFMET) JABSTRIK/ 58T086
Ch						
0	YEMODA HO	YEMODA HO	YEMODA HO	YEMODA HO	YEMODAHO	YEMODA HO
1	u 7 m	xxxxxx	u 11 m	u 11 m	u 11 m	u 7/11 m
2	u 23 m	xxxxxx	u 27 m	u 27 m	u 27 m	u 23/27 m
3	u 39 m	xxxxxx	u 43 m	u 43 m	u 43 m	u 39/43 m
4	u 56 m	xxxxxx	xxxxxx	xxxxxx	xxxxxx	u 56 m
5	u 72 m	u 72/76 m	u 76 m	u 76 m	u 76 m	u 72/76 m
6	u 96 m	xxxxxx	xxxxxx	xxxxxx	xxxxxx	u 96 m
7	u 123 m	xxxxxx	u 117 m	u 117 m	u 117 m	u 123/117 m
8	dir 7 m	xxxxxx	dir 11 m	dir 11 m	dir 11 m	dir 7/11 m
9	dir 56 m	xxxxxx	dir 43 m	dir 43 m	dir 43 m	dir 56/43 m
10	xxxxxx	xxxxxx	dir 76 m	dir 76 m	dir 76 m	dir 76 m
11	dir 123 m	dir 123 m	dir 117 m	dir 117 m	dir 117 m	dir 123/117 m
12	t 2 m	t 2 m	t 2 m	t 2 m	t 2 m	t 2 m
13	t 6 m	xxxxxx	t 11 m	t 11 m	t 11 m	t 6/11 m
14	t 22 m	xxxxxx	t 27 m	t 27 m	t 27 m	t 22/27 m
15	t 39 m	xxxxxx	xxxxxx	xxxxxx	xxxxxx	t 39 m
16	t 55 m	xxxxxx	xxxxxx	xxxxxx	xxxxxx	t 55 m
17	t 71 m	xxxxxx	t 76 m	t 76 m	t 76 m	t 71/76 m
18	t 95 m	xxxxxx	xxxxxx	xxxxxx	xxxxxx	t 95 m
19	t 122 m	t 122 m	t 117 m	t 117 m	t 117 m	t 122/117 m
20	t_d 2 m	t_d 2m	xxxxxx	xxxxxx	xxxxxx	t_d 2 m
21	t_d 122 m	t_d 122 m	xxxxxx	xxxxxx	xxxxxx	t_d 122 m
22	xxxxxx	xxxxxx	pressure	pressure	pressure	pressure
23	xxxxxx	xxxxxx	var 11 m	var 11 m	var 11 m	var 11 m
24	xxxxxx	xxxxxx	var 43 m	var 43 m	var 43 m	var 43 m
25	xxxxxx	xxxxxx	var 76 m	var 76 m	var 76 m	var 76 m
26	xxxxxx	xxxxxx	xxxxxx	xxxxxx	t_d Cam	t_d Cam
27	xxxxxx	xxxxxx	xxxxxx	xxxxxx	t Cam	t Cam
28	xxxxxx	xxxxxx	xxxxxx	xxxxxx	rel hum	rel hum
29	xxxxxx	xxxxxx	xxxxxx	xxxxxx	sun %	sun%

ch = channel
xxxxxx = the symbol for data with (inserted) unrealistic, high absolute values
u = wind speed
dir = wind direction
t = temperature
t_d = dewpoint temperature
var = wind direction variance
t_d Cam = Cambridge dewpoint
t Cam = Cambridge temperature
rel hum = relative humidity

4.3 Wind data reduction

When it comes to analyses of extreme events, the nature of the problem calls for a drastic reduction in the amount of data available. In order to have a sufficient amount of data for a proper statistical analysis, it is therefore of great importance to have a long-term recording period at one's disposal. This long-term approach might, however, lead to a problem in identifying and selecting reasonably homogeneous wind data of reliable quality.

One of the advantages of the Risø data is the simultaneous recordings of the same meteorological phenomenon. Even though these recordings are performed at various heights this gives a skilled wind technician an opportunity to find and exclude erroneous recordings at a particular height. Furthermore, it helps identifying periods containing extreme events when a recording at the level of interest has temporarily been out of operation.

In the present study, the wind speed data from the 72/76-m level have been chosen for the statistical analyses. The primary reason for this selection is the (relatively) continuous recordings through the whole period of interest (1958 – 1986) at this level.

7 MAY 1986.

		WIND SPEED (M/SEC)					WIND DIRECTION (DEG)				WIND DIRECTION VARIANCE (DEG)		
		11M	27M	43M	76M	117M	11M	43M	76M	117M	11M	43M	76M
08	00	11.6	12.5	12.5	13.3	14.1	125	128	128	128	3.7	3.2	2.7
	10	11.5	12.3	12.1	12.6	13.7	125	130	130	130	4.4	3.9	3.5
	20	10.9	11.5	11.7	12.4	13.5	127	131	129	129	4.5	4.0	3.3
	30	12.0	12.7	12.5	13.1	13.9	124	128	129	128	4.0	3.5	2.7
	40	12.5	13.3	13.2	14.0	14.6	123	128	127	127	3.7	3.0	2.1
	50	11.9	12.8	13.0	13.9	14.6	124	127	126	127	3.5	3.1	2.3
09	00	11.6	12.4	12.5	13.3	14.1	126	130	129	128	3.8	3.3	2.8
	10	11.7	12.5	12.3	12.7	13.3	124	127	127	129	4.5	3.5	2.5
	20	11.6	12.1	12.1	12.7	13.6	125	129	128	128	4.8	3.7	3.1
	30	11.7	12.7	12.7	13.4	14.1	123	128	127	127	4.3	3.3	2.6
	40	11.6	12.5	12.5	13.1	13.7	126	129	127	126	4.0	3.6	2.8
	50	11.6	12.1	11.9	12.4	13.1	129	131	128	127	4.4	3.6	2.8
10	00	11.8	12.6	12.5	12.9	13.6	125	129	128	127	4.3	3.6	3.0
	10	11.3	11.9	11.9	12.6	13.6	128	132	130	128	4.3	3.9	3.1
	20	11.6	12.5	12.4	13.1	13.7	124	128	127	126	4.2	3.7	2.6
	30	11.0	11.7	11.4	11.8	12.4	126	129	126	125	5.0	4.5	3.5
	40	11.0	11.7	11.7	12.1	12.4	128	131	130	129	4.8	4.5	3.8
	50	12.1	12.9	12.7	13.0	12.9	122	126	125	126	4.6	3.6	2.7

Figure 22: Recordings of wind direction and wind direction variance in periods with high wind speeds ($u_{76} \geq 10$ m/s). Illustrative example.

The apparent lack of influence on the wind speed from the near-site terrain as seen in Section 3.4 is another argument for choosing this level. Compared with the higher levels, the quality of the data at the 72/76 m level seems to be better – especially before the mounting of the triangular booms – presumably due to "tower shadow" effects at the higher levels. Regarding the simultaneous wind direction recording, a natural choice of level would of course be the 72/76-m one. Due to operational problems and discontinuation in the reading procedure (see Section 4.1), there is an extensive lack of wind direction data from this specific level.

Table 11: Number of missing wind speed observations for different levels of instrumentation.

	Anemometer heights						
	7/11 m	23/27 m	39/43 m	56 m	72/76 m	96 m	123/117 m
No. of missing obs.*	54040	54870	54465	155312	13840	155444	64541
Percentage of total No. of obs.*	22.8%	23.2%	23.0%	65.6%	5.8%	65.7%	27.4%

*Observations from 1973 and 1974 excluded.

Instead, the wind speed data are linked to the wind direction data of the 117/123-m level. When it comes to higher wind speeds ($u_{76} \geq 10$ m/s), the error imposed by this procedure is found to be of a magnitude comparable to the standard deviation of the wind direction (over the 10-min averaging period (see Fig. 22).

As a consequence of poor quality (especially for heights above 27 m) wind data from the period between 1 January 1973 and 1 January 1975 have not been used. Influences on the long-term statistical approach from this exclusion are dealt with in Section 6 where a detailed description of further wind data reduction is found.

4.4 Identification of missing and erroneous data

Unfortunately, the importance of high quality data on the rare extreme events is often counter to the problem of fall-out of the instrumentation. The passing of low pressures (cold fronts) in the winter season, responsible for these events, often causes icing of the anemometers. The usual fall in temperature with height implies that this phenomenon is more frequently met in the instrumentation at the higher levels.

Whenever instrumentation at lower levels is functioning, knowledge of the wind velocity profile can help reconstruct the wind speed at the height of interest. To some extent, this can help identify with assurance these rare events that can have a significant influence on the statistics of extremes.

In the actual study this method has been used combined with information on wind speed from other meteorological sites in Denmark, (The Meteorological Yearbook) when for some reason wind speed data from the 72/76-m level are missing.

Erroneous data are somewhat more difficult to handle. They can arise from a number of causes and be of a very complex nature. Of course, the method invoked when dealing with missing data could be applied when identifying erroneous data. It is, however, necessary to include an analysis of long-term effects on the data such as drift from worn-out recording gears etc.
Anyway, to a large extent you have to rely on a conscientious updating of data and calibration of the instrumentation.

Regarding the aspect of missing and erroneous data the 72/76-m level is found to be an appropriate choice. As seen in Table 11 the number of missing wind speed observations are by far the smallest at the 72/76-m level compared with the other levels. Furthermore, six clearly recognized major fall-outs are responsible for the bulk part of the missing observations, the rest being shorter periods of, say up to 3–4 days (see Table 12). Using the Meteorological Yearbook, the periods of the six major fall-outs have been examined for any extreme events that might influence the statistical approach employed. This subject is dealt with in Section 6.

In order to be able to identify erroneous data it is essential to have a close co-operation with the technicians involved in the instrumentation and hardware. Through such a cooperation it has been possible to identify periods with major instrumental problems. Then, by checking other sources, it is possible to recognize any extreme events not accounted for by the (erroneous) data. As a result of this work, the period between 1 January 1973 and 31 December 1974 has been excluded in the present study due to the presence of an extensive amount of erroneous data, especially for levels above 27 m.

Table 12: Overview of missing wind speed observations from the 72/76-m level.

Year	No. of missing observations $u_{72/76}$	No. of observations from other heights with $u_{72/76}$ out of operation	Comment
1958	805	51	recordings started 1 Feb. 1958
59	170	107	
1960	116	87	
61	24	24	
62	32	19	
63	0	–	
64	3058	147	change of hardware 18 Mar – 9 Jul 64
65	1381	114	unreliable hardware major fall-out 12 Feb – 23 Mar
66	508	8	adjustment of hardware 10 – 27 May
67	156	144	
68	1	–	
69	22	–	
1970	1895	1849	dismounting of instrumentation 18 Feb – 6 May for rebuilding of mast
71	97	6	
72	34	–	
*73	1314	1	new instrumentation and hardware major fall-out 1 Jan – 9 Feb
*74	529	1	
75	1508	1156	major fall-out 10 June – 28 Jul
76	165	–	
77	136	–	
78	253	32	
79	400	–	
1980	182	49	
81	191	–	
82	111		
83	141		
84	601	58	major fall-out 7 Feb – 21 Feb
85	110		
86	1742		recordings ended 21 Oct
Total 15.682 $\simeq$ 653.4 days		3853 $\simeq$ 160.5 days	

* The data need proper updating. The lowest two registration levels (u_{11} and u_{27}) seem reliable when it comes to identifying extreme events.

5 Extrapolation of wind data

Since the Danish Wind Atlas (Wind Atlas for Denmark) was first published in 1980, there has been a growing interest in the methodology outlined therein, culminating in the publication of the European Wind Atlas (1989).

The objective of the Danish Wind Atlas was to evaluate the wind resources with the purpose of locating sites for wind power plants in Denmark. For wind energy production purposes the main attention is put on mean wind properties. Therefore, the applicability of the method to extreme wind speeds still remains to be justified. Before going into a more detailed description of the extrapolating procedure, some basic concepts on meteorology are introduced.

5.1 Basic concepts

In this part of the world, high wind speeds are usually related to low pressures known as cyclones. They are created along the polar front through an exchange of energy between the warm equatorial air and cold air from the polar area. Once a pressure gradient is established, air starts moving toward the low pressure and the Coriolis force (a force arising from the rotation of earth) will influence the air and turn it towards the right (in the Northern Hemisphere). If the isobars are close to straight lines and the frictional force from earth is negligible, the system will approach an equilibrium between the two driving forces (the pressure gradient and the Coriolis force). Thence, the air will move at a constant speed parallel to the isobars in a counter-clockwise direction "around" the low pressure (in the northern hemisphere).

The wind generated under these conditions is called the *geostrophic wind* or free wind because it is not influenced by the frictional forces acting on the surface of the earth. If the curvature of isobars causes a significant deviation from straight lines, the effect of the centripetal force must be taken into account. Having included this effect on the wind, the real wind becomes the *gradient wind.* The free wind condition is usually fulfilled if the height is more than one kilometer above terrain. Below this height is the *planetary boundary layer.* In this layer the wind vector is turned a small angle counter-clockwise relative to the direction of the geostrophic wind. As the vertical extrapolation is performed through this layer, some fundamental characteristics regarding the dynamical behaviour of the boundary layer are of major importance. The first one is the *stability.*

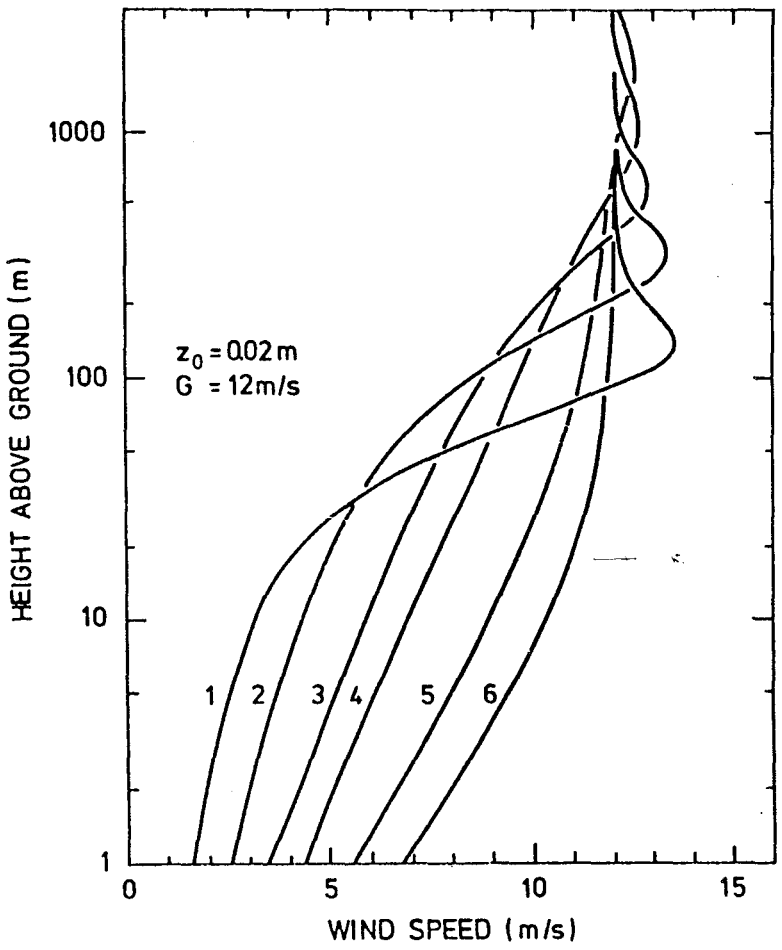

Figure 23: Wind velocity profiles through the boundary layer in different conditions. 1) strongly stable, 2) stable, 3) near-neutral, 4) neutral, 5) unstable, 6) strongly unstable conditions.

The boundary layer is said to be neutral if the change of temperature with height is -1°C for each 100-m increase of altitude (equal to an adiabatic expansion). It is said to be stable/unstable if the decrease of temperature is respectively less/more than 1°C for a 100-m increase of height. The prevailing stability has a strong influcence on the wind conditions (see Fig. 23).

Measurements at Risø show that unstable, neutral, and stable atmospheric conditions occur approximately 6%, 60%, and 34% of the time, respectively (Jensen, 1973).

Another important condition is that the geostrophic wind be constant with height. This is called *barotropy*; if this were not the case, *baroclinic* conditions would prevail. Strong *baroclinity* is attached to frontal zones and is most often transient.

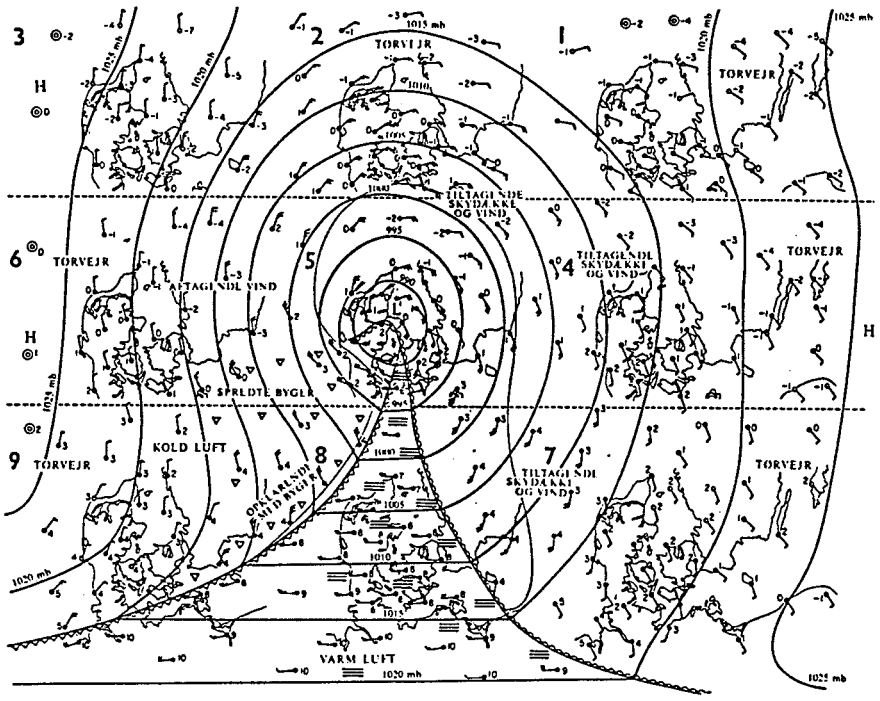

Figure 24: Nine weather maps illustrating the wind conditions when a low pressure passes A) south (maps 1–3), B), right across (maps 4–6), and C) (map 7–9) north of Denmark in an easterly direction. Analyses of 22 storms (B≥ 10) indicate that approximately 70%, 25%, and 5% belong to the A, B and C-events, respectively. From Nørrevang and Meyer (1968).

The physical modelling of the wind atlas does not include baroclinity, nor the effect of curved isobars (see pages 61–62 in Wind Atlas for Denmark), i.e. the gradient wind = the geostrophic wind. Note that this may cause some deficiency when extrapolating isolated exteme wind data.

5.2 Vertical extrapolation

Having provided a qualified terrain description of the Risø site (Section 3) and performed an updating of raw data (Section 4), the next step is the vertical extrapolation of data.

The European Wind Atlas procedure is based on the "double-vertical extrapolation method" which will also be used in the present study. The principle of the method is shown in Fig. 25. This method takes its origin in surface observations, extrapolates these to the top of the boundary layer, then interpolates or extrapolates the geostrophic wind in the horizontal direction.

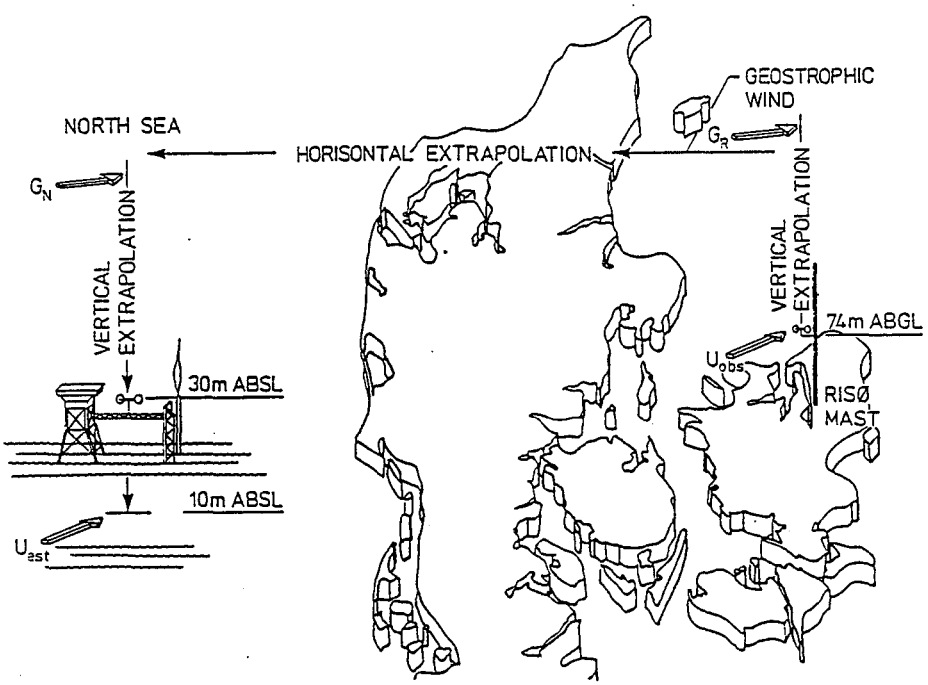

Figure 25: The principle of the double-vertical extrapolation method.

Finally, it is extrapolated downward again to a specified height at a specified site. This procedure is somewhat different from the method outlined in the Danish Wind Atlas as the starting procedure is calulating the geostrophic wind on the basis of pressure measurements.

The basic equation governing the vertical extrapolation is the *geostrophic drag law* which links the friction velocity u_*, the surface roughness z_0, and the stability parameter μ to the geostrophic wind velocity G:

$$G = \frac{u_{*cor}}{\kappa}\sqrt{\left[\ln\left(\frac{u_{*cor}}{f\,z_{0,\infty}}\right) - A(\mu)\right]^2 + B^2(\mu)} \tag{9}$$

where

$$\begin{array}{ll} \kappa = 0.4 & \text{(von Kármán's constant)} \\ f = 1.21\times10^{-4}\,s^{-1} & \text{(Coriolis parameter)} \\ \mu = \frac{u_{*cor}}{fL} & \text{(stability parameter)} \end{array}$$

u_{*cor} is the friction velocity related to homogeneous upstream conditions which again correspond to a roughness classification $z_0 = z_{0,\infty}$ (see Section 3.1). $A(\mu)$ and $B(\mu)$ are empirical functions defined as

$$A(\mu) = \begin{cases} b_0 - \ln(b_2) + \ln(b_2 - \mu) & ; \quad \mu < 0 \\ b_0 + \sqrt{b_1} - \sqrt{b_1 + \mu} & ; \quad \mu > 0 \end{cases} \tag{10}$$

$$B(\mu) = \begin{cases} \kappa + \frac{a_0 - \kappa}{1 - a_1 \mu} & ; \quad \mu < 0 \\ a_0 + \sqrt{\mu} & ; \quad \mu > 0 \end{cases} \tag{11}$$

with $a_0 = 4.5, a_1 = 0.04, b_0 = 1.8, b_1 = 5$ and $b_2 = 0.894$.

To a large extent the stability parameter μ is governed by the Monin-Obukhov length L, defined as

$$L = -\frac{T_0 \, u_{*,obs}^2}{g \, \kappa \theta_*} \tag{12}$$

where

T_0	is the absolute temperature near the surface
$\theta_* \, u_{*,obs}$	is a measure of the surface heat flux.

For neutral stability which is often prevailing in periods with high wind speeds (this has been verified by checking the temperature profiles in periods of storm) and over-water conditions, L will approach infinity $L \rightarrow \infty$ thence the stability parameter μ will approach 0. Accordingly, for *neutral conditions* the geostrophic drag law is given by

$$G_{\mu=0} = \frac{u_{*cor}}{\kappa} \sqrt{\left[\ln\left(\frac{u_{*cor}}{f \, z_{0,\infty}} \right) - b_0 \right]^2 + a_0^2} \tag{13}$$

where $a_0 = 4.5$ and $b_0 = 1.8$.

Introducing the Rossby number

$$Ro = \frac{G}{f \, z_0} \tag{14}$$

N.O. Jensen (1978) suggests the following simple approximation to Eq. (13)

$$G_{\mu=0} = 2 u_{*cor} \cdot \ln Ro \quad . \tag{15}$$

In the lower part of the boundary layer, denoted the *surface layer*, a special relationship exists between the observed wind speed u_{obs} and the friction velocity u_{*obs}.

Assuming neutral conditions, this relationship is given by

$$u_{obs} = \frac{u_{*obs}}{\kappa} \ln\left(\frac{z_{obs}}{z_{00}}\right) \tag{16}$$

where

z_{obs}	is the anemometer height
z_{00}	is the roughness length corresponding to the immediate surroundings
κ	$= 0.4$

The surface roughness for water can be approximated by

$$z_0^{water} = 0.014 \frac{u_*^2}{g} \quad . \tag{17}$$

Assuming neutral stability, we have accordingly established a relationship between the observed wind speed (u_{obs}) at a specified location and height and the geostrophic wind speed (G).

Applying the inverse procedure, this will of course yield an estimate of the wind speed u_{est} at another specified location and height.

Finally, the angle (α) between the surface and geostrophic wind is given by

$$\sin\alpha = -\frac{u_{*cor}}{\kappa G} \tag{18}$$

again assuming neutral stability.

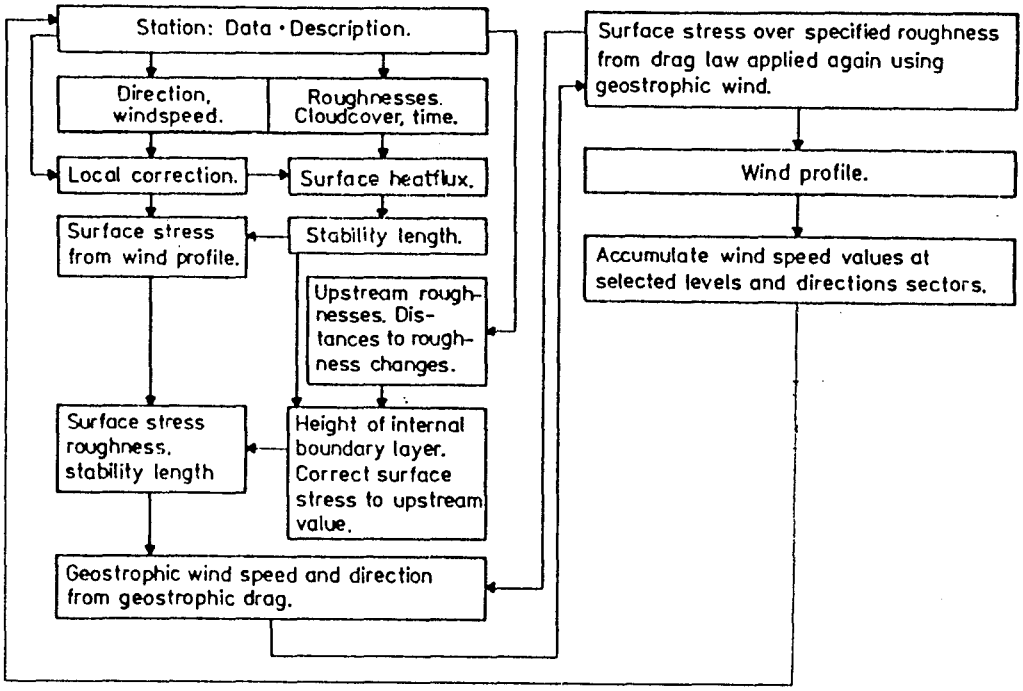

Figure 26: Schematic representation of the computational scheme for the double-vertical extrapolation.

5.3 Horizontal extrapolation

The horizontal extrapolation is performed above the planetary boundary layer and should accordingly be unaffected by the terrain below.

The theoretical justification of this statement is based on the assumption that terrain features such as gently sloping hills etc. will cause a pressure perturbation which is adequately described by potential flow theory (Section 3.3).

In mountainous regions, however, flow will cause pressure perturbation which will extend above the boundary layer and probably not be adequately described by a potential flow theory. In addition, local wind systems will occur (mistral, foehn, etc.), which will make a horizontal extrapolation rather troublesome, passing such terrain features.

Fortunately, these problems are not encountered within Danish territory. Furthermore, the weather system responsible for the strong winds will cover an area larger than that of Denmark.

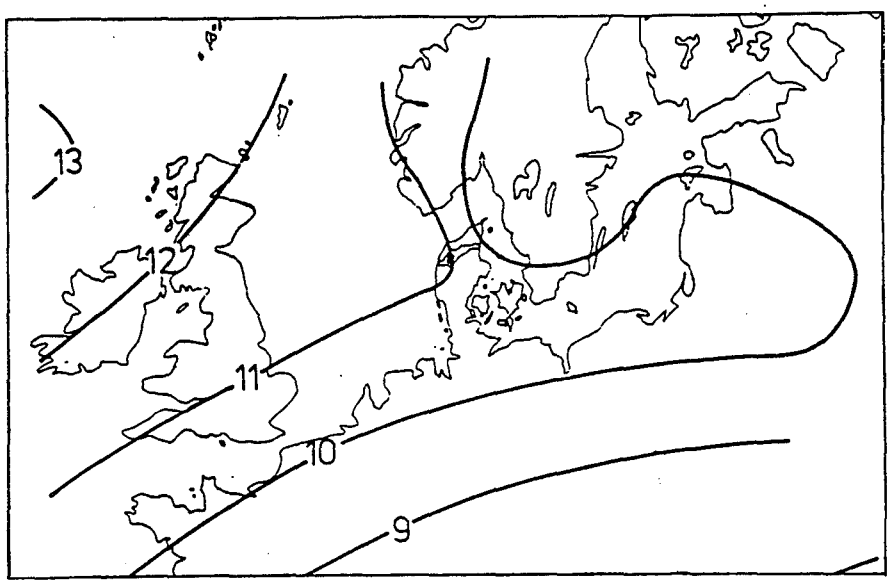

Figure 27: The mean wind speed at 850 mb computed from the analysis of weather maps and radiosonde data covering Northern Europe.

Concerning a geographic variation of the geostrophic mean wind speed over northern Europe, an analysis of weather maps and radiosonde data has been performed. The result shown in Fig. 27 indicates a variability of the geostrophic mean wind speed within Danish territory. This detection is not supported by a similar analysis performed in the Danish Wind Atlas.

Regarding extreme wind speeds, a comparison study (Section 7) performed on extrapolated data and data from the North Sea does not substantiate a geographical variation of the geostrophic extreme wind speed within Danish territory.

6 Application of statistical models

One of the major tasks of this study is to establish a reliable long-term statistics of extreme wind speeds in the Danish territorial waters, introducing a method which makes it easy to transform the result to other terrain categories. This section deals with the statistical theory and application for the meteorological data at hand.

First a short description will be given of the basic concepts and assumptions in statistical modelling.

6.1 Basic concepts and assumptions

Examining the variability of wind speed and direction in turbulent air generated primarily from differences in the atmospheric pressure surely leads to the conclusion that an exact predictability of this phenomenon would imply computational modelling beyond any reasonable capacity.

Alternatively, implementation of stochastic modelling seems advantageous. Introducing meteorological features such as wind speed as stochastic variables makes it possible, through the statistical representation (mean, variance, etc.) and the theory of frequency analysis, to produce estimates of future rare events including an estimate on the uncertainty of the predictions.

Historical data as the present wind speed data are considered to be a realization of a stochastic process emerging from an ensemble of realizations taken simultaneously from the same phenomenon at a given location. In order to invoke the stochastic modelling on historical data with only one realization, it is necessary to assume that the statistical representation of the stochastic variable over time equals the representation of the ensemble.

This is known as the *ergodic theorem*. This basic assumption is closely related to the next assumption introduced – the so-called *stationarity assumption* which implies that the representation of the stochastic variable is independent of the averaging period and starting time. This assumption will evidently not hold for the wind speed time series (periods of storm, seasonal variation, etc.). However, selecting an appropriate averaging period often secures *self stationarity*, i.e. pooling of stationary periods bit by bit excluding a general

drift, which will prove satisfactory when statistical models are applied. The mathematical formulation of the stochastic representation will be introduced at a later stage.

Finally, the *independent assumption* should be mentioned as the mathematical description of the process is highly simplified if this assumption holds. This aspect will be treated in greater detail later on. The interested reader is referred to Box and Jenkins, 1976 for a comprehensive introduction to the time series analysis.

6.2 Time series of wind speed and related stochastic processes

It can often be a troublesome task to identify the type and characteristics of a stochastic process if the information on the process is limited to the actual time series of the physical phenomenon.

Relating usual mathematical formulation such as mean value and variance to the process contains important information about the process of course, but in the field of time series analysis the most important formulation might be the *autocorrelation function (acf)* defined as

$$\rho(\tau) = \frac{c_{ww}(\tau)}{\sigma(w)^2} \tag{19}$$

where

$c_{ww}(\tau)$ is the autocovariance function, i.e. the covariance between $w(t_1)$ and $w(t_2)$, τ being the difference $t_2 - t_1$; $\sigma(w)^2$ is the variance of the stochastic process.

Certain problems arise when estimating the autocovariance function in practice. As in other statistical estimating procedures the problem of bias arises from the (usual) limited time series at hand. In case of a discrete time series of N observations, a central estimate of the autocovariance function is given by

$$\hat{c}_{ww}(\tau) = \frac{1}{N-\tau} \sum_{t=1}^{N-\tau} (w_t - \bar{w})(w_{t+\tau} - \bar{w}) \tag{20}$$

The stochastic assumption yields that $\hat{c}_{ww}(\tau) \to 0$ when $\tau \to \infty$. This is often not the case as the estimates $\hat{c}_{ww}(\tau_1)$ and $\hat{c}_{ww}(\tau_2)$ are correlated. Furthermore, the assumption of stationarity might not be fulfilled.

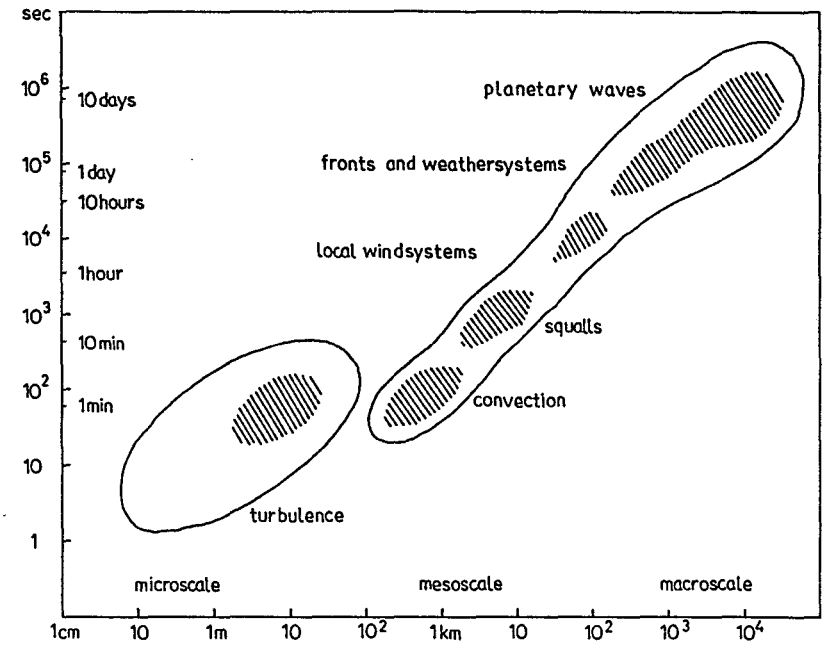

Figure 28: The figure illustrates the difference in length and time scale for various meteorological phenomena related to the wind climate.

In order to illustrate some fundamental property of the autocorrelation function, a short part of the time series has been extracted for further analysis (Fig. 29).

Starting with the basic continuous time series produced by the moving-ink coil system (see Section 4), the first reduction procedure creates a discrete time series of 10-min averages. This process clearly reduces the information from the continuous time series as the turbulence component is excluded in the discrete time series. Whether this "extraction of energy" from the process causes any deficiency in the further analysis depends on the issue of the study.

As the major interest of the present study is related to wind speed variations in connection with passing of low pressures with a time scale of hours and days, this reduction procedure is clearly justified.

A further reduction in the data material is performed, using only the 10-min average measurements around each full hour. This is not a standardardized method in the field of data reduction as a more appropriate method would be to extract an hourly mean value. The storage of the available data makes such a method rather troublesome. Instead a test was carried out regarding the influence on the data material from the applied reduction procedure. A number of 25 storm events has been extracted, covering a period of six years. From each storm event the maximum 10-min continuous average wind

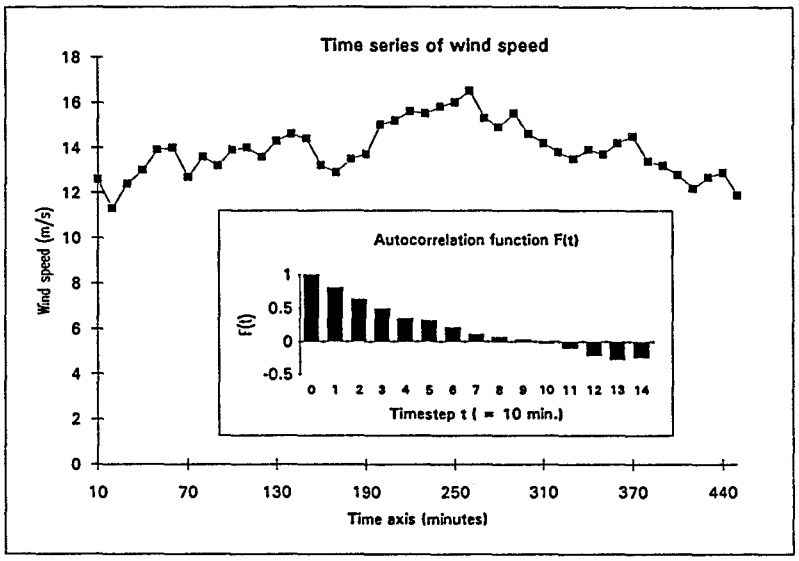

Figure 29: Autocorrelations and process time series.

speed ($u^{con}_{10,max}$) is compared to the maximum 10-min average each full hour ($u^{1hour}_{10,max}$). The ratio $\frac{u^{1hour}_{10,max}}{u^{con}_{10,max}}$ is found to be approximately 0.98. As expected the maximum mean value over one hour ($u_{1hour,max}$) is found to be less than $u^{1hour}_{10,max}$ for each storm event.

The ratio $\frac{u^{con}_{10,max}}{u_{1hour,max}}$ is found to be approximately 0.94. Again, with reference to Fig. 29, illustrating the reduced discrete time series and related estimates of the autocorrelation functions, the process seams to resemble an autoregressive process, i.e. a process in which the present value is a function of previous process values and random noise. The slowly dampened *acf* of the continuous time series indicates a higher degree of dependency between successive events compared to the series of $u^{1hour}_{10,max}$. A further reduction of the data material and corresponding stochastic processes will be dealt with in Sections 6.4 and 6.5.

6.3 Probability models for wind speed and direction

The next step in the statistical modelling, having identified the basic stochastic process, is the implication of a theoretical distribution function suitable for describing the probability of the random variable. Our primary interest is to find a suitable "initial" distribution for the wind speed variable and a conditional distribution for wind speeds given a specific wind direction. No theoretical justification is given (or can be given) for the choice of distribution, but they are simply chosen on a well-proven empirical background.

Table 13: Critical values (d_{crit}) in the Kolgomorov-Smirnov test as a function of the level of significance α.

$\alpha = 0.20$	$\alpha = 0.10$	$\alpha = 0.05$	$\alpha = 0.01$
$\frac{1.07}{\sqrt{n}}$	$\frac{1.22}{\sqrt{n}}$	$\frac{1.36}{\sqrt{n}}$	$\frac{1.63}{\sqrt{n}}$

6.3.1 Statistical tests

Having selected a distribution function, representing the random variable, a natural task is to perform a goodness-of-fit test.

Several statistical tests to evaluate distributional assumptions have been evolved. Some are valid for specific models, others are applicable for a wide range of distributions. In the present case a test called the Kolmogorov-Smirnov test has been selected which is a "distribution-free" test, simple to compute. We want to test the hypothesis that

H_0: the distribution provides an adequate representation for the random variable (w) (no rejection)
against H_1: the specified distribution does not provide an adequate representation for the random variable (w) (rejection)

We introduce a test property D:

$$D = \sup \mid \frac{i}{n+1} - F(w_i) \mid \tag{21}$$

i.e. computing the maximum difference between the distributional model and cumulated histogram of the observations. We can test this property against a critical value d_{crit} which will depend only on the number of observations n and the level of significance α on which we will accept the hypothesis. Usally a significance level of $\alpha = 0.05$ is found appropriate, corresponding to the confidence level of $1 - \alpha = 0.95$.

In Table 13 is listed a number of values for d_{crit} corresponding to different levels of significance.

We will accept the H_0-hypothesis, if

$$D \leq d_{crit} \quad .$$

Strictly speaking this procedure is valid only if the distribution model is independent of the observation, i.e. the parameter estimates must not be performed on the data against which they are tested. Having a large number of observations, this is rather a theoretical than an actual practical problem.

6.3.2 Marginal distributions

The two-parameter Weibull distribution is generally used to represent the random wind speed variable (w – horizontal 10-min average wind speed). Its probability density function is

$$f(w; c, A) = \frac{c}{A}\left(\frac{w}{A}\right)^{c-1} \exp\left[-\left(\frac{w}{A}\right)^{c}\right] \quad . \tag{22}$$

The cumulative Weibull distribution is given by

$$F(w; c, A) = 1 - \exp\left[-\left(\frac{w}{A}\right)^{c}\right] \quad . \tag{23}$$

Important statistical representation of the Weibull distribution is listed below:

$$\text{Mean value:} \quad \mu_w = A\Gamma\left(1 + \frac{1}{c}\right) \tag{24}$$

$$\text{Variance:} \quad \mathrm{Var[w]} = \mathrm{A}^2\left[\Gamma\left(1 + \frac{2}{\mathrm{c}}\right) - \Gamma^2\left(1 + \frac{1}{\mathrm{c}}\right)\right] \tag{25}$$

$$\text{Modal value:} \quad \mathrm{Mod[w]} = \mathrm{A}\left(\frac{\mathrm{c}-1}{\mathrm{c}}\right)^{1/\mathrm{c}} \tag{26}$$

$$\text{Mean square:} \quad \overline{w^2} = A^2\Gamma\left(1 + \frac{2}{c}\right) \tag{27}$$

Simple moment estimates of the parameters can be computed through the following equations.

$$\hat{A} = \frac{\overline{w^2}}{\mu_w} \cdot \frac{\Gamma\left(1+\frac{1}{\hat{c}}\right)}{\Gamma\left(1+\frac{2}{\hat{c}}\right)} \tag{28}$$

$$\frac{\Gamma\left(1+\frac{2}{\hat{c}}\right)}{\left[\Gamma\left(1+\frac{1}{\hat{c}}\right)\right]^2} = \frac{\overline{w^2}}{\mu_w^2} \tag{29}$$

with estimates of

$$\hat{\mu}_w \simeq \bar{x}_w = \frac{1}{n}\sum_{i=1}^{n} w_i$$

$$\hat{\overline{w^2}} \simeq \overline{x_w^2} = \frac{1}{n}\sum_{i=1}^{n} w_i^2 \quad .$$

where n is the number of observations.

Maximum likelihood estimates can be obtained by solving the two equations as follows with respect to A and c

$$n \cdot A^c - \frac{1}{A^c}\sum_{i=1}^{n} w_i^c = 0 \tag{30}$$

$$\frac{n}{c} + \sum_{i=1}^{n} \ln w_i - \frac{1}{A^c}\sum_{i=1}^{n} (\ln w_i \cdot w_i^c) = 0 \tag{31}$$

In the present case a *maximum likeness* estimation procedure has been used – first grouping the observation in a histogram and then using a (modified) maximum likelihood procedure to obtain estimates of A and c so that the corresponding Weibull density distribution has the best possible fit to the histogram. Figure 30 shows the marginal histogram of wind speed $\left(U_{10min}^{1hour}\right)$ from the 76-m level on the Risø mast.

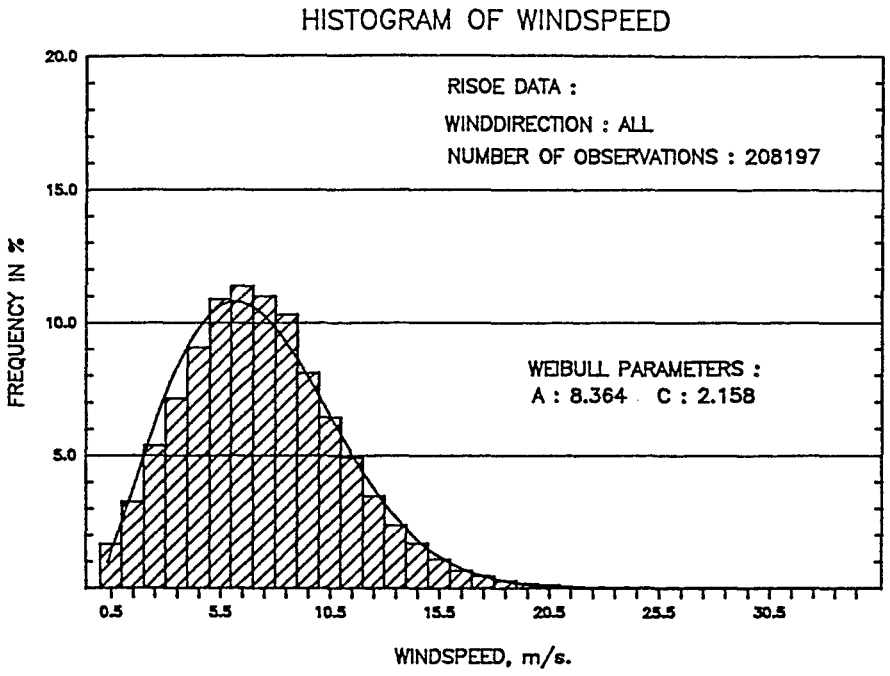

Figure 30: Histogram of U_{10min}^{1hour} from the 76-m level on the Risø Mast and associated probability density distribution.

A goodness-of-fit test yields the following.

$$\delta_{crit}^{\alpha=0.05} = \frac{1.36}{\sqrt{n}} = \frac{1.36}{\sqrt{208197}} = 0.003 \quad .$$

The test property D is found to be 0.158 indicating a significant rejection of the Weibull distribution as a suitable model for the wind speed distribution. This result shall not, however, be attached too much importance as an acceptance of the hypothesis is almost impossible to gain with a number of more than 200,000 observations. The result should merely serve as a guideline in the further analysis with respect to the problem of finding the "true" distribution which rarely (never) exists when it comes to describing physical phenomena.

Selecting a probability distribution representing the wind direction variable (θ) is somewhat more difficult. This problem will not be given much attention but some of the basic parameters of "circular" distributions will be given in the following.

For a unimodal frequency distribution (i.e. a distribution with a single peak) the following important representation can be deducted.

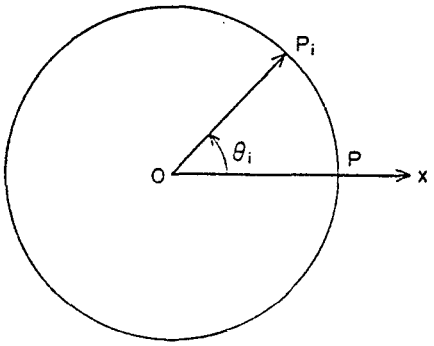

Figure 31: Representations of the sample point θ_i. $OP = 1$. Note the counter-clockwise direction of the θ_i-angle.

First, we define

$$\bar{c} = \frac{1}{n}\sum_{i=1}^{n} \cos\theta_i \tag{32}$$

$$\bar{s} = \frac{1}{n}\sum_{i=1}^{n} \sin\theta_i \tag{33}$$

$$\bar{R} = \sqrt{\bar{c}^2 + \bar{s}^2} \tag{34}$$

$$\bar{c} = \bar{R}\cos\bar{x}_\theta \tag{35}$$

and

$$\bar{s} = \bar{R}\sin\bar{x}_\theta \quad . \tag{36}$$

This leads to a formula for the mean value $\bar{x}_\theta$ of the sample $\theta_i, 1 < i \leq n$. To obtain $\bar{x}_\theta$, it is convenient to use

$$\bar{x}_\theta \quad = \begin{cases} \bar{x}'_\theta & \text{if} \quad \bar{s} \geq 0, \bar{c} > 0 \\ \bar{x}'_\theta + \pi & \text{if} \quad \bar{c} < 0 \\ \bar{x}'_\theta + 2\pi & \text{if} \quad \bar{s} < 0, \bar{c} > 0 \end{cases} \tag{37}$$

where

$$\bar{x}'_\theta = \arctan\left(\frac{\bar{s}}{\bar{c}}\right) \qquad -\frac{\pi}{2} < \bar{x}'_\theta < \frac{\pi}{2} \quad . \tag{38}$$

The circular variance s_θ around $\bar{x}_\theta$ is given by

$$s_\theta = 1 - \frac{1}{n}\sum_{i=1}^{n} \cos\left(\theta_i - \bar{x}_\theta\right) \quad . \tag{39}$$

As $\cos(\theta_i - \bar{x}_\theta) = \cos\theta_i \cos\bar{x}_\theta + \sin\theta_i \sin\bar{x}_\theta$ then, using Eqs. (35) and (36) Eq. (39) reduces to

$$s_\theta^{rad} = 1 - \bar{R} \tag{40}$$

where $\bar{R}$ is the mean resulting length,

$$s_\theta^{deg} = \frac{180^\circ}{\pi} \times s_\theta^{rad} \quad . \tag{41}$$

Note that the angular standard deviation, s_θ, cannot be taken as $s_\theta^{1/2}$, but has to undergo a transformation to the range $(0, \infty)$. For further treatment of this subject, see Mardia (1972).

The most important unimodal probability (density) distribution in statistical inference on the circle is the von Mises distribution defined as

$$f(\theta; \mu_\theta, \kappa) = \frac{1}{2\pi \cdot I_0(\kappa)} \cdot \exp\left[\kappa \cos\left(\theta - \mu_\theta\right)\right] \tag{42}$$

with $\quad 0 < \theta \leq 2\pi \quad , \quad \kappa > 0 \quad , \quad 0 \leq \mu_\theta < 2\pi$

where $I_0(\kappa)$ is the modified Bessel function of the first kind and order zero, i.e.

$$I_0(\kappa) = \sum_{r=0}^{\infty} \frac{1}{r!^2} \left(\frac{1}{2}\kappa\right)^{2r} \quad . \tag{43}$$

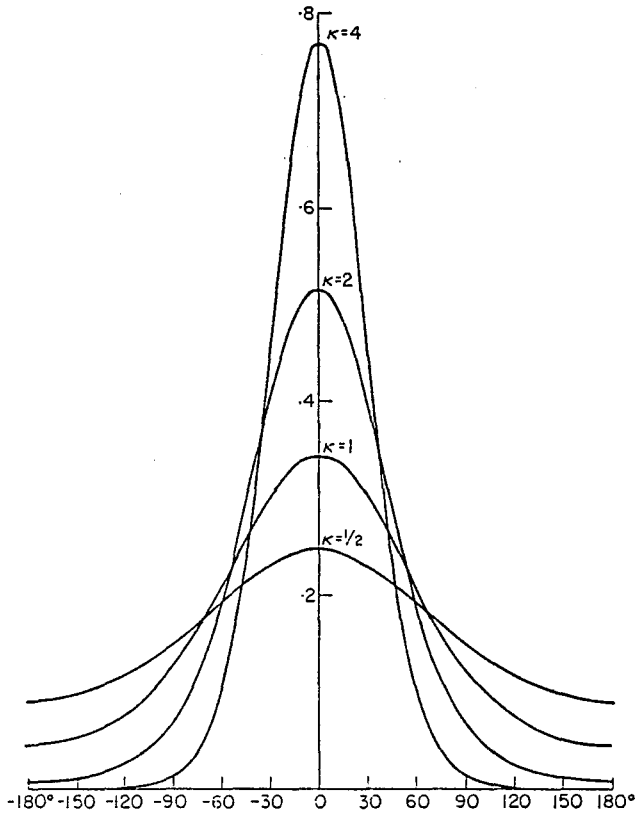

Figure 32: Density of the von Mises distribution for $\mu_\theta = 0°$ and $\kappa = \frac{1}{2}$, 1, 2, 4.

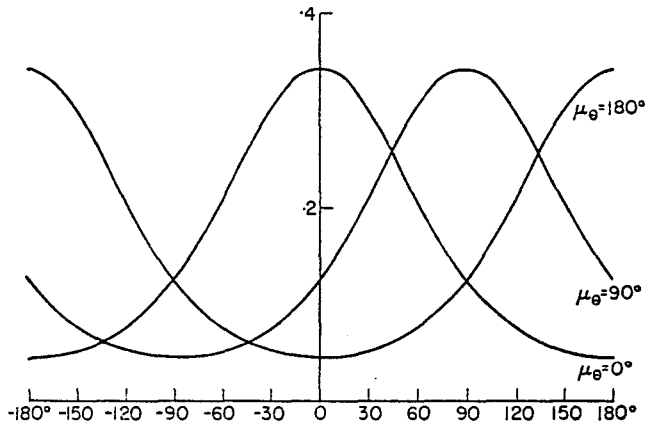

Figure 33: Density of the von Mises distribution for $\kappa = 1$ and $\mu_\theta = 0°$, 90°, 180°.

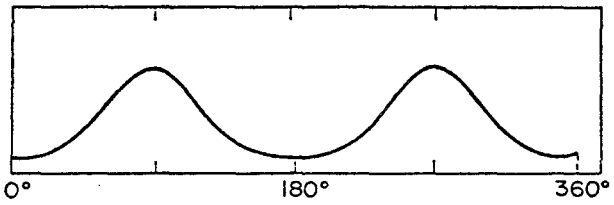

Figure 34: Density of the bimodal von Mises type distribution for $\kappa = 1$, $\mu_{\theta,1}$ = 90°, and $\mu_{\theta,2} = 270°$.

The parameter μ_θ is the mean direction while the parameter κ may be regarded as a concentration parameter.The maximum likelihood estimates of κ and μ_θ are found by solving the following equations:

$$\hat{\mu}_\theta = \bar{x}_\theta \quad . \tag{44}$$

$$\frac{I_1(\kappa)}{I_0(\kappa)} = \bar{R} \quad . \tag{45}$$

For different values of $\bar{R}$ this solution is tabulated in Mardia (1972).

In practice, density distributions on the circle are often multimodal (i.e. they have more than one peak).

They can be obtained by extending the range of a unimodal distribution on $(0, 2\pi/\ell)$ to $(0, 2\pi)$.

A multimodal density function with ℓ-modes situated $2\pi/\ell$ radians apart with the first mode at $\mu_{\theta,1} = \mu_\theta$ is given by

$$f(\theta, \mu_{\theta,\ell}, \kappa) = \frac{1}{2\pi I_0(\kappa)} \exp\left[\kappa \cos \ell\,(\theta - \mu_\theta)\right] \tag{46}$$

with $\quad 0 < \theta \leq 2\pi \quad , \quad 0 < \mu_\theta < 2\pi/\ell.$

From the wind direction histogram of the Risø site (Fig. 35) three modals, situated around the southeast, west, and north direction, are recognized.

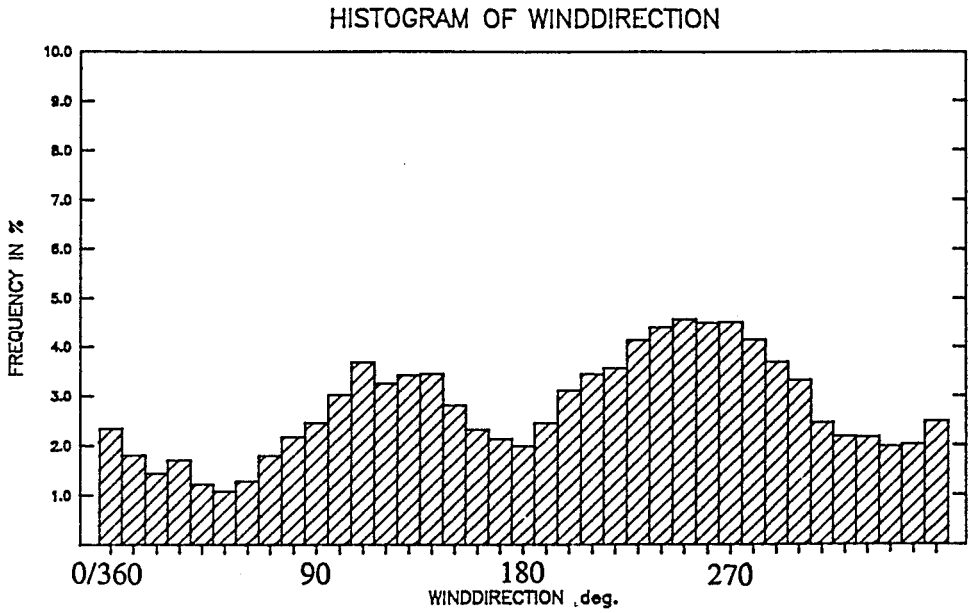

Figure 35: Wind direction histogram from the 117/123 m level on the Risø mast 1958–1986.

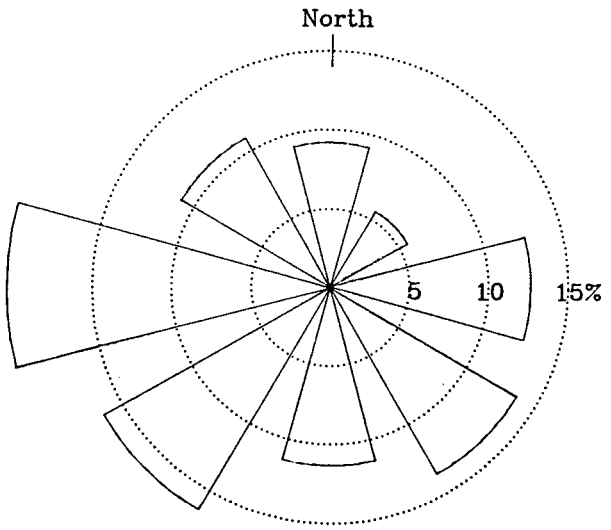

Figure 36: Rose diagram of the wind direction from the 117/123 m level at the Risø mast, 1958–1986 .

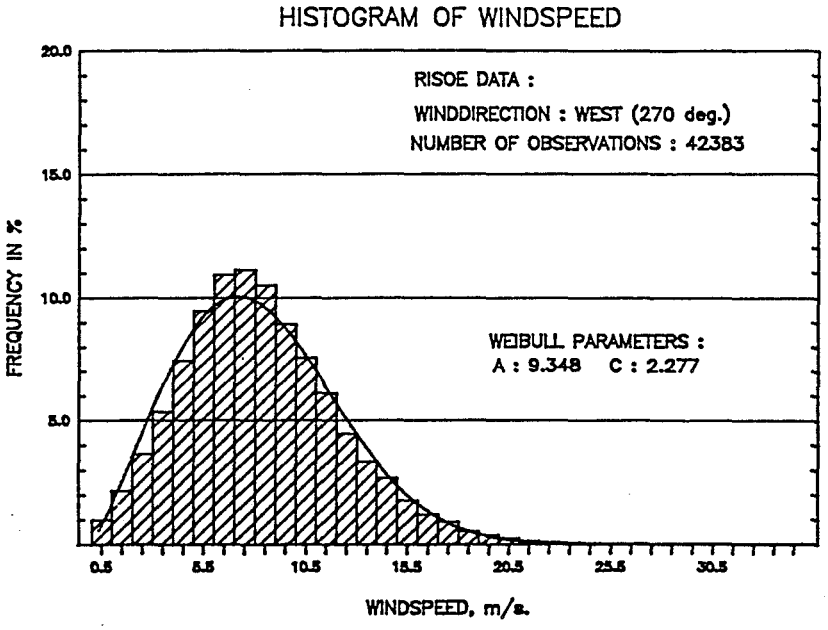

Figure 37: Histogram of wind speed from the west sector recorded from the 72/76 m level on the Risø mast, 1958 - 1986. Histograms for other sectors are found in Appendix B .

It is, however, also clear that the concentration factor (κ) (i.e. the variance around each modal) differs from modal to modal. Therefore, no attempt has been made to fit a three-modal von Mises distribution to the data. As previously mentioned the primary interest of this study is aimed at the distribution of wind speed, especially the conditional distribution of wind speed given a specific wind direction. A theoretical approach as to establishing joint distributions for wind speed and direction is not within the scope of this study.

6.3.3 Conditional distributions

In classic probability theory the probability of an event A, given the occurrence of an event B, called the conditional probability of A, is given by:

$$\Pr(A \mid B) = \frac{\Pr(A \cap B)}{\Pr(B)} \quad . \tag{47}$$

$\Pr(A \cap B)$is the probability that both A and B will occur, known as their "joint probability", and $\Pr(B)$ is the probability of the event B.

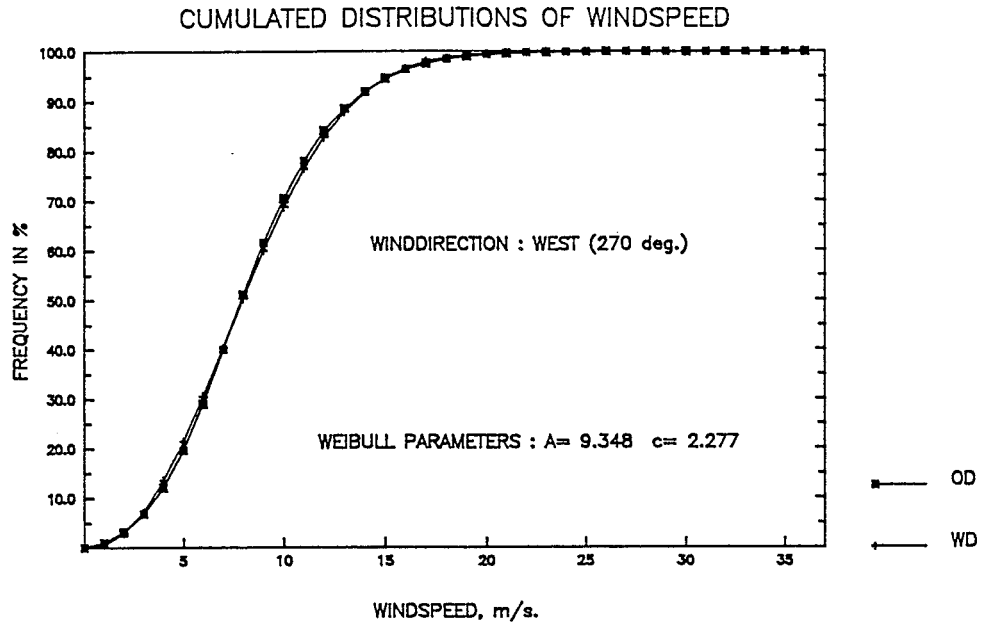

Figure 38: Cumulated distribution of wind speed from the west sector recorded from the 72/76 m level on the Risø mast, 1958 – 1986. OD: observed distribution. WD: Weibull distribution.

For a continuous variable the probability distribution function $F(w)$ is defined as

$$F(w) = \Pr(W \leq w) \quad .$$

Introducing the wind speed variable W and wind direction variable Θ, the distribution of W conditioned that $\theta_1 < \Theta \leq \theta_2$ is given by

$$F(w \mid \theta_1 < \Theta \leq \theta_2) = \frac{F(w, \theta_2) - F(w, \theta_1)}{F(\theta_2) - F(\theta_1)} \tag{48}$$

where $F(\theta)$ is the marginal cumulative probability distribution of wind direction, and $F(w, \theta)$ is the joint cumulative probability distribution of wind speed and direction.

As none of the two distributions have been derived or approximated to the data, a more theoretical approach to determine the conditional distribution of wind speed given a specific wind direction seems infeasible. Instead an empirical approch has been used, assigning Weibull distributions to the histogram of conditional wind speed data (see Fig. 37).

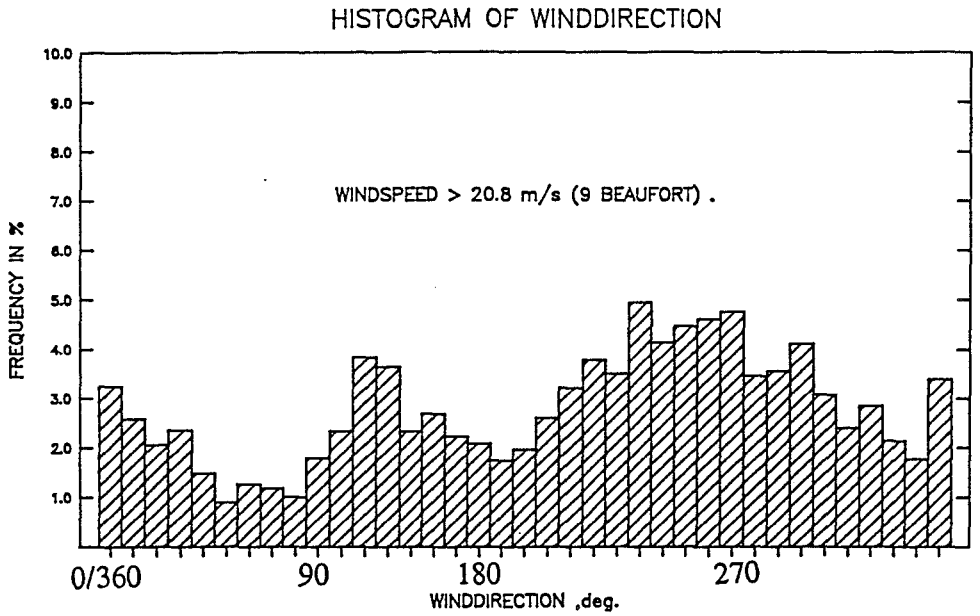

Figure 39: Histogram of conditional wind direction data from the 117/123 m level on the Risø mast, 1958 – 1986.

The parameters are estimated on the basis of maximum likeness procedure. A Kolomogorov-Smirnov test of the goodness-of-fit shows a clear rejection of the H_0-hypothesis on the 95% confidence level for all the eight wind direction sectors (see Section 6.3.1).

This rejection does not imply that further statistical treatment is based on erroneous premises. As will be shown in the next section, the primary interest is attended to the tail behaviour of the initial distribution.

Finally is shown the conditional density distribution of wind direction Θ conditioned that $W > w_1$

$$F(\theta \mid W > w_1) = \frac{1 - F(w_1, \theta)}{1 - F(w_1)} \tag{49}$$

where $F(w)$ is the marginal cumulative probability distribution of wind speed and $F(w, \theta)$ is the joint cumulative probability distribution of wind speed and direction.

Again, no attempt has been made to fit an appropriate distribution (see Fig. 39). However, it is clear that there is no major difference between the conditional and marginal wind direction distribution.

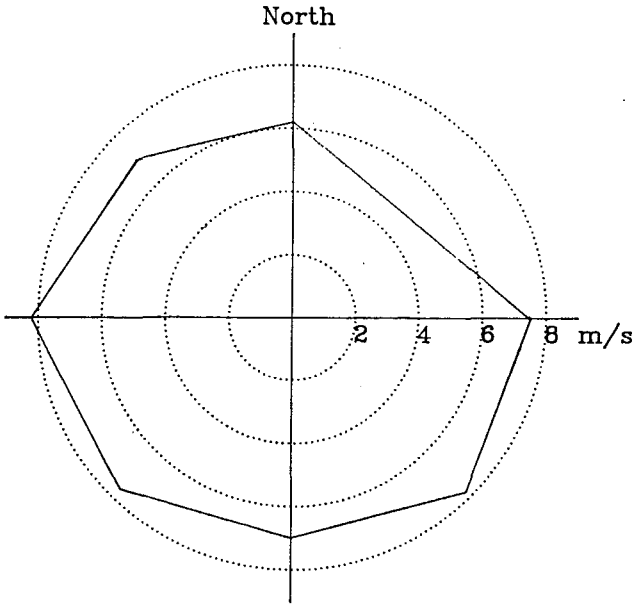

Figure 40: Mean wind speed for different wind directions. The wind speed is from the 72/76 m level and the direction is from the 117/123 m level on the Risø mast, 1958 – 1986.

6.4 Extraction of extreme data

The discrete time series of 10-min average of measured wind speed values was introduced in Section 6.2 (Fig. 29). As the major interest of the present study concerns extreme events (i.e. storm events), the bulk part of this series must be regarded as being of less informatory value when it comes to rare extreme events.

In the classic approach to frequency analysis of extreme events the so-called annual maximum (AM) series plays a significant role. The AM series conveys from the initial series by taking the largest value from each year. Another fundamental approach to the problem of extracting information on extreme events from the initial series is to introduce a threshold and then selecting only well-defined peak values above this threshold. This will create a new series, a so-called peak over threshold series (POT) where each value W_{max}^{peak} is separated in time (i.e. time steps) according to a random variable T which can be shown to follow a geometric distribution. Special attention should be drawn to the independence assumption when applying this method. A further description of this approach is given in Section 6.6. First, the AM-series will be treated in greater detail.

The creation of AM and POT-data from an initial series is illustrated in Fig. 42.

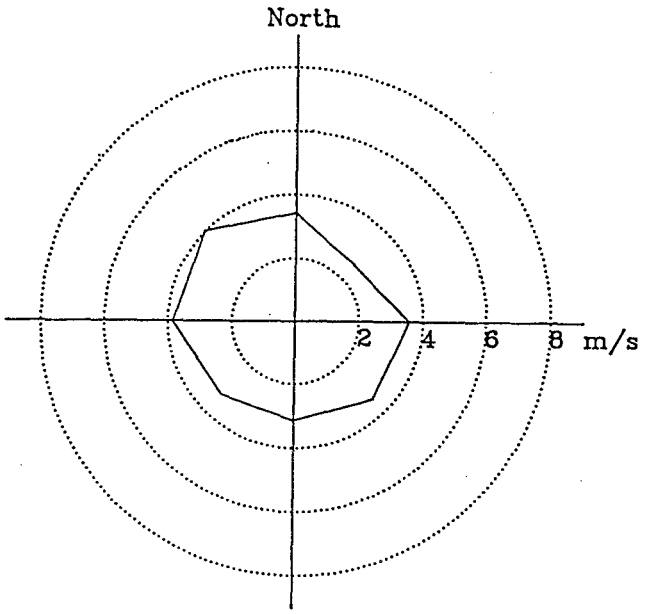

Figure 41: Standard deviation of wind speed for different wind directions. The wind speed is from the 72/76 m level, and the wind direction is from the 117/123 m level on the Risø mast, 1958–1986.

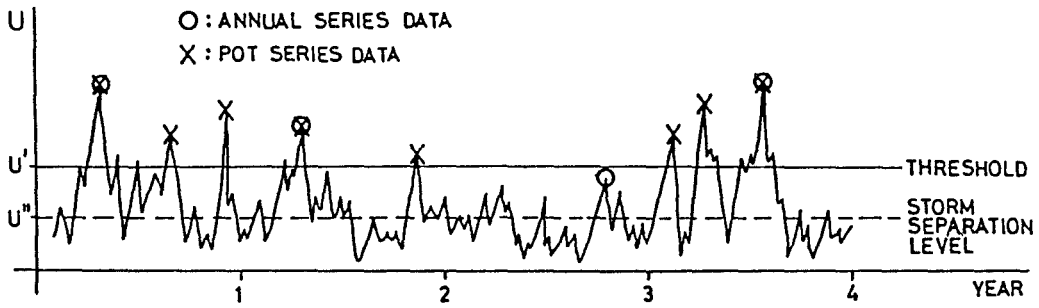

Figure 42: Schematic representation of data abstraction to constitute annual and partial series (POT-series).

6.5 Annual maximum (AM) series

6.5.1 Theory

In Section 6.3.2 the two-parameter Weibull distribution was used to represent the random variable of horizontal hourly 10-min average wind speeds (W). However, this distribution, in the following called the initial distribution, did not pass the goodness-of-fit test and can therefore not be regarded as the "true" representation of the random wind speed variable.

Concerning the theoretical derivation of a an appropriate extreme value distribution, this problem is overcome by assuming some basic characteristics of the initial distribution in which of course the tail behaviour is of main interest.

Taking n independent (!) values of $W_i, 1 \leq i \leq n$ which are supposed to be represented by the same initial distribution function $F(w)$, the *maximum* value of $W_i : X = \sup W_i, 1 \leq i \leq n$ will follow a distribution function given by:

$$F_X(x) = [F_W(x)]^n \quad . \tag{50}$$

This is a simple consequence of the *independence assumption* in a *binomial process.*

Not knowing the true initial distribution, we have to make some assumptions concerning the tail behaviour of the initial distribution.

a) As $F(x)$ and $F(w)$ approach infinity, they shall tend to the same asymptotic expression. This is known as the *stability postulate.*

b) The type of initial distribution must be established (Exponential, cauchy, etc.).

c) To check whether the inital distribution is censored upward, downward, or both (i.e. knowing some fundamental characteristics of the physical process).

Based on the assumption of an unbounded initial distribution of the Exponential type (Fisher an Tippett, 1928), (Gumbel, 1958) known as the EV1 or Gumbel distribution, the first asymptotic distribution is given by

$$F(x;\alpha,\beta) = e^{-e^{-\alpha(x-\beta)}} \quad . \tag{51}$$

Thence the probability density function is

$$f(x;\alpha,\beta) = \alpha e^{-\alpha(x-\beta)} \cdot e^{-e^{-\alpha(x-\beta)}} \tag{52}$$

where α and β are the distribution parameters.

Mean and variance are

$$E[x] = \beta + \frac{\gamma_E}{\alpha} = \beta + \frac{0.577}{\alpha} \tag{53}$$

where γ_E = Euler's constant,

$$\text{Var[x]} = \frac{\pi^2}{\alpha^2 \cdot 6} \tag{54}$$

and the coefficient of skewness and kurtosis are

$$C_s = \frac{\mu^3}{(\mu_2)^{3/2}} = 1.14 \tag{55}$$

$$C_k = \frac{\mu_4}{\mu_2^2} = 5.4 \tag{56}$$

where μ_i are the central moments of order i:

$$\begin{aligned} \mu_i &= \int_{-\infty}^{\infty} (x-\mu)^i f(x)\, dx \\ \mu &= E[x] = \beta + \frac{\gamma_E}{\alpha} \quad . \end{aligned} \tag{57}$$

Fisher and Tippett derived two other asymptotic probability distributions for the largest value of which only the second (EV2) will be mentioned here. If a random variable W_i is bounded to the left, and if the tail falls off according to a potential variation (i.e. a cauchy type initial distribution), then the distribution function of the largest value is given by

$$F(x;\alpha,\beta) = e^{-\left(\frac{x}{\beta}\right)^{-\alpha}} \quad 0 < x < \infty \quad ; \quad \alpha,\beta > 0 \tag{58}$$

where zero is the lower limit of the variable. Thence the probability density function is

$$f(x;\alpha,\beta) = \frac{\alpha}{\beta}\left(\frac{x}{\beta}\right)^{-(\alpha+1)} \cdot e^{-\left(\frac{x}{\beta}\right)^{-\alpha}} \quad . \tag{59}$$

For this distribution moments exist only for orders larger than the value of the α-parameter.

Mean and variance are

$$E[x] = \beta\Gamma\left(1 - \frac{1}{\alpha}\right) \quad \alpha > 1 \quad , \tag{60}$$

$$\mathrm{Var[x]} = \beta^2\left[\Gamma\left(1 - \frac{2}{\alpha}\right) - \Gamma^2\left(1 - \frac{1}{\alpha}\right)\right] \quad \alpha > 2 \quad . \tag{61}$$

An interesting relationship exists between the type 1 and type 2 distribution. If x is distributed according to the type 2 distribution with parameters α and β, then $\ln x$ is distributed according to type 1 with the parameters α and $\ln\beta$. This transformation could be utilized in connection with the extreme probability paper that exists for the type 1 distribution.

A general extreme-value distribution (GEV) exists, combining in one form the three asymptotic distributions. This distribution function was first introduced by Jenkinson (1955). The functional equation reads

$$F(x;\alpha,\beta,k) = e^{-[-(1-\alpha k(x-\beta))^{1/k}]} \quad . \tag{62}$$

α and β are scale and location parameters, respectively; k is a shape parameter determining which asymptotic distribution is represented. Type 1, 2, and 3 correspond to $k = 0, k < 0$ and $k > 0$, respectively. For $k > 0, x$ is bounded from the above by

$$x \leq \beta + \frac{1}{\alpha \cdot k} \quad k > 0 \quad , \tag{63}$$

and from below if $k < 0$

$$x \geq \beta + \frac{1}{\alpha \cdot k} \quad k < 0 \quad . \tag{64}$$

The mean of the distribution is

$$E[x] = \beta + \frac{1}{\alpha k}(1 - \Gamma(1 + k)) \quad . \tag{65}$$

A measure of dispersion is given in the next subsection.

Three different extreme value distributions have been presented for the largest value in a binomial process. The EV1-distribution has a shortcoming because it is unbounded to the left (i.e. assigning negative wind speed values). This problem is of course also inherited in the GEV-distribution. In addition, the lower and upper bound for $k < 0$ and $k > 0$, respectively, is not consistent with the physical phenomenon.

Nevertheless, both the EV1 and GEV-distribution have been widely used irrespective that all conditions are not fulfilled. Theoretically, the EV2-distribution is limited to a small number of initial distributions. In connection with the problem of parameter estimation due to lack of certain moments, this aspect has limited its application.

As a consequence of the longer tail of the EV2 compared to the EV1-distribution, the former will give higher extreme estimates. This was also found in a comparison between the two distributions, using the west sector data. None of the two distributions seemed to be superior to the other when it came to goodness-of-fit. The following analysis therefore only includes the EV1 and GEV-distributions.

Parameter estimation A fairly simple method is applied which has proven highly efficient for even small-size samples. The method is the probability-weighted moment (PWM) procedure. The generalized probability-weighted moment of a random variable x with a distribution function $F(x)$ (Greenwood et al., 1979) is given by

$$\mu_{\ell,m,n} = E\left[x^{\ell} F(x)^m \cdot (1 - F(x))^n\right] \tag{66}$$

where ℓ, m and n are real numbers.

For a practical approach a reduced form of Eq. (66) is preferable. Hosking et al. (1985) suggest the moments:

$$\mu_{1,m,0} = E\left[x \cdot F\left(x\right)^m\right] \qquad (m = 0, 1, 2 \ldots) \tag{67}$$

for which an unbiased estimator of Eq. (67) is given by Landwehr et al. (1979):

$$b_m = \frac{1}{n} \sum_{r=1}^{n} \frac{(r-1)(r-2)\cdot\cdots\cdot(r-m)}{(n-1)(n-2)\cdot\cdots\cdot(n-m)} \cdot x_r \tag{68}$$

where n is the number of observations and r the rank of the observation.

Several studies indicate (Arora et al., (1987), Kumar et al., (1987), Hosking et al.(1985)) that compared to other methods, the PWM-method yields little bias and only moderate variance on the parameter estimates for the EV1 and GEV-distributions, being superior even to the maximum likelihood method for small-size samples. The only drawback of the method is that it can be applied only to distributions expressed in the inverse form $x = x(F)$.

For the EV1-parameters the PWM-estimates are

$$\hat{\alpha}_1 = \frac{\ln 2}{2\, b_1 - b_o} \quad , \tag{69}$$

$$\hat{\beta}_1 = b_0 - \frac{0.577}{\hat{\alpha}_1} \quad . \tag{70}$$

For the GEV-parameters they are

$$\hat{\alpha} = \frac{\Gamma(1+\hat{k})(1-2^{-\hat{k}})}{(2b_1 - b_0)\hat{k}} \quad ; \tag{71}$$

$$\hat{\beta} = b_0 + \frac{1}{\hat{\alpha}\hat{k}}\left(\Gamma(1+\hat{k}) - 1\right) \quad ; \tag{72}$$

$$\hat{k} = 7.859 \cdot c + 2.9554\, c^2 \quad . \tag{73}$$

$$c = \frac{2b_1 - b_0}{3b_2 - b_0} - \frac{\ln 2}{\ln 3} \tag{74}$$

Equation (73) only holds for $-0.5 < k < 0.5$. An exact solution requires iterative methods for Eq. (75):

$$(3b_2 - b_0)/(2b_1 - b_0) = (1 - 3^{-\hat{k}})/(1 - 2^{-\hat{k}}) \quad . \tag{75}$$

$2b_1 - b_0$ can be interpreted as a measurement for the scale of the distribution (Hosking et al, 1985).

Extreme T-year events One of the primary tasks of a frequency analysis is the extrapolation of the selected probability model beyond existing data. A T-year event, x_T, is an event that will occur once each T-year on the average. The T-year period or recurrence interval is related to the probability distribution $F(x)$ through the following equation.

$$T = \frac{1}{1 - F(x)} \quad . \tag{76}$$

Using Eq. (76) and expressing the T-year event through the inverse form $x = x(F)$ of EV1 and GEV yields as follows.

T-year event for the EV1-distribution:

$$x_T^{EV1} = \frac{-\ln\ln\left(\frac{T}{T-1}\right)}{\alpha} + \beta \tag{77}$$

and for the GEV-distribution:

$$x_T^{GEV} = \frac{1 - \left(-\ln\left(1 - \frac{1}{T}\right)\right)^k}{k\alpha} + \beta \quad . \tag{78}$$

The T-year event is a random variable as a consequence of the uncertainty in the *parameter estimation* due to the limited size of the sample. Accordingly, confidence limits should be assigned to the estimates.

To illustrate the method of deriving standard errors on T-year estimates, the procedure is applied to the EV1-distribution. Assigning standard errors s_T on the T-year estimate x_T, the method of moment is utilized. Estimates of mean and variance through the method of moments is given by

$$E[x] \simeq \bar{x} = \beta + \frac{\gamma_E}{\alpha} \tag{79}$$

and

$$\mathrm{Var[x]} \simeq \mathrm{s_x^2} = \frac{\pi^2}{\alpha^2 \cdot 6} \quad . \tag{80}$$

$\bar{x}$ and s_x are the sample mean and standard deviation, respectively. Then, expressing x_T by $\bar{x}, s_x$ and a frequency factor k_T:

$$x_T = \bar{x} + k_T s_x \quad . \tag{81}$$

Using Eqs. (77), (79) and (80), the frequency factor is then found to be

$$k_T = \frac{\sqrt{6}}{\pi}\left(-\ln\ln\left(\frac{T}{T-1}\right)\right) - \frac{\gamma_E \cdot \sqrt{6}}{\pi} \quad . \tag{82}$$

The variance of x_T:

$$\mathrm{Var}[x_T] = \mathrm{Var}[\bar{x}] + k_T^2\,\mathrm{Var}[s_x] + 2\,k_T\,\mathrm{Cov}[\bar{x}, s_x] \tag{83}$$

can then be assessed by utilizing

$$\mathrm{Var}[\bar{x}] = \frac{\mu_2}{n}; \tag{84}$$

$$\mathrm{Cov}[\bar{x}, s_x] \simeq \frac{1}{n}\frac{\mu_3}{\sqrt{\mu_2}} \quad ; \tag{85}$$

$$\mathrm{Var}[s_x] \simeq \frac{1}{n}\frac{\mu_4 - \mu_2^2}{4\,\mu_2} \quad , \tag{86}$$

and introducing the coefficients of skewness (Eq.(55)) and kurtosis (Eq.(56)), Eq. (83) becomes

$$\mathrm{Var}[x_T] \simeq \frac{\mu_2}{n}[1 + k_T \cdot C_s + k_T^2 \frac{C_k - 1}{4}] \quad . \tag{87}$$

Inserting the numerical values for C_s and C_k and replacing μ_2 by the estimate s_x^2 leads to the following expression for the standard error:

$$s_T = \frac{s_x}{\sqrt{n}}[1 + 1.14\, k_T + 1.1\, k_T^2]^{1/2} \quad . \tag{88}$$

Kite (1970) has shown that the T-year estimate may be assumed normally distributed, and accordingly a 95% confidence interval is obtained by

$$x_T \pm 1.96\, s_T \quad . \tag{89}$$

6.5.2 Application

The annual maximum wind speed has been extracted from the record of transformed Risø data for the period 1958 – 1986 inclusive, but excluding the years 1973 and 1974 due to unreliable data (see Section 4.4). Thence a total number of 27 yearly maxima from eight different wind sectors are to be analysed plus 27 yearly wind-direction-independent maxima.

Adopting Gumbel's (1958) requirements for an appropriate plotting position, the Weibull plotting position is used

$$P = \frac{R}{n - 1} \tag{90}$$

where R is the rank of observation, n the total number of observations. The data are tested against the EV1 and GEV-distributions.

Data Presentation The ranked annual maximum data from the west sector are found in Table 14. Data from the other sections are found in Appendix C .

Table 14: Data covering the west sector for the Annual Maximum (AM) Model. Data from all other sectors are found in Appendix C .

Obs. Rank R	Plot. Pos. $P_r = \frac{r}{n+1}$	W Sector		
		Date	u_{max} m/s	Dir. °)
1	0.036	671017^{21}	29.3	274
2	0.071	811124^{20}	26.5	283
3	0.107	830118^{11}	26.3	290
4	0.143	750126^{09}	23.7	252
5	0.179	771224^{15}	22.8	268
6	0.214	680115^{18}	22.5	275
7	0.250	691029^{18}	22.4	275
8	0.286	801223^{19}	22.1	274
9	0.321	661218^{18}	22.0	265
10	0.357	760301^{13}	21.6	292
11	0.393	851106^{11}	21.5	248
12	0.429	711022^{21}	21.4	275
13	0.462	650105^{04}	21.1	276
14	0.500	610326^{22}	20.5	276
15	0.536	620212^{10}	20.5	266
16	0.571	821216^{08}	20.2	272
17	0.607	780911^{15}	19.8	272
18	0.643	580209^{14}	19.3	286
19	0.679	590220^{15}	18.8	276
20	0.731	700104^{07}	18.8	266
21	0.750	860516^{11}	18.3	248
22	0.786	791127^{04}	18.2	292
23	0.821	841021^{13}	18.1	275
24	0.857	720403^{13}	18.0	276
25	0.893	640126^{17}	17.9	266
26	0.929	600422^{16}	17.5	286
$n = 27$ (No. of years)	0.964	631012^{05}	17.0	276

Table 15: Annual Maximum (AM) Model

$b_0 = \bar{x} = \frac{1}{n}\sum_{i=1}^{n} x_i$	20.967
$b_1 = \frac{1}{n}\sum_{R}\frac{(R-1)}{(n-1)}x_R$	11.30
$b_2 = \frac{1}{n}\sum_{R}\frac{(R-1)(R-2)}{(n-1)(n-2)}x_R$	7.87
$s_x =$	2.977
Parameter Estimation, EV1-Distribution	
$\hat{\alpha}^1_{PWM} = \frac{\ln 2}{2b_1 - b_0}$	0.425
$\hat{\beta}^1_{PWM} = b_0 - \frac{0.577}{\hat{\alpha}_{PWM}}$	19.61
Parameter Estimation, GEV-Distribution	
$c = \frac{2b_1 - b_0}{3b_2 - b_0} - \frac{\ln 2}{\ln 3}$	-0.014
$\hat{k}_{PWM} = 7.859 \cdot c + 2.9554\, c^2$	-0.106
$\hat{\alpha}_{PWM} = \frac{\Gamma(1+\hat{k})(1-2^{-\hat{k}})}{(2b_1 - b_0)\hat{k}}$	0.473
$\hat{\beta}_{PWM} = b_0 + \frac{1}{\hat{\alpha}\cdot\hat{k}}(\Gamma(1+\hat{k}) - 1)$	19.51

Parameter estimation Applying the PWM method for estimating the parameters, Table 15 lists the estimates for the west sector for both the EV1 and the GEV distributions. Parameter estimates for other wind directions can be found in Appendix C .

Estimated T-year events Estimated T-year events are found in Tables 16 and 17 for the EV1 and GEV-disribution, respectively. A plot of the two models versus data from the west sector is found in Section 6.7.

Note: ***Data from the North-east sector should be regarded with caution due to a considerable tower shadow effect, see figs. 16 - 21 and comments in Appendix A.***

Table 16: Estimated T-Year events on the basis of the EV1-distribution. x_T: Estm. T-Year Event, s_T: Estm. Spread on T-Year Event.

EV1 - Distribution: $F(x;\alpha,\beta) = e^{-e-\alpha(x-\beta)}$ *PWM*-Parameter Estimates: $\hat{\alpha}_{PWM} = \frac{\ln 2}{2b_1 - b_0}$ $\hat{\beta}_{PWM} = b_0 - \frac{0.577}{\hat{\alpha}_{PWM}}$			Return Period (T-Year) 1.11	2	5	10	20	50	100
$y_T = -\ln\ln\frac{T}{T-1}$			-0.83	0.37	1.50	2.25	2.97	3.90	4.60
$\kappa_T = \frac{y_T}{1.28}$ - 0.45			-1.102	-0.161	0.722	1.308	1.870	2.597	3.144
$l_T = [1 + 1.14\kappa_T + 1.1\kappa_T^2]^{1/2}$			1.039	0.919	1.548	2.091	2.642	3.373	3.932
N Sector:	$\hat{\alpha}_{PWM} = 0.506$	$\hat{\beta}_{PWM} = 15.47$							
$s_x = 2.393$	$x_T = \frac{y_T}{\alpha} + \beta$		13.8	16.2	18.4	19.9	21.3	23.2	24.6
	$s_T = \frac{s_x}{\sqrt{n}} \cdot l_T$	68%	0.48	0.42	0.71	0.96	1.22	1.55	1.81
		95%	0.96	0.85	1.43	1.93	2.43	3.11	3.62
NE Sector:	$\hat{\alpha}_{PWM} = 0.439$	$\hat{\beta}_{PWM} = 13.05$							
$s_x = 3.116$	$x_T = \frac{y_T}{\alpha} + \beta$		11.2	13.9	16.5	18.2	19.8	21.9	23.5
	$s_T = \frac{s_x}{\sqrt{n}} \cdot l_T$	68%	0.62	0.55	0.93	1.25	1.58	2.02	2.36
		95%	1.25	1.10	1.86	2.51	3.17	4.05	4.72
E Sector:	$\hat{\alpha}_{PWM} = 0.592$	$\hat{\beta}_{PWM} = 17.26$							
$s_x = 2.021$	$x_T = \frac{y_T}{\alpha} + \beta$		15.9	17.9	19.8	21.1	22.3	23.9	25.0
	$s_T = \frac{s_x}{\sqrt{n}} \cdot l_T$	68%	0.40	0.36	0.60	0.81	1.03	1.31	1.53
		95%	0.81	0.72	1.20	1.63	2.06	2.62	3.06
SE Sector:	$\hat{\alpha}_{PWM} = 0.573$	$\hat{\beta}_{PWM} = 16.46$							
$s_x = 2.128$	$x_T = \frac{y_T}{\alpha} + \beta$		15.0	17.1	19.1	20.4	21.6	23.3	24.5
	$s_T = \frac{s_x}{\sqrt{n}} \cdot l_T$	68%	0.43	0.38	0.63	0.86	1.08	1.38	1.61
		95%	0.85	0.75	1.27	1.71	2.16	2.76	3.22
S Sector:	$\hat{\alpha}_{PWM} = 0.550$	$\hat{\beta}_{PWM} = 15.55$							
$s_x = 2.249$	$x_T = \frac{y_T}{\alpha} + \beta$		14.0	16.2	18.3	19.6	21.0	22.6	23.9
	$s_T = \frac{s_x}{\sqrt{n}} \cdot l_T$	68%	0.45	0.40	0.67	0.91	1.14	1.46	1.70
		95%	0.90	0.80	1.34	1.81	2.29	2.92	3.40
SW Sector:	$\hat{\alpha}_{PWM} = 0.542$	$\hat{\beta}_{PWM} = 18.02$							
$s_x = 2.259$	$x_T = \frac{y_T}{\alpha} + \beta$		16.5	18.7	20.8	22.2	23.5	25.2	26.5
	$s_T = \frac{s_x}{\sqrt{n}} \cdot l_T$	68%	0.45	0.40	0.67	0.91	1.15	1.47	1.71
		95%	0.90	0.30	1.35	1.82	2.30	2.93	3.42
W Sector:	$\hat{\alpha}_{PWM} = 0.425$	$\hat{\beta}_{PWM} = 19.61$							
$s_x = 2.977$	$x_T = \frac{y_T}{\alpha} + \beta$		17.7	20.5	23.1	24.9	26.6	28.8	30.4
	$s_T = \frac{s_x}{\sqrt{n}} \cdot l_T$	68%	0.60	0.53	0.89	1.20	1.51	1.93	2.25
		95%	1.20	1.06	1.78	2.40	3.02	3.86	4.50
NW Sector:	$\hat{\alpha}_{PWM} = 0.468$	$\hat{\beta}_{PWM} = 18.33$							
$s_x = 2.672$	$x_T = \frac{y_T}{\alpha} + \beta$		16.6	19.1	21.5	23.1	24.7	26.7	28.2
	$s_T = \frac{s_x}{\sqrt{n}} \cdot l_T$	68%	0.53	0.47	0.80	1.08	1.36	1.73	2.02
		95%	1.07	0.95	1.59	2.15	2.72	3.47	4.04
All Sectors:	$\hat{\alpha}_{PWM} = 0.499$	$\hat{\beta}_{PWM} = 20.75$							
$s_x = 2.568$	$x_T = \frac{y_T}{\alpha} + \beta$		19.1	21.5	23.8	25.3	26.7	28.6	30.0
	$s_T = \frac{s_x}{\sqrt{n}} \cdot l_T$	68%	0.51	0.45	0.77	1.03	1.31	1.67	1.94
		95%	1.03	0.91	1.53	2.07	2.61	3.33	3.89

Table 17: Estimated T-year events on the basis of the GEV-distribution.

GEV Distribution: $F(x) = e^{[-\{1-k\alpha(x-\beta)\}^{1/k}]}$ *PMW* Parameter Estimates $\hat{\alpha}_{PWM} = \frac{\Gamma(1+\hat{k})(1-2^{-\hat{k}})}{(2b_1-b_0)\cdot\hat{k}}$ $\hat{\beta}_{PWM} = b_0 + \frac{1}{\hat{\alpha}\cdot\hat{k}}\left(\Gamma(1-\hat{k})-1\right)$ $\hat{k}_{PWM} = 7.859\cdot c + 2.9554\cdot c^2$ $x_t = \frac{1-\left(-\ln\left(1-\frac{1}{T}\right)\right)^{\hat{k}}}{\hat{k}\hat{\alpha}} + \hat{\beta}$			Return Periods (T-Year)						
			1.11	2	5	10	20	50	100
N Sector:	$\hat{\alpha}_{PWM} = 0.450$ $\hat{k}_{PWM} = 0.145$	$\hat{\beta}_{PWM} = 15.61$ x_T	13.6	16.4	18.6	19.9	21.0	**22.2**	23.1
NE Sector:	$\hat{\alpha}_{PWM} = 0.490$ $\hat{k}_{PWM} = -0.107$	$\hat{\beta}_{PWM} = 12.91$ x_T	11.3	13.7	16.2	18.1	20.1	**22.8**	25.0
E Sector:	$\hat{\alpha}_{PWM} = 0.460$ $\hat{k}_{PWM} = 0.395$	$\hat{\beta}_{PWM} = 17.61$ x_T	15.5	18.4	20.1	20.9	21.4	**21.9**	22.2
SE Sector:	$\hat{\alpha}_{PWM} = 0.563$ $\hat{k}_{PWM} = 0.020$	$\hat{\beta}_{PWM} = 16.48$ x_T	15.0	17.1	19.1	20.4	21.6	**23.2**	24.3
S Sector:	$\hat{\alpha}_{PWM} = 0.464$ $\hat{k}_{PWM} = 0.228$	$\hat{\beta}_{PWM} = 15.76$ x_T	13.8	16.5	18.5	19.6	20.4	**21.3**	21.9
SW Sector:	$\hat{\alpha}_{PWM} = 0.442$ $\hat{k}_{PWM} = 0.285$	$\hat{\beta}_{PWM} = 18.29$ x_T	16.2	19.1	21.1	22.1	22.8	**23.6**	24.1
W Sector:	$\hat{\alpha}_{PWM} = 0.473$ $\hat{k}_{PWM} = -0.106$	$\hat{\beta}_{PWM} = 19.51$ x_T	17.8	20.3	23.0	24.9	26.9	**29.7**	32.0
NW Sector:	$\hat{\alpha}_{PWM} = 0.349$ $\hat{k}_{PWM} = 0.514$	$\hat{\beta}_{PWM} = 19.15$ x_T	16.2	20.1	22.2	23.0	23.5	**24.0**	24.2
All Sectors:	$\hat{\alpha}_{PWM} = 0.539$ $\hat{k}_{PWM} = -0.078$	$\hat{\beta}_{PWM} = 20.69$ x_T	19.2	21.4	23.6	25.3	26.9	**29.2**	31.0

Goodness-of-fit test Using the Kolmogorov-Smirnov test described in Section 6.3.1 with a confidence level of 95%, the property d_{crit} is calculated to be

$$d_{crit} = \frac{1.36}{\sqrt{27}} = 0.26 \quad .$$

In Fig. 43 the EV1-distribution is plotted with the cumulated frequencies of the west-sector observations. It appears that on the 95% confidence level the EV1-distribution provides an adequate representation. Following the same line of method for the other sectors for the GEV-representation, no argument is found for rejecting the two distributions.

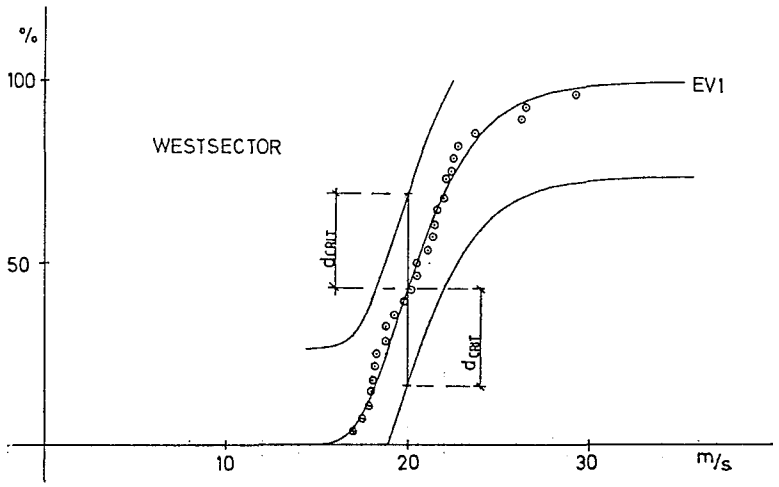

Figure 43: A Kolmogorov-Smirnov test of the EV1-distribution assumption for the west sector. ⊙ : observations.

Sensitivity analysis It could be of some interest to check the influence by the highest-ranking observations on the extreme T-year estimates. These observations are subjected to the same "data disease" as other data, but in addition they can be outliers, i.e. single data that have an abnormal or inconsistent appearance with the rest, making them particularly conspicuous.

As an example of an outlier, the highest-ranking observations from the north-east sector is an obvious choice. Withdrawing this observations (u = 25.6 m/s) and inserting the highest but one observation from the same year (u = 10.7 m/s) yields the following alteration in the EV1-distribution for the 50-year estimate, x_{50}:

$$x_{50} \quad (u = 10.7) \quad = \quad 19.6 \quad \text{m/s}$$
$$s_{50} \quad (u = 10.7) \quad = \quad 1.46 \quad \text{m/s}$$

compared to the original values:

$$x_{50} \quad (u = 25.6) \quad = \quad 21.9 \quad \text{m/s}$$
$$s_{50} \quad (u = 25.6) \quad = \quad 2.02 \quad \text{m/s}$$

which is a significant reduction. It might be an extreme example, but it emphasizes the importance of a careful data handling. In general, if an outlier is not proven to be erroneous it should be included in the sample, alternatively assigned to another recurrence if evidence approves it.

6.6 Peak-over-threshold (POT) series

6.6.1 Theory

As described in Section 6.4 there is another fundamental approach to the problem of extracting data with informative value in evaluating extreme events. Introducing a threshold w' and selecting only the peak value above this threshold, under appropriate conditions the extracted data will then constitute a partial duration series with independent data. This procedure is known as the peak over threshold (POT) method. Contrary to the AM-series where the maximum value from each year was selected (i.e. a binomial process), we are now dealing with a compound event of two random variables:

a) The period of time between successive threshold crossings or, expressed in another way, the number of events in a specified interval (N).

b) The magnitude of peak values exceeding the threshold (W).

If the condition is met that the peak exceedances have an *independent* occurrence at a *constant average rate*, the Poisson model will be a suitable representation of N. The Poisson density function is given by

$$f(n;\lambda) = \frac{\lambda^n}{n!} e^{-\lambda} \quad \lambda > 0 \quad n = 0, 1, 2, \ldots \tag{91}$$

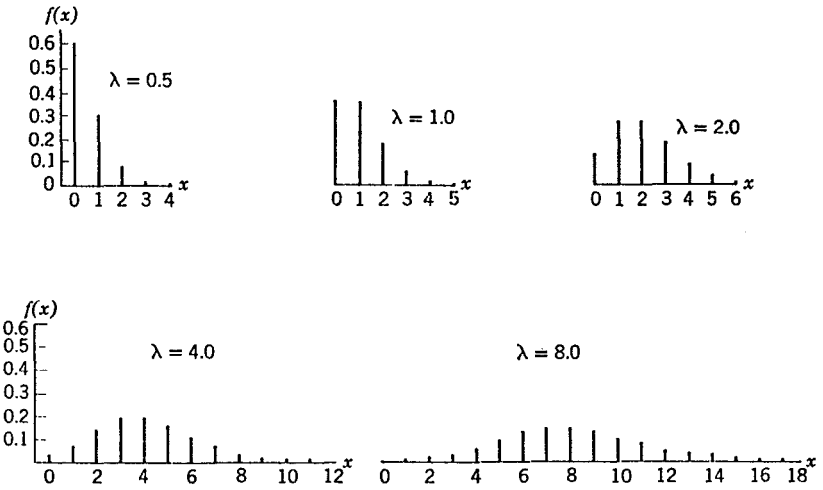

Figure 44: Poisson distributions with different values of λ.

where $f(n;\lambda)$ is the probability of exactly n events in a specified interval and the parameter λ is the rate of occurrence. The mean and variance are

$$E[n] = \lambda \quad , \tag{92}$$

$$\mathrm{Var[n]} = \lambda \quad . \tag{93}$$

Regarding λ as an intensity over a year with peak values larger than an arbitrary level, $w(w > w')$,the expected number of events in t years becomes

$$\lambda_w = \lambda t\,[1 - F(w)] \tag{94}$$

where $F(w)$ is the distribution function for W:

$$F(w) = P(W < w \mid W > w') \quad .$$

The maximum value of W in the period of t years denoted w_t corresponds to the probability of 0 events larger than w_t in t years. Inserting $n = 0$ and Eq. (94) in Eq. (91), the extreme value distribution for w_t becomes

$$F(w_t) = e^{-\lambda t[1-F(w)]} \quad . \tag{95}$$

In case of exponentially distributed peak exceedances:

$$F(w;\alpha) = 1 - \mathrm{e}^{-\frac{1}{\alpha}(w-w')} \tag{96}$$

where

w' is the threshold and α the distribution parameter. The mean and variance are

$$E[w] = \alpha + w' \quad , \tag{97}$$

$$\mathrm{Var}[w] = \alpha^2 \quad . \tag{98}$$

The extreme value distribution for w_t becomes

$$F(w_t) = e^{-\lambda t e^{-\frac{1}{\alpha}(w_t - w')}} \tag{99}$$

where λt is equal to the number of observations exceeding w' in t years.

Other distribution functions than (Eq. (96)) can be used in Eq. (95), see Rosbjerg (1987). However, this simple model, containing only one parameter (α), yields good results when it comes to parameter estimation which again has a positive influence on the standard error of the T-year estimate (s_{wT}).

Parameter estimation Maximum likelihood estimates of the λ and α-parameters are

$$\hat{\lambda} = \frac{n}{t} \tag{100}$$

where n is the total number of occurrences in t years and

$$\hat{\alpha} = \bar{x} - w' \tag{101}$$

where $\bar{x}$ is the sample mean for peek exceedances above the threshold w'.

Extreme T-year events Recalling the definition of the T-year event ($\lambda_w = 1$) and utilizing Eq. (94), w_T can be expressed by

$$w_T = F_w^{-1}\left(1 - \frac{1}{\lambda T}\right) \quad . \tag{102}$$

Using Eq. (96) and inserting $1 - \frac{1}{\lambda T}$ gives

$$w_T = w' + \alpha \ln(\lambda T) \tag{103}$$

which is the T-year event in a Poisson process with exponentially distributed peak exceedances. Confidence limits on the T-year estimate is obtained as follows. Using a Taylor expansion for Eq. (103) gives the approximation:

$$\mathrm{Var}[w_T] \simeq \left(\frac{\partial}{\partial\hat{\alpha}}\right)^2 \mathrm{Var}[\hat{\alpha}] + \left(\frac{\partial}{\partial\hat{\lambda}}\right)^2 \mathrm{Var}[\hat{\lambda}] + 2\left(\frac{\partial}{\partial\hat{\alpha}}\right)\left(\frac{\partial}{\partial\hat{\lambda}}\right) \mathrm{Cov}[\hat{\alpha},\hat{\lambda}] \ , \tag{104}$$

partial derivatives of Eq.(103) yield

$$\frac{\partial}{\partial\hat{\alpha}} = \ln(\lambda T) \quad ; \quad \frac{\partial}{\partial\hat{\lambda}} = \frac{\alpha}{\lambda} \quad ,$$

$$\mathrm{Var}[\hat{\alpha}] = \frac{\alpha^2}{\lambda \cdot T} \quad ; \quad \mathrm{Var}[\hat{\lambda}] = \frac{\lambda}{T}$$

and finally according to Cunnane (1973)

$$\mathrm{Cov}[\hat{\alpha},\hat{\lambda}] = 0 \quad .$$

By inserting these values in Eq. (104), the variance of the T-year can be expressed as

$$\mathrm{Var}[w_T] \simeq \frac{\alpha^2}{\lambda T}(1 + (\ln(\lambda T))^2) \tag{105}$$

or

$$s_{wT} \simeq \frac{\alpha}{\sqrt{\lambda T}} \sqrt{1 + (\ln(\lambda T))^2} \quad . \tag{106}$$

Assuming the T-year estimate to be normally distributed, the 95% confidence interval is obtained by

$$w_T \pm 1.96 \cdot s_{wT} \quad .$$

Note that there is a difference between assigning T-year events in a Poisson process (T_{pos}) and a binomial process (AM-series) (T_{ann}). The following relation between T_{pos} and T_{ann} is given by Rosbjerg (1977)

$$T_{pos} = -\frac{1}{\ln\left(1 - \frac{1}{T_{ann}}\right)} \quad . \tag{107}$$

In this context it should be mentioned that the binomial distribution

$$f(x; n, p) = \binom{n}{x} p^x (1-p)^{n-x} \tag{108}$$

approaches the Poisson distribution as n becomes arbitrarily large and p becomes arbitrarily small, i.e. np remains constant ($np \simeq \lambda$).

Application The problem of independent observations seems to be more obvious for the POT-method than for the AM-method (see Gumbel (1958) page 164). Therefore, it is important to engineer a method for the POT-procedure that secures surely independet observations.

Dealing with wind data it would e.g. not be recommendable to use more than one peak value for each low pressure. Furthermore, it is of vital importance to choose a sufficently high threshold. The method used in the present study is illustrated in Fig. 45 for the west sector.

Table 18: Applied thresholds with the corresponding number of peak exceedances for each wind direction sector.

Sector	Selected threshold w'	Total No. of obs. exceeding w'
N	12.5	120
NE	10.5	115
E	14.5	110
SE	14.5	104
S	13.5	122
SW	15.5	106
W	17.5	107
NW	16.5	114
All	18.5	142

Four clear peak exceedances belonging to the west sector are recognized. However, only the two highest exceedances from each pair (marked $\otimes$) are extracted while the lower peak exceedance clearly belongs to the same low pressure also responsible for the higher peak exceedance. Thresholds and a corresponding number of observations for the different wind direction sectors are found in Table 18.

Data presentation The 27 highest ranking observations from the west sector with corresponding Weibull plotting positions are found in Table 19. Data from other sectors are found in Appendix C .

Parameter estimation Maximum likelihood estimates of the parameters for the west sector in the Poisson model are found in Table 20. Parameter estimates for other wind direction sectors can be found in Appendix C .

Note: ***Data from the North-east sector should be regarded with caution due to a considerable tower shadow effect, see figs. 16 - 21 and comments in Appendix A.***

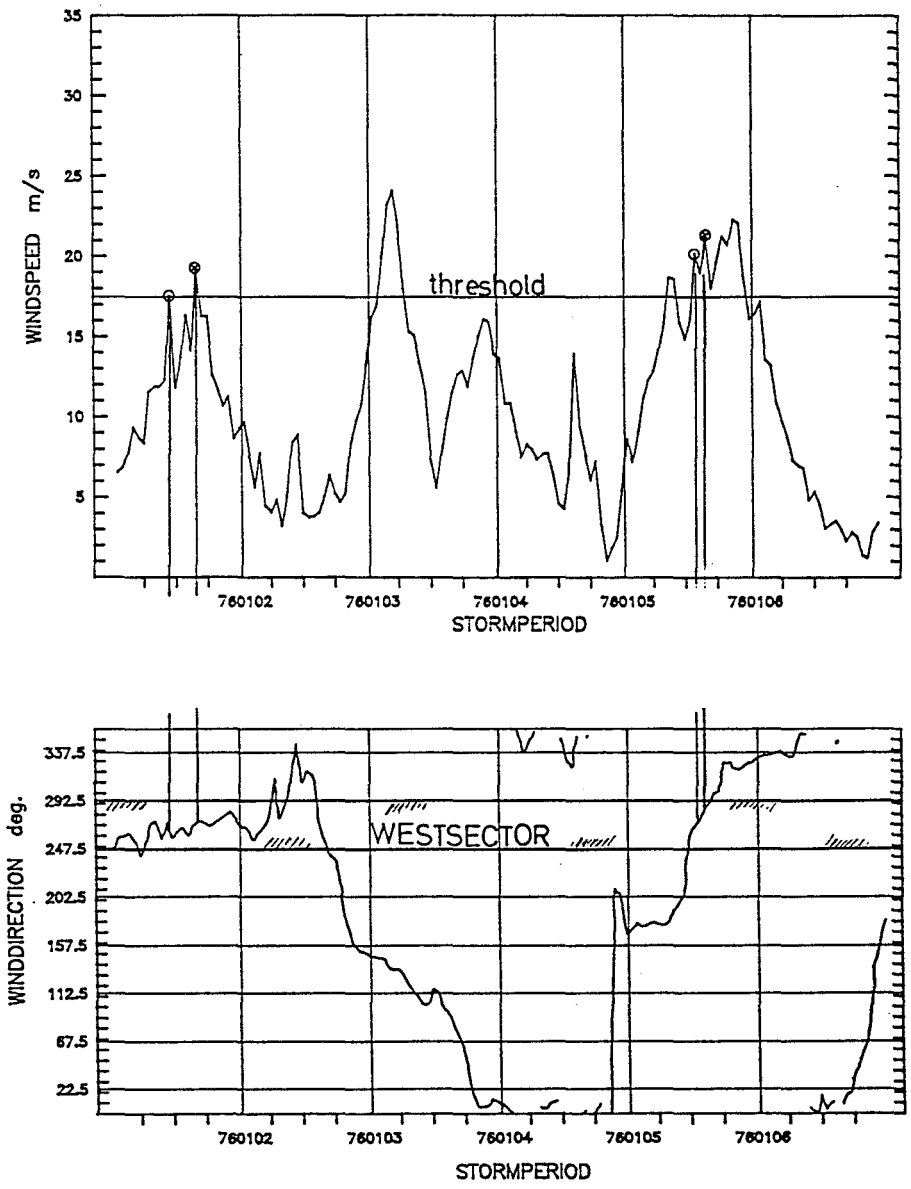

Figure 45: An example of how to extract independent peak exceedances in a storm event. ⊗: independent peak exceedances belonging to the west sector.

Table 19: Data from the Peak over Threshold (POT) Model (west sector).

Obs. Rank R	Plot. Pos. $P_r = \frac{r}{n+1}$	West Sector		
		Date	u_{max} m/s	Dir. °)
1	0.036	671017^{21}	29.3	274
2	0.071	811124^{20}	26.5	283
3	0.107	830118^{11}	26.3	290
4	0.143	811102^{12}	24.6	286
5	0.179	810101^{14}	24.2	292
6	0.214	811121^{04}	23.7	278
7	0.250	750126^{09}	23.7	252
8	0.286	670224^{01}	23.5	265
9	0.321	670420^{15}	22.8	265
10	0.357	771224^{15}	22.8	268
11	0.393	680115^{18}	22.5	275
12	0.429	691029^{18}	22.4	275
13	0.462	810208^{12}	22.3	290
14	0.500	690922^{12}	22.2	275
15	0.536	801223^{19}	22.1	274
16	0.571	661218^{18}	22.0	265
17	0.607	760301^{13}	21.6	292
18	0.643	851106^{11}	21.5	248
19	0.679	850906^{12}	21.5	286
20	0.731	760121^{07}	21.4	283
21	0.750	830129^{10}	21.4	282
22	0.786	711022^{21}	21.4	275
23	0.821	650105^{04}	21.1	276
24	0.857	670204^{12}	21.1	266
25	0.893	711116^{23}	20.8	266
26	0.929	710716^{13}	20.7	266
$n = 27$	0.964	670303^{19}	20.6	266

Table 20: Peaks over Threshold (POT) Model.

West Sector		
Threshold level	w':	17.5 m/s
No. of observations	N:	107
Mean	$\bar{x} =$	19.74
Standard deviation	$s_x =$	2.88
Parameter est.in the Poisson model:		
Intensity	$\hat{\lambda} = \frac{N}{n}; n = 27$	3.96
Mean above	$w' : \hat{\alpha} = \bar{x} - w'$	2.24

Estimated T-year events Estimated T-year events are found in Table 21. A plot of the Poisson model versus the 27 highest ranking observations (for the west sector) is found in Section 6.7.

Goodness-of-fit test The POT-model is a compound model consisting of two models:

1. A distribution model for the number of events in a specified interval, in this context assumed to be a Poisson distribution.
2. A distribution model for the peak exceedances, in this context assumed to be an exponential distribution.

Before examining the compound model it would therefore be appropriate to check the goodness-of-fit of the Poisson and exponential distributions.

The Poisson distribution
First the Kolmogorov-Smirnov test is implemented on the Poisson distribution . Note that this is not in accordance with the theory of the Kolmogorov-Smirnov test which, strictly speaking, should be applied only to continuous distributions. The test property D is found to be

$$D = \sup \mid F_N - F_{obs} \mid = 0.164$$

(see Table 22) which compared to the critial value

$$d_{crit} = \frac{1.36}{\sqrt{27}} = 0.262$$

will not lead to a rejection of the Poisson assumption on the 95% confidence level.

Another approach in testing the Poisson assumption could be to assign confidence bounds on λ (see Table 23).

Table 21: POT Model: Table of estimated T-Year events

Estimated T-Year Event $w_T = w' + \hat{\alpha}\ln(\hat{\lambda}\cdot T)$ Estimated Spread on T-Year Event $s_{wT} = \frac{\hat{\alpha}}{\sqrt{\hat{\lambda}T}}(1+(\ln\hat{\lambda}T)^2)^{1/2}$					Return Period (T-Year) 1.11	2	5	10	20	50	100
N Sector:	$\hat{\alpha}=2.32$	$\hat{\lambda}=4.44$	$w'=12.5$								
$N=120$			w_T		16.2	17.6	19.7	21.3	22.9	25.0	26.6
			s_{wT}	68%	0.40	0.51	0.69	0.83	0.97	1.16	1.31
				95%	0.80	1.02	1.38	1.66	1.95	2.33	2.62
NE Sector:	$\hat{\alpha}=1.87$	$\hat{\lambda}=4.26$	$w'=10.5$								
$N=115$			w_T		13.4	14.5	16.2	17.5	18.8	20.5	21.8
			s_{NT}	68%	0.32	0.41	0.56	0.68	0.79	0.95	1.07
				95%	0.65	0.83	1.12	1.35	1.59	1.90	2.14
E Sector:	$\hat{\alpha}=2.01$	$\hat{\lambda}=4.07$	$w'=14.5$								
$N=110$			w_T		17.5	18.7	20.6	22.0	23.3	25.2	26.6
			s_{wT}	68%	0.35	0.45	0.61	0.74	0.87	1.04	1.17
				95%	0.69	0.89	1.22	1.47	1.73	2.07	2.34
SE Sector:	$\hat{\alpha}=1.64$	$\hat{\lambda}=3.85$	$w'=14.5$								
$N=104$			w_T		16.9	17.9	19.4	20.5	21.6	23.1	24.3
			s_{wT}	68%	0.28	0.37	0.50	0.61	0.72	0.86	0.97
				95%	0.57	0.73	1.00	1.22	1.43	1.72	1.94
S Sector:	$\hat{\alpha}=1.68$	$\hat{\lambda}=4.52$	$w'=13.5$								
$N=122$			w_T		16.2	17.2	18.7	19.9	21.1	22.6	23.8
			s_{wT}	68%	0.29	0.37	0.50	0.60	0.70	0.84	0.94
				95%	0.58	0.74	1.00	1.20	1.40	1.68	1.88
SW Sector:	$\hat{\alpha}=2.06$	$\hat{\lambda}=3.93$	$w'=15.5$								
$N=106$			w_T		18.5	19.8	21.6	23.1	24.5	26.4	27.8
			s_{wT}	68%	0.36	0.46	0.63	0.76	0.90	1.08	1.21
				95%	0.71	0.92	1.26	1.52	1.79	2.15	2.42
W Sector:	$\hat{\alpha}=2.24$	$\hat{\lambda}=3.96$	$w'=17.5$								
$N=107$			w_T		20.8	22.1	24.2	25.7	27.3	29.4	30.9
			s_{wT}	68%	0.39	0.50	0.68	0.83	0.97	1.17	1.31
				95%	0.77	1.00	1.36	1.65	1.94	2.33	2.63
NW Sector:	$\hat{\alpha}=2.09$	$\hat{\lambda}=4.22$	$w'=16.5$								
$N=114$			w_T		19.7	21.0	22.9	24.3	25.8	27.7	29.1
			s_{wT}	68%	0.36	0.46	0.63	0.76	0.89	1.07	1.20
				95%	0.72	0.92	1.26	1.52	1.78	2.13	2.40
All:	$\hat{\alpha}=1.81$	$\hat{\lambda}=5.26$	$w'=18.5$								
$N=142$			w_T		21.7	22.8	24.4	25.7	26.9	28.6	29.8
			s_{wT}	68%	0.31	0.39	0.52	0.62	0.72	0.86	0.96
				95%	0.62	0.78	1.04	1.24	1.45	1.72	1.93

Table 22: The Poisson distribution versus cumulated observations from the west sector.

n	$f(n;\lambda) = \frac{3.96^n}{n!}e^{-3.96}$	$F_N = \sum_{i=0}^{n} \frac{3.96^n}{n!}e^{-3.96}$	n^{obs}	$F^{obs} = \sum \frac{n^{obs}}{27}$	$\mid F_N - F_{obs} \mid$
0	0.019	0.019	1	0.037	0.018
1	0.075	0.094	5	0.222	0.128
2	0.149	0.243	5	0.407	0.164
3	0.197	0.440	4	0.556	0.116
4	0.195	0.635	2	0.630	0.005
5	0.155	0.790	3	0.741	0.049
6	0.102	0.892	3	0.852	0.040
7	0.058	0.950	1	0.889	0.061
8	0.029	0.979	0	0.889	0.090
9	0.013	0.992	2	0.963	0.029
10	0.005	0.997	0	0.963	0.034
11	0.002	0.999	0	0.963	0.036
12	0.0006	0.9996	0	0.963	0.037
13	0.0002	0.9998	0	0.963	0.037
14	0.00005	0.99985	1	1.000	

In Table 24 the estimated intensities $\hat{\lambda}$ are listed as well as the corresponding maximum and minimum frequencies of (independent) threshold passages observed in the different wind direction sectors in a 12-month period. Comparing these values with the confidence bounds in Table 23 leads to a rejection of the estimated intensities $\hat{\lambda}$ as being the "true" values.

The somewhat doubtful acceptance of the Poisson distribution as an adequate representation is in keeping with the tendency of predominant strong low pressures in some years. This problem will be dealt with more thoroughly in Section 6.7.

The exponential distribution
The Kolmogorov-Smirnov test performed on the exponential distribution assumption in Table 25 shows no rejection on the 95% confidence level.

The exponential density distribution based on maximum likelihood estimates of the α-parameter is plotted together with the histogram of peak exceedances for the west sector in Fig. 46.

Table 23: 95% confidence level for λ in sampling from a Poisson distribution.

Obs. frequency	Corresponding 95% limits of the intensity λ	
	Lower band (97.5%)	Upper band (97.5%)
0	0.0000	3.69
1	0.0253	5.57
2	0.242	7.22
3	0.619	8.77
4	1.09	10.24
5	1.62	11.67
6	2.20	13.06
7	2.81	14.42
8	3.45	15.76
9	4.12	17.08
10	4.80	18.39
11	5.49	19.68
12	6.20	20.96
13	6.92	22.23
14	7.65	23.49
15	8.40	24.74
16	9.15	25.98
17	9.90	27.22
18	10.67	28.45
19	11.44	29.67
20	12.22	30.89

Table 24: Test of the estimated intensities, see Table 23.

Sector	Estimated intensities $\hat{\lambda}$	Obs. max. frequency in 12 months	Obs. min. frequency in 12 months	Rejecting $\hat{\lambda}$ on 95% confidence level
N	4.44	14	0	yes
NE	4.26	13	0	yes
E	4.07	9	0	yes
SE	3.85	11	0	yes
S	4.52	11	0	yes
SW	3.93	8	0	yes
W	3.96	14	0	yes
NW	4.22	12	0	yes
All	5.26	15	0	yes

Table 25: Test of exponential distributed peak exeedances above w' at the 95% confidence level.

Sector	No. of observ. N	Test property $D = \sup \mid \frac{i}{n+1} - F(w) \mid$	95% confidence level $d_{crit} = \frac{1.36}{\sqrt{N}}$	$D > d_{crit}$
N	120	0.061	0.124	no
NE	115	0.017	0.127	no
E	110	0.057	0.130	no
SE	104	0.032	0.133	no
S	122	0.047	0.123	no
SW	106	0.055	0.132	no
W	107	0.014	0.131	no
NW	114	0.051	0.127	no
All	142	0.023	0.114	no

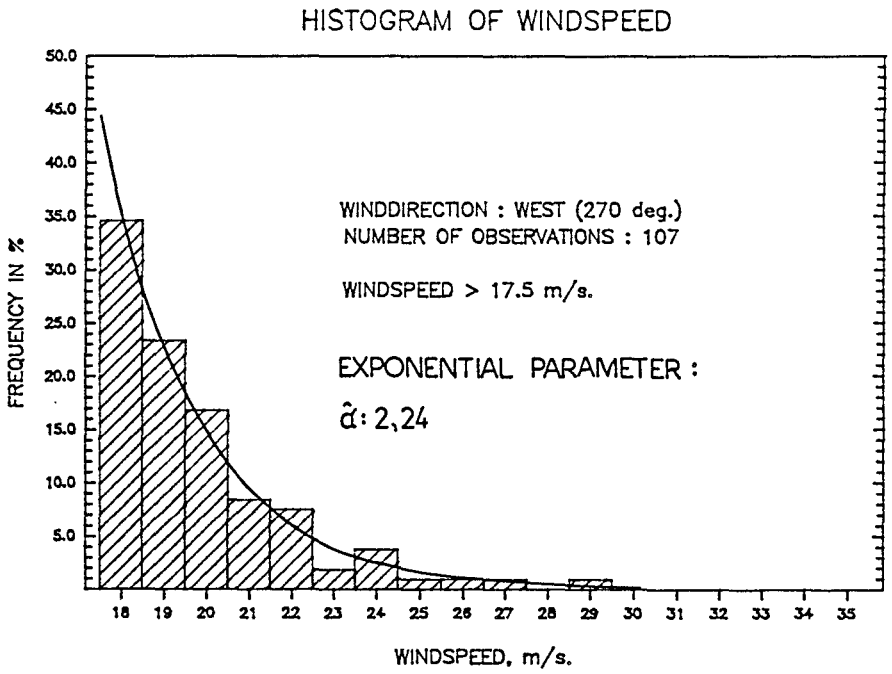

Figure 46: Histogram of wind speeds above the threshold $w' = 17.5$ m/s from the west sector. The same histogram are found in Appendix D for other wind direction sectors.

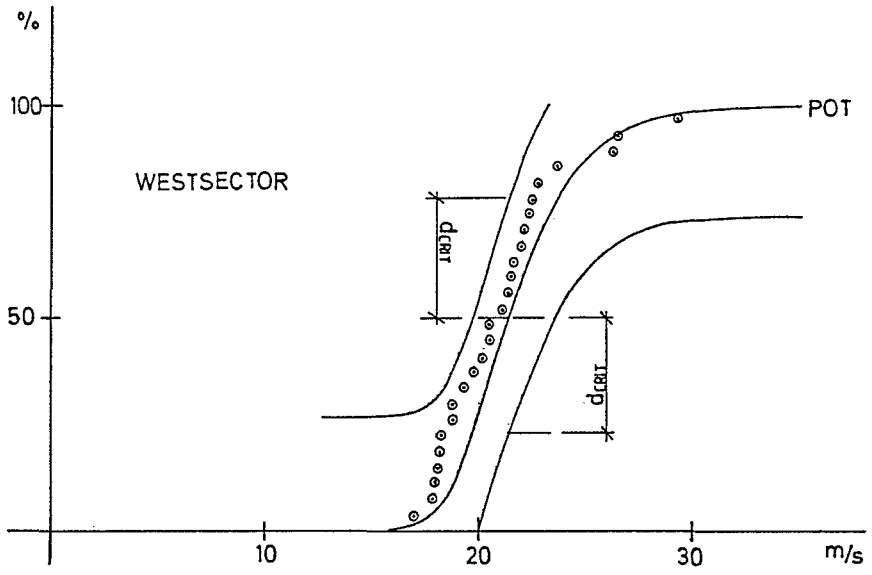

Figure 47: A Kolmogorov-Smirnow test of the compound POT model assumption for the west sector. ⊙: observations.

The compound POT-model
The extreme value distribution derived in Section 6.6.1 is valid for the *maximum peak exceedance in T-year*. Resembling the annual maximum series, the extreme value distribution for the *maximum peak exceedance in one year* becomes :

$$F(w_1) = e^{-\lambda e^{-\frac{1}{\alpha}(w_1 - w')}} \tag{109}$$

This distribution is tested against the annual maximum peak exceedance in Fig. 47 (not the 27 highest ranking observations).

The critcal value in the Kolmogorov-Smirnov test is:

$$d_{crit} = \frac{1.36}{\sqrt{26}} = 0.267$$

A performance of the same test for the other wind direction sectors does not lead to a rejection of the POT-model at the 95% confidence level.

Table 26: Mean estimates and standard errors on the 50-year event.

Sector	50-year event w_{50}			$\bar{w}_{50}$	$s_{w_{50}}$
	EV1	GEV	POT[1]		
N	23.2	22.2	25.0	23.5	1.42
NE	21.9	22.8	20.5	21.8	1.14
E	23.9	21.9	25.2	23.7	1.63
SE	23.3	23.2	23.1	23.2	0.08
S	22.6	21.3	22.6	22.2	0.75
SW	25.2	23.6	26.4	25.1	1.39
W	28.8	29.7	29.4	29.3	0.47
NW	26.7	24.0	27.7	26.1	1.92
All	28.6	29.2	28.6	28.8	0.33

[1]Note that according to Eq. (107) there is a difference between assigning a T-year event in a Poisson process and in an annual maximum process. Regarding the 50-year return period, the difference is insignificant.

6.7 Evaluation

The EV1 and GEV-distributions representing the models for the AM-series are plotted in Fig. 48 together with annual maximum observations from the west sector, marked $\odot$. In the same figure, the POT model is plotted together with the 27 highest ranking observations from the west sector, marked $\times$. The POT model is plotted according to the stipulated return periods from Table 21 in Section 6.6.2. Furthermore, 97.5% upper and lower confidence bounds are plotted on the EV1 and Poisson models. Despite a few outliers in the upper tail of the distributions (dealt with in Section 6.5.2), the models seem to give a good representation of the data. Note the narrow 95% confidence band on the POT model compared with the more wide band on the EV1-distribution. Primarily, this is a consequence of the larger number of observations used in the POT model. Having introduced an error band due to uncertainty in the parameter estimation within the different models, it is natural to check the variability between the models in the 50-year estimates.

In Table 26 mean estimates $\bar{w}_{50}$ and spread $s_{w_{50}}$ are found on the 50-year event for the different wind direction sectors.

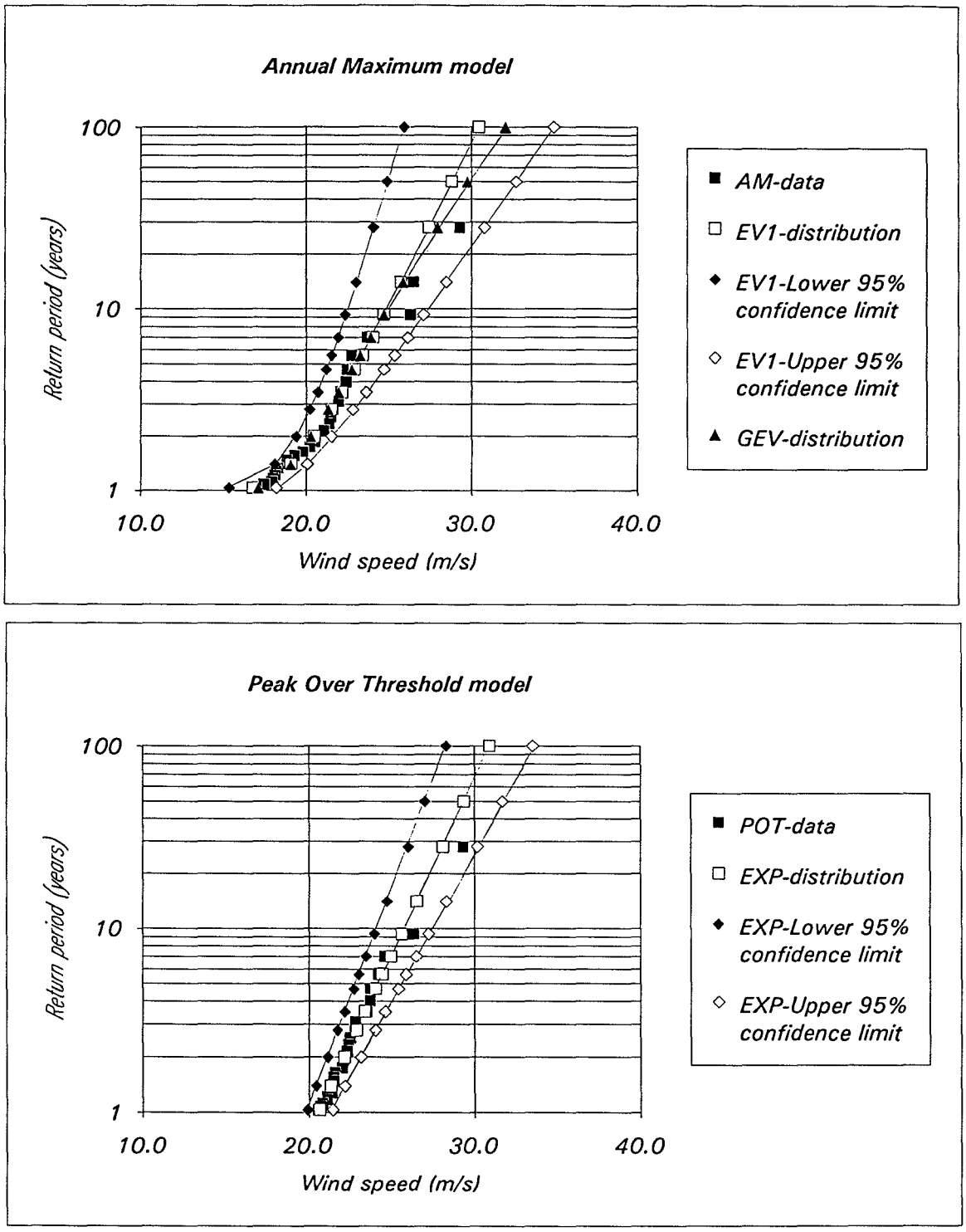

Figure 48: The EV1, GEV, and POT models versus data from the west sector. The same representation are found in Appendix E for the other wind direction sectors.

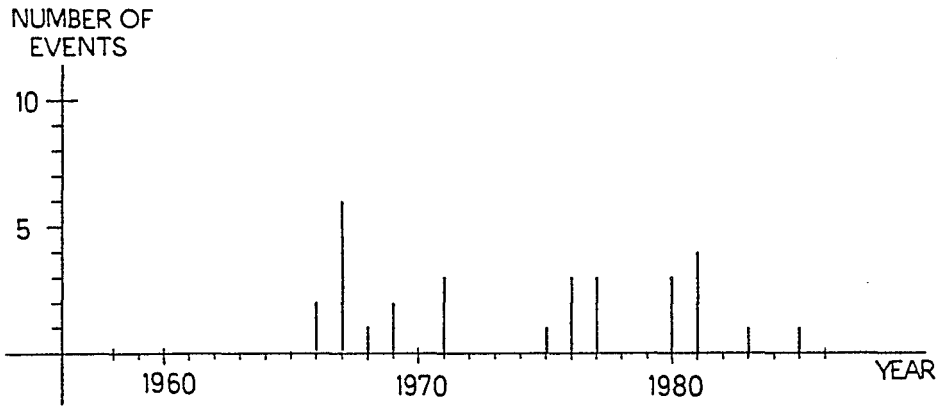

Figure 49: Occurrence of storms ($u > 9$ Beaufort) in the period 1958 – 1986.

Assuming the mean estimate to be normally distributed, the 95% confidence interval is given by

$$\bar{w}_{50} \pm 1.96\ s_{w50} \quad . \tag{110}$$

As to the Poisson process model one of the fundamental assumptions is that the events occur at a *constant rate* over a specified interval. The first problem in this connection is the well-known fact that strong low pressures (responsible for storm events) pass Denmark more frequently in the winter period (October – March). Another more serious problem in this respect is that strong low pressures seem to accumulate in some years. Whether this occurs in some periodic manner is difficult to tell because of the relatively short recording period at hand.

In Fig. 49 the occurrence of the 30 worst storms in the period 1958 – 1986 are plotted on a time scale clearly rejecting the constant rate assumption.

An updated record of sea floods through history (1200 AC →) supports this picture (I.G. Jensen, not yet published).

A further investigation of this problem should be performed, eventually leading to a modified POT-model with this knowledge included.

Previous work on the climate of strong winds in Denmark (M. Jensen et al., 1970) was based on measurements of the velocity pressure

$$q = \frac{1}{2}\rho \cdot u^2 \tag{111}$$

where ρ is the air density ($\rho \simeq 1.28$ kg/m^3). A measuring station was placed at Thorsminde on the west coast of Jutland, to the west exposed to the North Sea. Transforming the 50-year event estimate from this station to conditions similar to those applied in this study (10-min mean, 10 m above sea level) yields

$$\hat{w}_{50} \simeq 30.3\,\mathrm{m/s}$$

which equals the 97.5% upper confidence bound on the mean estimate for the 50-year event in the west sector

$$\hat{w}_{50}^{max}(W) = 29.3 + 1.96 \times 0.47 = 30.3\,\mathrm{m/s} \quad .$$

The Danish code for wind loads on structures (DS 410 *Last på konstruktioner*) prescribes a basic wind speed of

$$w_b = 27\,\mathrm{m/s}$$

relating to a 10-min average wind speed 10 m above open farmland ($z_0 = 0.05$) with a recurrence interval of 50 years.

Transforming this wind speed to a basic wind speed over smooth terrain ($z_0 = 0.01$) and applying the roughness transformation $k_t = 0.19(z_0/z_{0r})^{0.078}$, $z_{0r} = 0.05$ yields

$$w_b^{0.01} \simeq 27 \times \frac{0.19}{0.17} = 30.2\,\mathrm{m/s} \quad .$$

The roughness classification for smooth terrain ($z_0 = 0.01$) should however not be assigned to open-water conditions. For wind speeds of 30 m/s, the roughness length in open-water is closer to the value of $z_0 \approx 0.003$., implying a wind speed of

$$w_b^{0.003} \approx 27 \times \frac{0.19}{0.153} = 33.5\,\mathrm{m/s}$$

which is significantly higher than the stipulated $\hat{w}_{50}^{max}(W)$.

Table 27: Mean estimates $\bar{w}_{50}(\theta)/\bar{w}_{50}(W)$ compared to basic wind speeds from various wind directions $w_b(\theta)/w_b(NNW)$ according to the recommendations of SBI-Anvisning 158.

Sector	$\bar{w}_{50}(\theta)/\bar{w}_{50}(W)$	$w_b(\theta)/w_b(WNW)$
N	0.80	
NNE		0.79
NE	0.74	
ENE		0.74
E	0.81	
ESE		0.81
SE	0.79	
SSE		0.76
S	0.76	
SSW		0.82
SW	0.86	
WSW		0.91
W	1.00	
WNW		1.00
NW	0.89	
NNW		0.92
All	0.98	

Finally, the results should be related to a new "Instructions for wind loads on buildings and structures" (SBI anvisning 158, Hansen and Dyrbye, 1989). The main conclusions in these instructions regarding dimensioning 10-min averages of mean wind velocity are

a) Severe storms have approximately the same strength within the boundaries of Denmark.

b) Storms from the west are predominant.

c) The basic wind speed w_b is a function of wind direction ($w_b(\theta)$), assigning the basic wind speed of $w_b(WNW) = 27$ m/s to the WNW wind direction.

The instructions set up a table for the basic wind speed from other wind directions related to $w_b(WNW)$. These values are compared to the mean estimates $\bar{w}_{50}(\theta)$ related to $\bar{w}_{50}(W)$ in the present study, see Table 27.

7 Verification

In order to verify the results of the present study it is important to recall the procedures of the physical modelling.

Reviewing Sections 3 and 5 of this report it is clear that the compound model is based on a complexity of submodels and assumptions. It is, however, not within the scope of this study to verify all constituting models and assumptions, but rather to illustrate the possibilities of the method presented.

For this purpose a comparison with storm data from the North Sea was found suitable while good correlation with the Risø storm data would give a significant support to the applicability of the method, especially bearing in mind the distance of approximately 500 km between the two locations.

Unfortunately, due to a poor quality of the Dan/Gorm field data, it was not possible (not considered worthwhile) to perform actual statistics on these data.

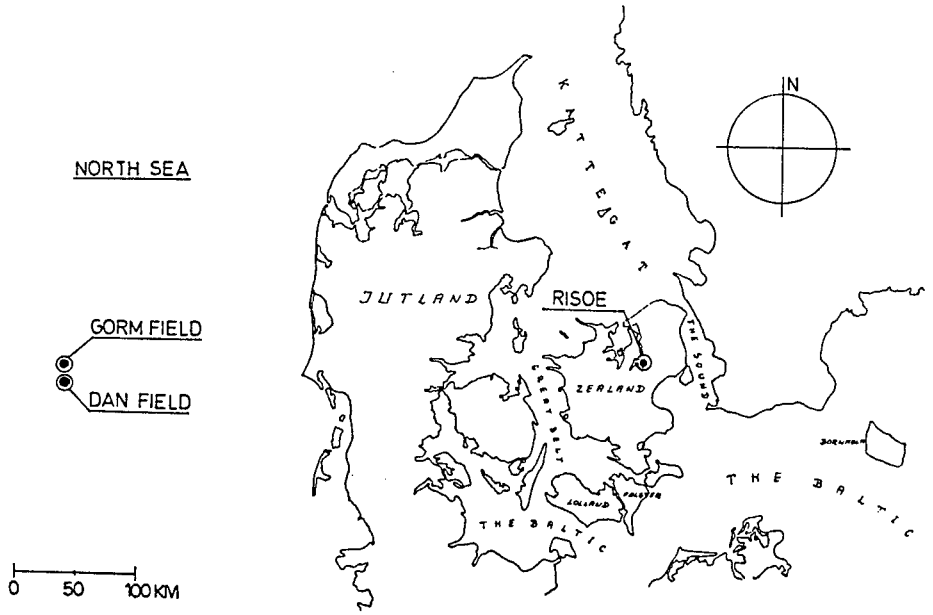

Figure 50: Location of the Dan and Gorm fields.

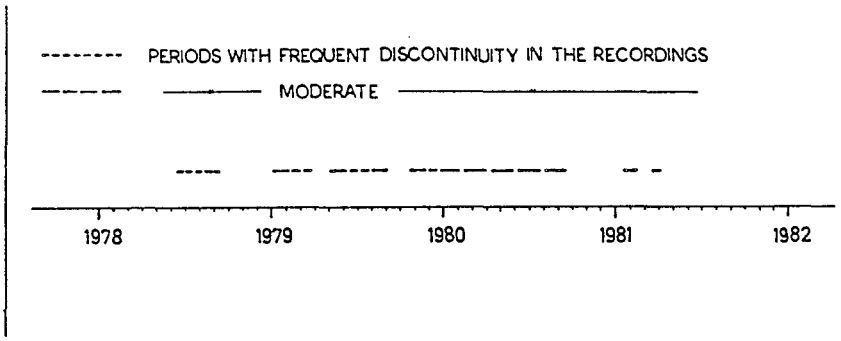

Figure 51: Periods with wind speed recording from the Dan field.

7.1 Presentation of North Sea wind data

As a consequence of the intensive offshore industry in the North Sea, a considerable amount of environmental monitoring has been going on. Many of the platforms are equipped with wind gauges and other meteorological gear, creating a possibility of sampling reliable wind data at sea contrary to traditional ship observations. It seems, however, that both the placing and updating of the anemometers are performed in a somewhat careless manner, causing extensive lee effects and fall-outs of the recordings.

Regarding the Danish sector, wind data recordings started at the Dan field (see Fig. 50) in the middle of 1978 and was running in a somewhat abrupt way until the beginning of 1981, see Fig. 51. The equipment was moved to the Gorm field (Figs. 53 and 54) where the recordings were resumed at the end of 1981.

The recording is still running even though the original data storing procedure at the Danish Hydraulic Institute (DHI) is now abandoned.

Recording at the Dan field
The recording covers the period from the middle of 1978 until the beginning of 1981. Note the frequent fall-outs, as seen in Fig. 51.

The wind data are recorded as 10-min averages of wind speed and logged every 20-min. The anemometer is placed on the bridge between the processing platform and flare tower, approximately 27 m above mean sea level, seeFig. 52. A considerable interference with the platform structure should be expeced from wind directions between 180 and 250 degrees and between 35 and 50 degrees.

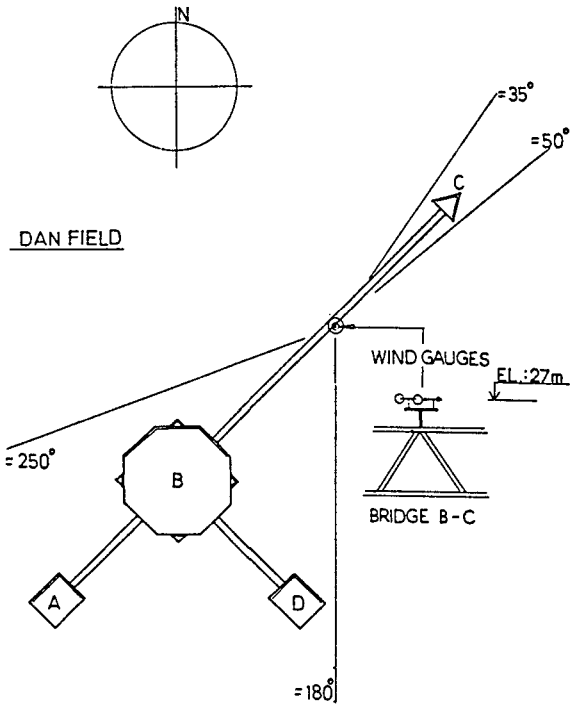

Figure 52: Location plan of the Dan field. Wind direction sectors with possible turbulence and lee effects are indicated.

A: Wellhead platform
B: Processing platform
C: Flare tower
D: Wellhead platform

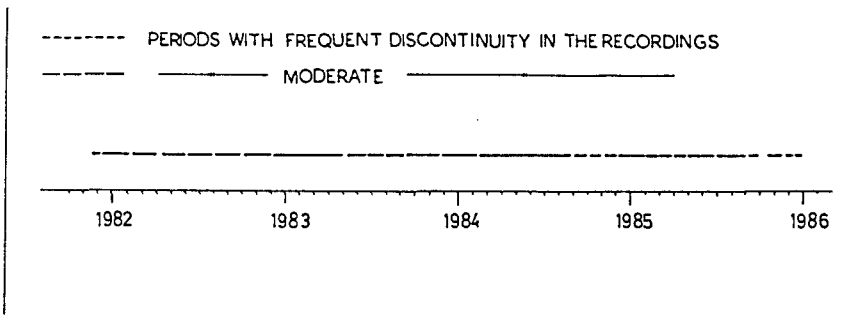

Figure 53: Periods of wind speed recording at the Gorm field.

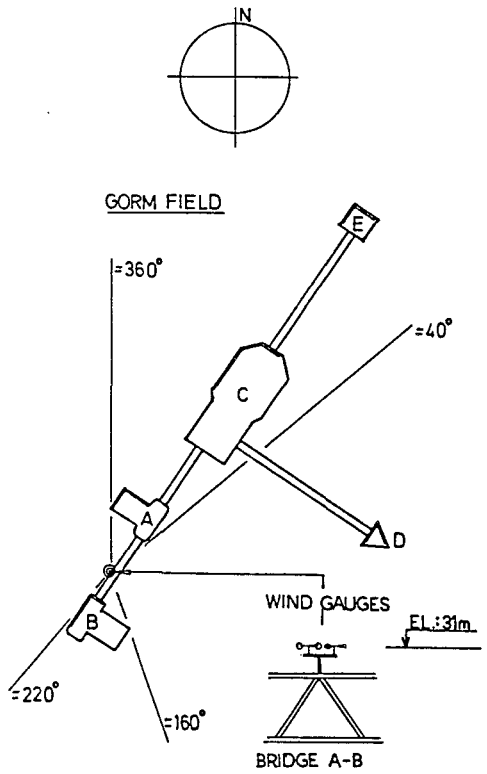

Figure 54: Location plan of the Gorm field. Wind direction sectors with possible turbulence and lee effects are indicated.

A: Wellhead platform
B: Wellhead platform
C: Processing platform
D: Flare tower
E: Riser platform

Recording at the Gorm field
The recording covers a period from the end of 1981 until 1986, see Fig. 53.

Wind data are recorded as 10-min average wind speeds logged every 5 min. Only 10-min averages of wind speed every full hour are used in the present study. The anemometer is placed on the bridge between wellhead platforms A and B, approximately 31 m above mean sea level, see Fig. 54. Disturbance of the wind field caused by the platform modules should be expected from wind directions between 0 and 40 degress and between 160 and 220 degrees.

7.2 Comparison with extrapolated storm data from Risø

A selection of storm events for comparison is made on the following criteria:

a) Storm severity

b) Principal storm direction.

As to the first criterion, the seven highest ranking storms covering the period from 1979 until 1986 were extracted from the extrapolated Risø data. For the comparison study Risø data were extrapolated to 30 m above mean sea level. Unfortunately, only the two highest ranking storms were represented in the Dan/Gorm field data, the remaining five periods were fall-outs. The two storms came from west/northwesterly directions implying reasonable undisturbed recordings from the Dan/Gorm fields. They are plotted in Figs. 55 and 56 revealing a good correlation between the two data set with a clear span of time between comparable events.

It is of interest to see whether this good correlation prevails when the storm is not quite as severe and from a another wind direction. Accordingly, an easterly storm has been selected for comparison. From this wind direction the wind gauges should be reasonably unaffected by the platform structures. Again a picture is drawn of a correlated process, now with an inverse span of time between comparable events. However, there is a significant difference in the severity of the "storm" at the two locations, indicating an influence of local character; perhaps a strong difference in air-sea temperature (Hasse, 1974).

Finally, a south/south-westerly storm is selected to illustrate the interference of the platform structure on the wind field, see Fig. 58. A very clear lee effect is seen when the wind direction approaches the southerly direction.

Summarizing the comparison study:

1. Good correlation betweeen the extrapolated Risø and North Sea data is achieved for severe westerly and northwesterly storms.

2. A significant lower correlation is found for more moderate storms and storms from other wind directions.

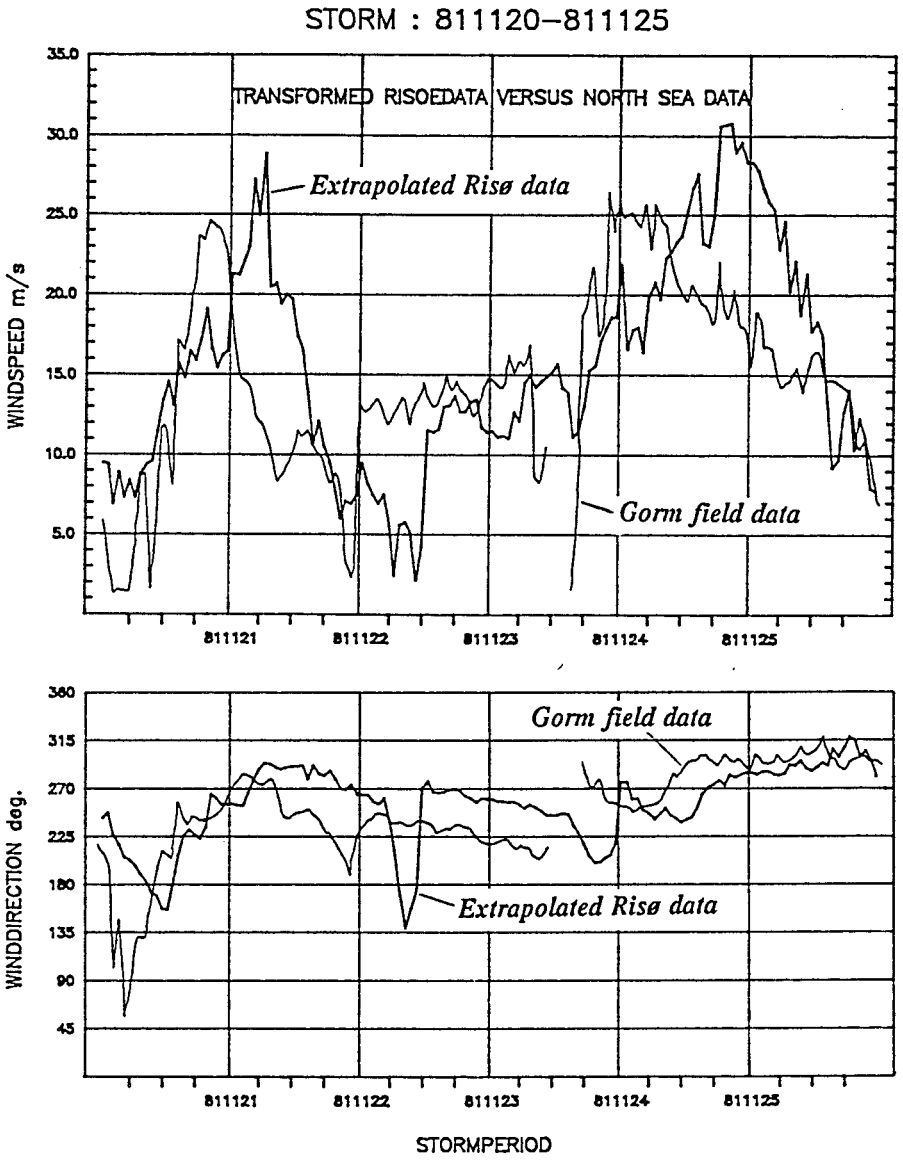

Figure 55: Simultaneous recordings of the highest ranking storm in the period 1979 – 1986.

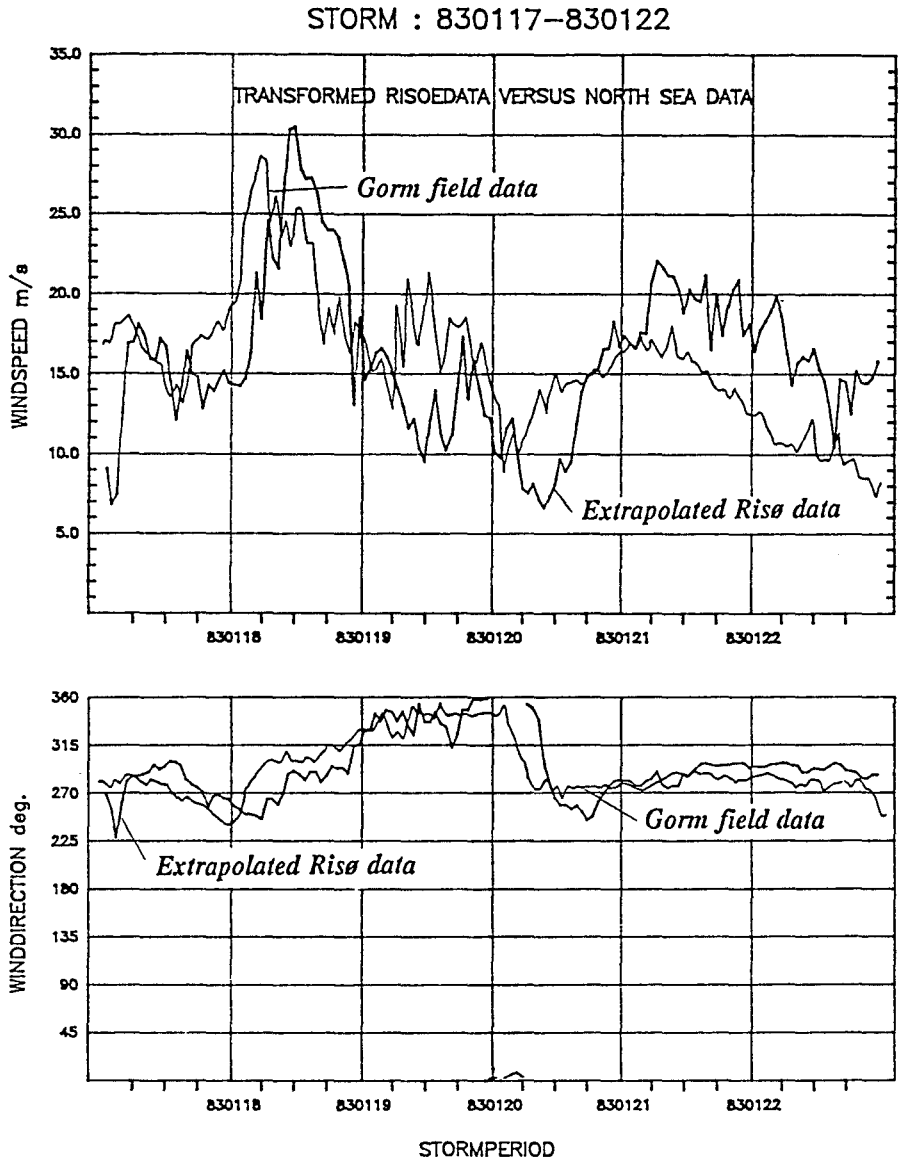

Figure 56: Simultaneous recordings of the highest ranking but one storm in the period 1979 – 1986.

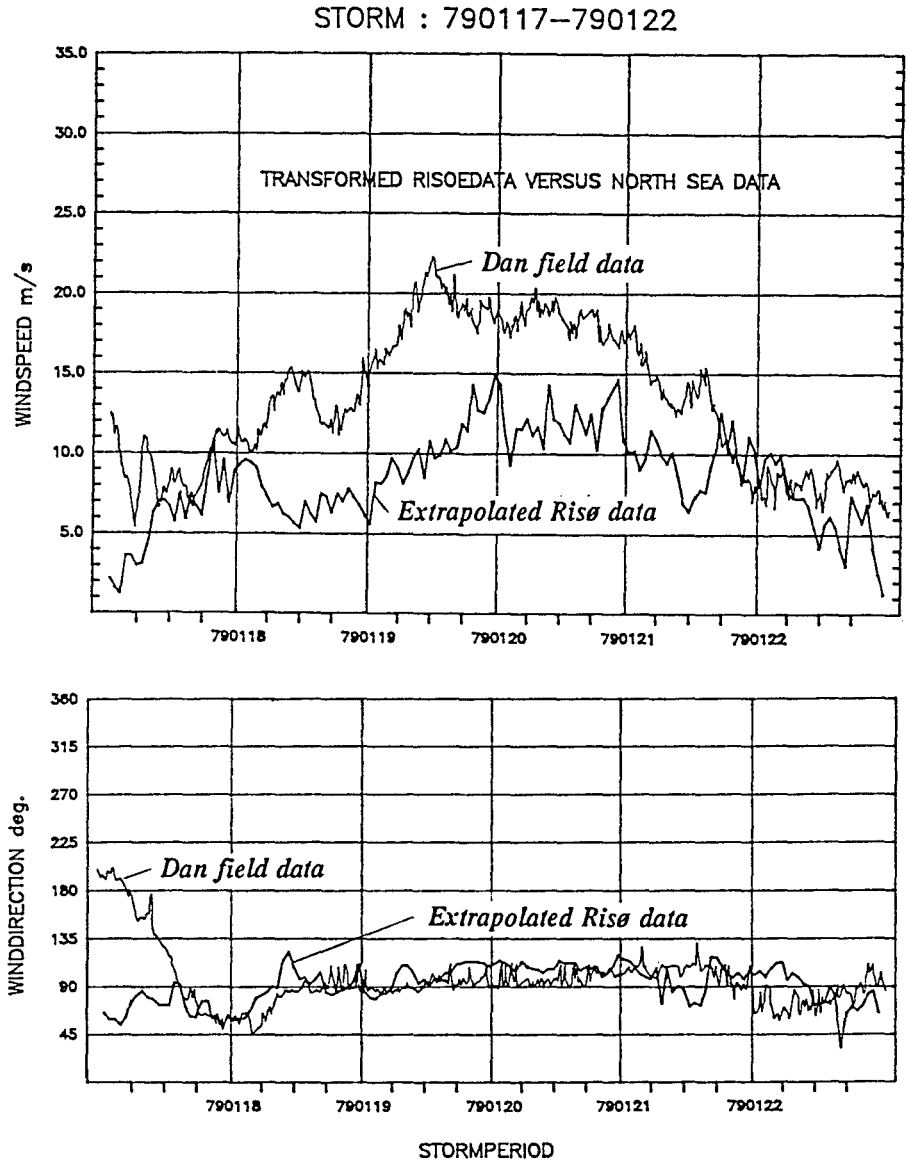

Figure 57: Simultaneous recordings of an easterly storm.

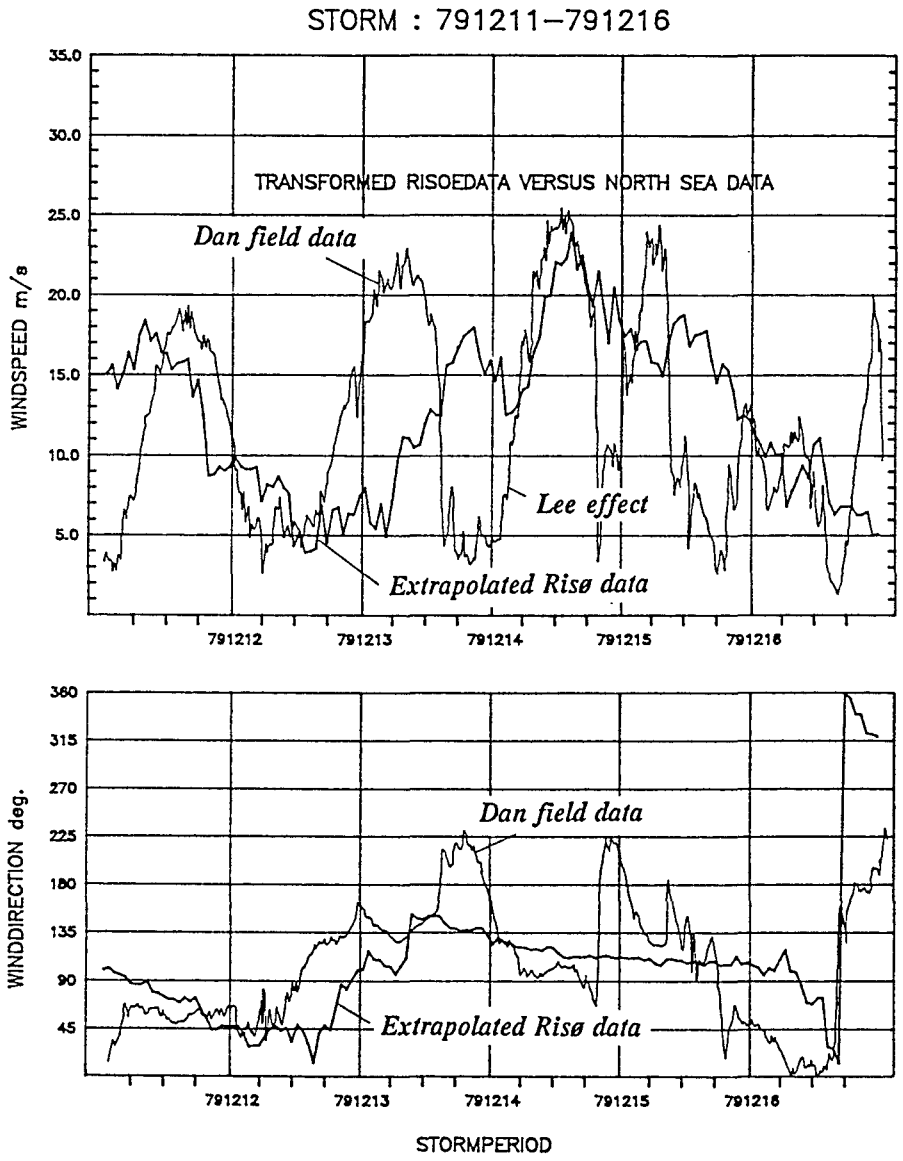

Figure 58: Simultaneous recordings of an south/southeasterly storm.

8 Conclusion

This chapter is a summary of the findings in the previous chapters. Finally, some general comments and recommendations are given for future work.

3 The terrain description model

Forming the basis of the extrapolation procedure, the terrain description model is an important part of the compound model. Unfortunately, the very complex terrain surrounding the Risø site invokes a great deal of subjectivity into the model. One of the problems has been to assign roughness lengths to a terrain, the appearance of which has clearly changed through a period of 30 years. When comparing the wind velocity profile based on the roughness change model with measured mean velocity profiles, an acceptable resemblance with a difference less than 5% seems to appear.

Corrections of the wind velocity profile through the shelter and orographic models seem appropriate for the lower recording levels (< 40 m) but will have no effect on measurements from the 72/76 m level.

4 Data material

The data from the 72/76 m recording level are found to be of a reliable and homogeneous quality.

There is an obvious advantage using the Risø data as the wind velocity is measured simultaneously at different recording levels. This makes it possible to identify erroneous data or periods with strong winds if e.g. the 72/76 m recording level is out of order. Furthermore, the long period of recording (31 years) provides a comparatively better basis than former studies of the subject (M. Jensen et al., 1970) (seven years) when it comes to statistical inference.

5 Extrapolation of storm data

The performance of the extrapolation procedure has not been checked even though it is apparent that several of the premises for the wind atlas method are not met under extreme wind conditions. This is primarily because the vertical extrapolation method *over land* is tightly related to the terrain description model. In order to evaluate the extrapolation method for extreme

wind conditions, it would be feasible to compare extreme wind measurements in open water with free wind computations at the same location.

As an example this verification procedure could include a modified surface layer profile which took into account the air-sea temperature difference. The available data from the North Sea are, however, not found to be of a sufficiently reliable quality for such a comparison study.

The basic assumption of neutral stability under high wind speeds is verified through analysing temperature profiles in the surface layer during storm periods. Neutral stability was prevailing in approximately 90% of the situations with a significant tendency of neutral stability during the peak periods of the storm.

As to horizontal extrapolation no evidence is found for a geographical variation of the extreme wind speed within Danish territory.

6 Application of statistical models

Two fundamental methods in frequency analysis are applied. The POT-method which makes use of a comparatively large number of observations resulting in a rather low standard error on the T-year estimate, and the AM-method with a limited number of observations (equal to the number of years) causing a higher standard error on the T-year estimate.

The POT-method is based on the assumption that the rate of events (storms) is Poisson-distributed, i.e. the events have a random occurrence at a constant rate. This condition is apparently not fulfilled as some years appear to be more "stormy" than others.

This implies that an improvement of the POT-method could be attained by applying another distribution function for the rate of occurrences, e.g. a negative binomial distribution. In spite of this, three probability models, one of which belongs to the POT-method, are tested against the data, and they all show acceptable goodness-of-fit. Accordingly, a very good basis is provided for assigning T-year estimates to 10-min average wind speeds 10 m above mean sea level in the respective wind direction sectors.

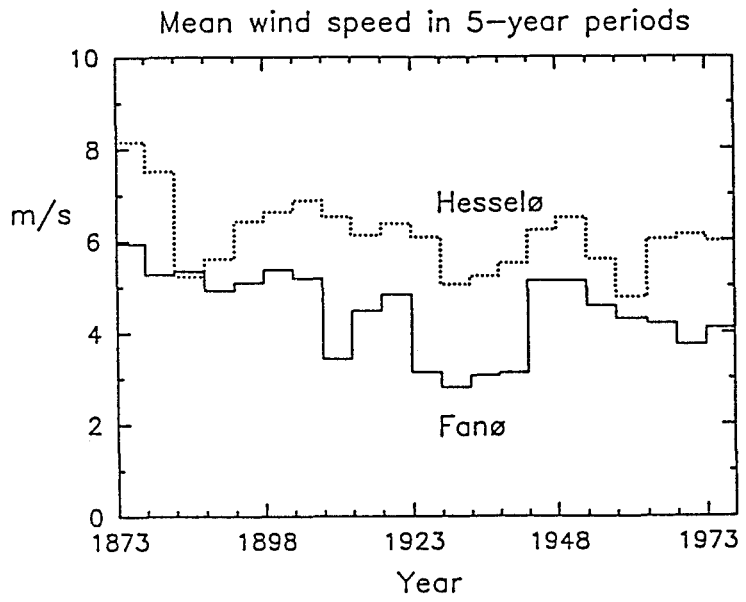

Figure 59: Five-year mean speeds at Fanø and Hesselø, based on the raw observations, S.E. Larsen et al., 1988 .

7 Verification

The extrapolated Risø data were compared with wind data from the Dan/-Gorm fields in the North Sea. Unfortunately, this data material turned out to be of a rather poor quality making the comparison study rather sparse. Good correlation was found for severe westerly storms. A significant lower correlation was found for more moderate storms and storms from other wind directions.

Comment on the supposed climate deterioration

In view of the intense speculations whether our climate is deteriorating in the sense of more frequent and severe storms, the following contribution is made.

a) No trend is found in the mean velocity recorded at the 72/76 m level on the Risø mast in the period February 1958 – October 1986.

b) Observed mean wind speeds from Fanø and Hesselø, covering a period of one hundred years (1873 – 1973) show no increase, rather a decrease in mean wind speed.

c) Recorded sea floods (I.G. Jensen, 1989) classified as large or very large from this century do not indicate an increasing trend, see Table 28.

Table 28: Number of large or very large sea floods in this century. According to I.G. Jensen, 1989.

Period	No. of large or very large sea floods
1900 – 1909	5
1910 – 1919	5
1920 – 1929	7
1930 – 1939	5
1940 – 1949	4
1950 – 1959	1
1960 – 1969	6
1970 – 1979	6
1980 – 1989	1

Future work

a) A more thorough testing on different stages of the model.

b) Methodology used to extrapolate extreme wind data to another homogeneous terrain roughness (e.g. $z_0 = 0.05$).

c) An updating using new wind speed data, say each five years supplemented with a trend analysis.

Acknowledgements

I would like to acknowledge the following staff members of the Department of Meteorology and Wind Energy at Risø National Laboratory.

Niels Otto Jensen for giving birth to many fruitful ideas during the study and for reading and making comments to the manuscript; Ib Troen, Erik Lundtang Petersen, and Niels G. Mortensen for useful guidance in connection with the terrain description model and wind atlas method; Morten Frederiksen for his "detective" work regarding updating of data; Birthe Skrumsager for excellent typing of the manuscript; other members of the department staff, all being very helpful.

Special thanks to Dan Rosbjeg, ISVA, The Technical University of Denmark, for guidance in connection with statistical methods applied. Furthermore, for his patient confidence in the project.

Postscriptum

Work on the present report commenced in 1985 and a draft copy of the report was completed in 1988 during a three month period where the author was employed as a research associate at the Department of Meteorology and Wind Energy at Risø National Laboratory.

The author has since then been preoccupied with other activities explaining the late completion of the final report.

However, it should be noted that other publications by the author such as: Abild and Nielsen (1991); Abild, Mortensen and Landberg (1991) and Abild, Andersen and Rosbjerg (1991); to a large extent has been based on work presented in the draft issue (1988) of the present report.

References

Abild, J.B. et al. (1983). Stokastisk analyse af stormbølger. SVAF, Danmarks Ingeniør Akademi, Bygningsretningen, internal report, not published, 164 pp.

Abild, J.B. and B. Nielsen (1991). Extreme values of wind speeds in Denmark. Risø–M–2842, 107 pp.

Abild, J.B., N.G. Mortensen, and L. Landberg (1992). Application of the wind-atlas method to extreme wind speed data. Proceedings of 8th International Conference on Wind Engineering, Canada 1991. *J. Wind Eng. and Ind. Aerodyn.*, **41**, 473–484.

Abild, J.B., E. Y. Andersen, and D. Rosbjerg (1992). The climate of extreme winds at the Great Belt, Denmark. Proceeds of 8th International Conference on Wind Engineering, Canada 1991. *J. Wind Eng. and Ind. Aerodyn.*, **41**, 521–532.

Box, G.E.P. et al. (1976). Time series analysis: forecasting and control. Holden-day.

Brink-Kjær, O. et al. (1984). Extreme wave conditions in the central North Sea. Sixteenth Annual Offshore Technology Conference, May, 283–293.

Busch, N.E. (1965). A micrometeorological data-handling system and some preliminary results. Risø Report No. 99, 88 pp.

Busch, N.E. (1965). A note on the similarity hypothesis for wind profiles. Risø Report No. 100.

Børresen, J.A. (1987). Vindatlas for Nordsjøen og Norskehavet. The Norwegian Meteorological Institute, Universitetsforlaget.

Christensen, J. (1965). Meteorological measurements at Risø 1962 – 1964. Risø Report No. 121, 67 pp.

Dansk Ingeniørforening (1982). Code of practice for loads for the design of structures, DS 410, 3rd edition.

Doran, J.C. and Gryning, S.E. (1987). Wind and temperature structure over a land-water-land area. *J. Clim. Appl. Meteor.*, **26**, 973–979.

Dyrbye, C. et al. (1989). Vindlast på bærende konstruktioner. SBI Anvisning No. 158, 204 pp.

Fisher, R.A. et al. (1928). Limiting forms of the frequency distribution on the largest or smallest member of a sample. Proceedings, *Cambridge Phil. Soc.*, **24**, p. 180.

Frederiksen, M. (1987). Hovedpunkter vedrørende klimatologiske målinger på Risøs meteorologimast. Risø National Laboratory, Dept. of Meteorology and Wind Energy, internal paper, not published, 6 pp.

Greenwood, J.A. et al. (1979). Probability weighted moments definition and relation to parameters of general distributions expressable in inverse form. *Water Resour. Res.*, **15**, 1049–1054.

Gumbel, E.J. (1958). Statistics of extremes. Colombia University Press, New York, 375 pp.

Hahn, J.G. et al. (1968). Statistical models in engineering. Wiley, New York, 347 pp.

Hansen, E. (1971). Analyse af hydrologiske tidsserier. Laboratoriet for Hydraulik, Danmarks tekniske Højskole, Polyteknisk Forlag, 169 pp.

Hasse, L. (1974). On the surface to geostrophic wind relationship at sea and the stability dependence of the resistance law. *Beitr./Phys. Atmos.*, **47**, 45–55.

Hoshing, J.R.M. et al. (1985). Estimation of the generalized extreme value distribution by the method of probability-weighted moments. *Technometrics*, **27**, 251–261.

Jackson, P.S. et al. (1975). Turbulent wind flow over a low hill. *Quart. J. Roy. Met. Soc.*, **101**, 929–955.

Jackson, P.S. (1979). The influence of local terrain features on the site selection for wind energy generating systems. Faculty of Engineering Science, University of Western Ontario, Report BLWT–1–1979, 83 pp.

Jenkinson, A.F. (1955). The frequency distribution of the annual maximum (or minimum) values of meteorological elements. *Quart. J. Roy. Met. Soc.*, **81**, 158–171.

Jensen, I.G. (1985). Sea Floods. Danish Meteorological Institute, Climatological Paper No. 13, 96 pp.

Jensen, I.G. (1989). Stormfloder. Internal report, Danish Meteorological Institute, 89 pp, not published.

Jensen, M. (1959). Aerodynamik i den naturlige vind. Teknisk Forlag, Copenhagen, 173–226.

Jensen, M. et al. (1970). The climate of strong winds in Denmark. Danish Technical Press, Copenhagen, 40 pp.

Jensen, N.O. (1978). On the escarpment wind profile. *Quart. J. Roy. Met. Soc.*, **104**, 719–728.

Jensen, N.O. (1978). Change of surface roughness and the planetary boundary layer. *Quart. J. Roy. Met. Soc.*, **104**, 351–356.

Jensen, N.O. (1981). Studies of the surface layer during change in surface conditions. Colloque: Construire avec le vent, Nantes, France, Paper No. 1–4, 20 pp.

Jensen, N.O. (1983). Escarpment induced flow perturbations, a comparison of measurements and theory. *J. Wind Eng. Ind. and Ind. Aerodyn.*, 1983, 342–251.

Jensen, N.O. and Troen, I. (1983). Vurdering af vindklimaet ved færgehavne i Storebælt. Contract Report for the Danish Railways, 22 pp + appendices.

Jensen, N.O., Petersen, E.L., and Troen, I. (1984). Extrapolation of mean wind statistics with special regard to wind energy applications. WMO, World Climate Programme, Report No. WCP–86, 85 pp.

ge Kishore, A. et al. (1987). An evaluation of seven methods for estimating parameters of EV1 distribution. Hydrologic frequency modelling. Proceeding of the International Symposium on Flood Frequency and Risk Analysis, May 1986, 383–394.

Kite, G.W. (1974). Assessment of the assumption of normality in computation of confidence limits. Inland Waters Directorate, Water Resources Branch Applied, Ottawa, Canada.

Kite, G.W. (1977). Frequency and risk analysis in hydrology. Water Resources Publications, Hydrology Division, Network Planning and Forecasting Section, P.O. Box 303, Fort Collins, CO, USA.

Kumar, A. et al. (1987). Entropy principle in the estimation of Gumbel parameters. Hydrologic frequency modelling. Proceedings of the International Symposium on Flood Frequency and Risk Analysis, May 1986, 419–431.

Landwehr, J.M. et al. (1979). Probability weighted moments compared with some traditional techniques in estimating Gumbel parameters and quantiles. *Water Resour. Res.*, **15**, 1055–1064.

Mardia, K.V. (1972). Statistics of directional data. Academic Press, London, 281 pp.

Møller, H.B. et al. (1959). Preliminary report on the meteorological measurements at Risø. Risø Report No. 8, 42 pp.

Nørrevang, A. and T.J. Meyer (1968). Danmarks Natur, Vol. 2 *Klima og Levevilkår*. Politikens Forlag, 79–94.

Panofsky, H.A. (1972). Wind profiels and change of terrain roughness at Risø. *Quart. J. Roy. Met. Soc.*, **98**, 845–854.

Petersen, E.L., Troen, I., Frandsen, S., and Hedegaard, K. (1981). Danish Wind Atlas. A rational method of wind energy siting. Risø–R–429, 229 pp.

Petersen, E.L. and Troen, I. (1989). European Wind Atlas. Risø National Laboratory, published for the EEC, 656 pp.

Prescott, P. et al. (1982). Maximum likelihood estimation of the parameters of the three parameter generalized extreme value distribution from censored samples. *J. Statis. Comput. Simul.*, **16**, 241–250.

Rosbjerg, D. (1977). Return periods of hydrological events. *Nordic Hydrology*, **8**, 57–61.

Rosbjerg, D. (1979). Noter til stokastisk hydrologi. ISVA, Danmarks Tekniske Højskole, internal paper, 41 pp.

Rosbjerg, D. et al. (1982). Uncertainty in reservoir design – benefits from using secondary data. Optimal Allocation of Watrer Resources. Proceedings of the Exeter Symposium, July, IAHS Publication No. 135, 59–67.

Rosbjerg D. and J. Knudsen (1984). POT-estimation of extreme sea states and the benefit of using wind data. *Statistical Extremes and Applications*, NATO ASI Series C, Vol. 131, Reidel, 611–620.

Rosbjerg, D. (1987). Partial duration series with log-normal distributed peak values. Hydrologic frequency modelling. Proceedings of the International Symposium on Flood Freqeuncy and Risk Analysis, May 1986. D. Reidel, Dordrecht, 117–129.

Rossi, E. (1984). Two-component extreme value distribution for flood frequency analysis. *Water Resour. Res.*, **20**, 847–856.

Taylor, P.A. et al. (1983). Progress Report to the International Energy Agency's programme on research and development on wind energy conversion systems, Task VI: Study of local wind flow at potential WECS hill sites. Atmospheric Environment Service, Canada.

Troen, I. and Mortensen, N.G. (1987). WA^{S}P– Wind Atlas and Application Programme. An Introduction. Risø National Laboratory. First edition 13 pp, second edition 10 pp.

Appendices:

Appendix A:

Model boundary layer profiles compared with measured wind velocity profiles for different azimuth sectors.

Introduction to the boundary profiles:

This Appendix contains wind velocity profiles based on measurements at different levels of the Risø mast together with model profiles established through the WA^{S}P computation described in chapter 3 of this report.

Wind velocity profiles are presented for eight wind direction sectors. A short description of the characteristics of each profile will be given in the following.

General comments:

The model boundary profile (bold line) is drawn starting at the theoretical level of the *geostrophic wind* (approx. 1000 m above ground level) and adjusting the profile for each change in roughness from a distance of 20 km from the site. A long-term (period: 1958-1986 indicated by ∇ in the plots) measured mean wind velocity profile has been made to fit the model boundary profile at the 74 m level of the Risø mast by applying an appropriate scaling factor. Accordingly, only the relative merits of the model profile and the measured profile can be evaluated in the figures. Only wind speeds above 10 m/s have been used in order to secure near neutral stability of the boundary layer.

With the purpose of investigating a possible change of roughness with time, two short-term measured wind velocity profiles have been included for comparison:

□: Short-term measured mean wind velocity profile, period 1958 - 1967.

◇: Short-term measured mean wind velocity profile, period 1982 - 1986.

Finally, corrections have been made to the long-term measured mean wind velocity profile to include the effects of shelter and/or orographic features in the near site terrain. The magnitude of these corrections are indicated on the figures as a plus or minus percentage for increase and decrease in wind speed, respectively. The adjusted profile is indicated with a ○ and a thin line in the figures.

The relative behaviour between the adjusted measured wind profile (thin line) and the roughness model profile (bold line) will thus provide illustrative information on the quality of the composed terrain model and can to some extent help pointing out measurements suffering from tower shadow effects and occasional overspeeding of cup anemometers.

North sector (357.5° - 22.5°):

The roughness change model provides a good description of the terrain, especially the change in roughness at the Risø peninsula seems to be well accounted for. It is not evident, however, that corrections due to shelter obstacles and orographic features improve the fit to the measured profiles. Note the apparent "historic" change of the roughness in the near site terrain as predicted by the measured □: 1958 - 1967 and ◇: 1982-1986 records.
Furthermore, beware that measurements taken from the 120 m recording level have been subject to a slight tower shadow effect during the early instrumentation, see Fig. 19.

North-east sector (22.5° - 67.5°):

This sector is subjected to a considerable tower shadow effect, see Figs. 16 - 21 in Chp. 4. This effect has been included directly in the input option of the roughness change model as a roughly estimated 5% decrease in the measured wind speed. Recent studies (Abild and Nielsen, 1991) indicate, that this reduction is likely to be as much as 10 - 15% with a predominant effect during the early recordings prior to the installation of the rolling booms. This finding is supported by looking at the difference in mean wind speed for the □: 1958 - 1967 and ◇: 1982-1986 records. The composed terrain model seems to provide a good description of the terrain even for the lower recording levels.
Note the significant "historic" changes in the roughness in the near site terrain. Due to the problem of assessing the tower shadow effect, data and extreme statistics from the north-east sector shall be treated with some caution.

East sector (67.5° - 112.5°):

The measured profiles indicate that the roughness change, approximately 700 m from the mast, should be more pronounced. This deficiency causes the model boundary layer profile to overestimate wind speeds for the lower recording levels. Note that due to disturbed flow conditions caused by the mast, wind data from the east sector might be subject to a slight overspeeding especially for the early measurements and recording levels below the 123 m level, see Figs. 16 and 19.

South-east sector (112.5° - 157.5°):

In general the composed boundary layer model appears to be in concordance with the measured wind profile. It seems recommendable to use a slightly higher surface roughness than the one adopted (z_0 = 0.054 m) for the terrain more than 700 m from the site. This might be explained by a combination of thermal and roughness effects as the wind flow passes land-water-land trajectories close to the site, see further comments in section 3.5. Note that a overspeeding effect is likely to be present for the early recordings at the 123 m level of the mast.

South sector (157.5°-202.5°):

The most significant difference between the model boundary layer profile and the measured profile relates to the roughness change across the bay at the Veddelev hill. It appears that a higher ground roughness should have been adopted for the terrain on the Veddelev hill. As for the south-east sector this might be explained by a combination of thermal and roughness effects, see comments in Chp. 3.5.
The orographic effect from the Veddelev hill is believed to be less than 0.5%, see section 3.3.1.

South-west sector (202.5° - 247.5°):

Apart from the corrections predicted by the obstacle model for the shelter effect from the DR2 Reactor, the roughness model boundary profile seems to be in convincing agreement with the measurements. Some flow disturbance, caused by the proximity of the mast to the instrumentation, must be expected for the early measurements from this sector, see figs. 16 and 19.

West sector (247.5° - 292.5°):

The composed boundary model provides an excellent fit to the measured profile. The roughness change at the Risø peninsula is clearly recognized. Note the significant change of roughness with time as identified in the measurements at the lower recording levels.

North-west sector (292.5° - 337.5°):

The model boundary layer profile provides an acceptable fit to the measured profile and the shelter model evidently improves the performance of the composed terrain model. As for the west sector the roughness change at the Risø peninsula is clearly identified, however, comparatively more accentuated in the measurements. Note the radical change of roughness with time as revealed in the measurements at the lower recording levels. Beware of overspeeding effects for early measurements, see Figs. 16 and 19.

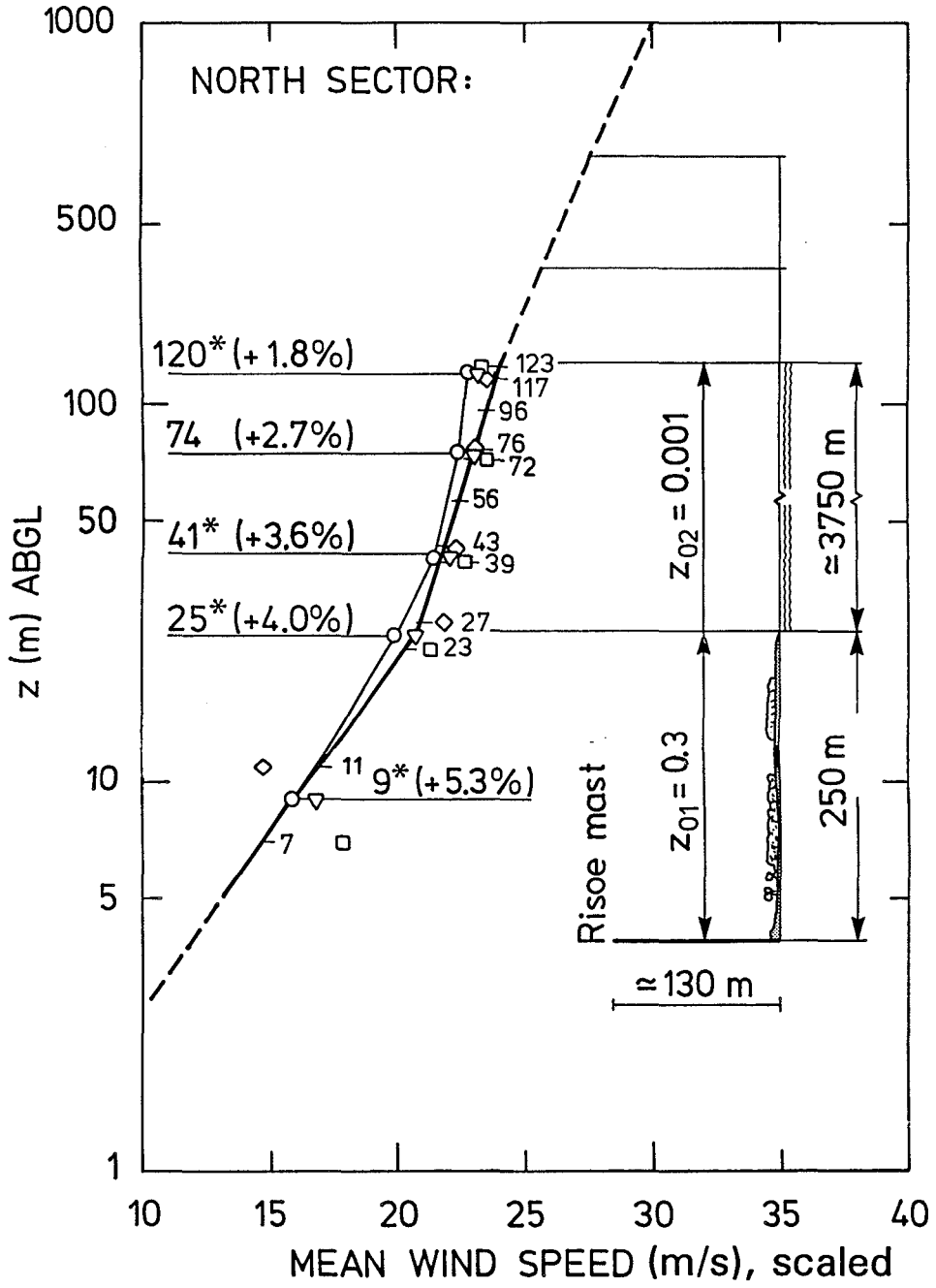

▽ : *Long-term measured mean wind velocity profile, period: 1958-1986.*
○ : *Long-term adjusted mean wind velocity profile, period: 1958-1986.*
◇ : *Short-term measured mean wind velocity profile, period: 1982-1986.*
□ : *Short-term measured mean wind velocity profile, period: 1958-1967.*

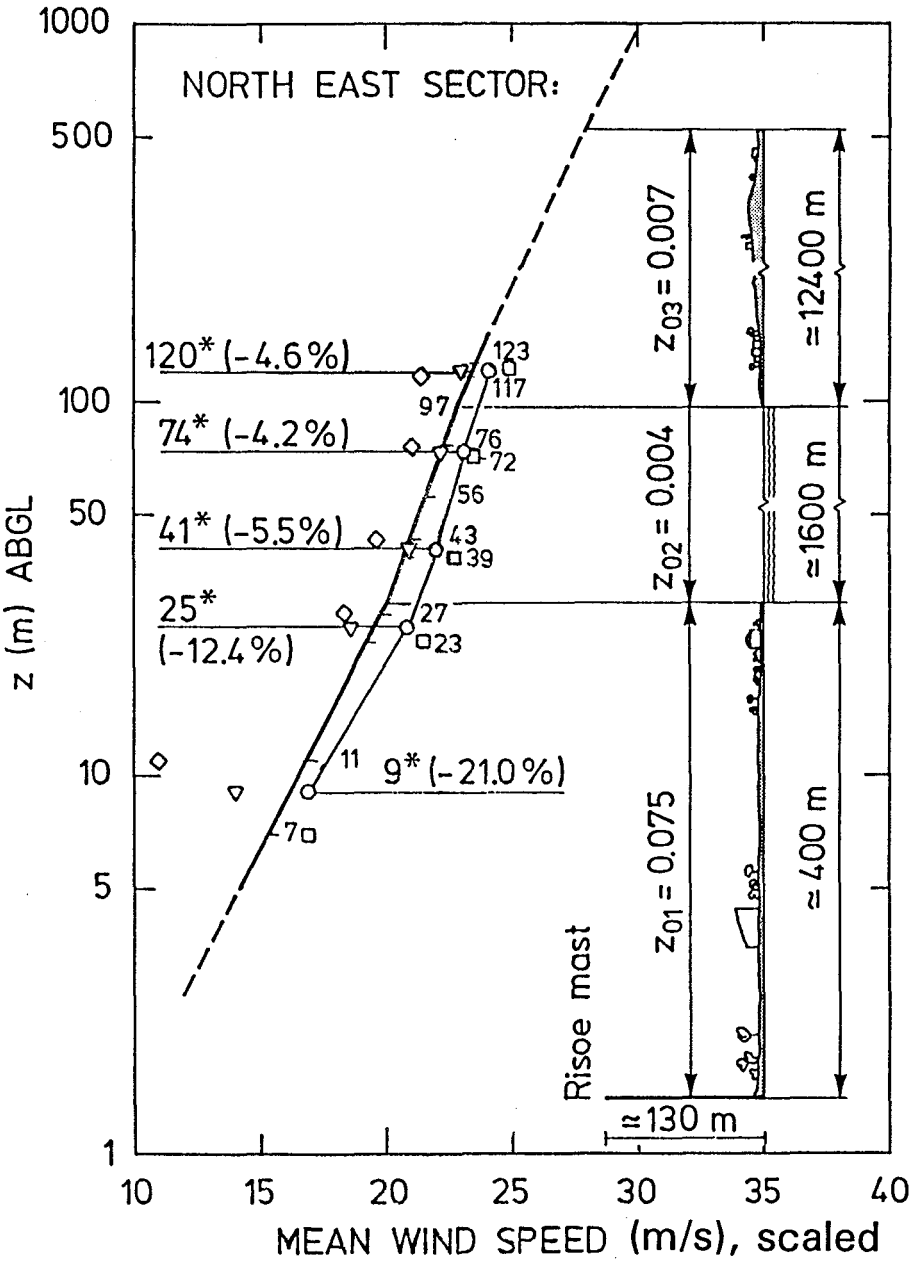

▽ : *Long-term measured mean wind velocity profile, period: 1958-1986.*
○ : *Long-term adjusted mean wind velocity profile, period: 1958-1986.*
◇ : *Short-term measured mean wind velocity profile, period: 1982-1986.*
□ : *Short-term measured mean wind velocity profile, period: 1958-1967.*

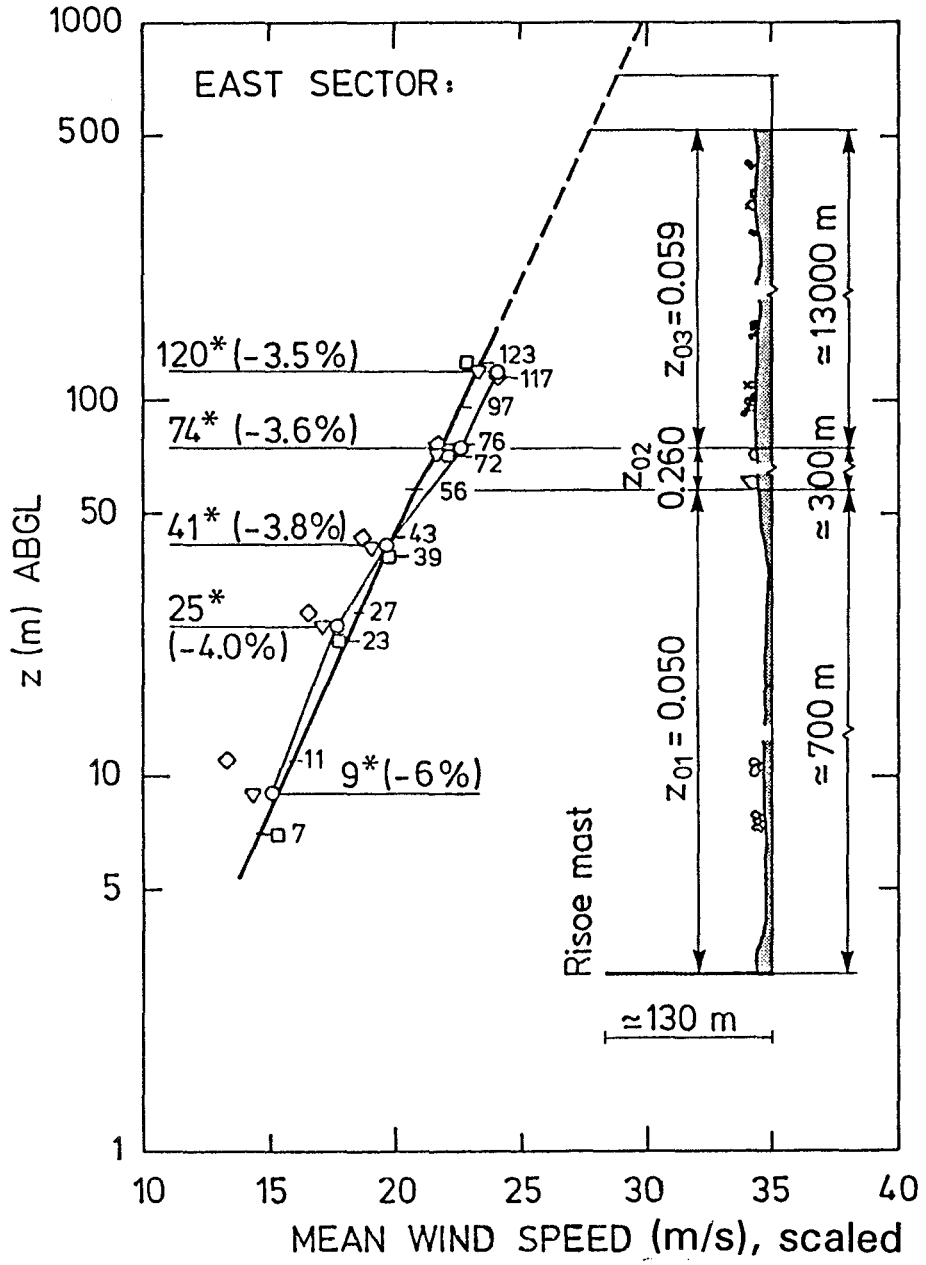

▽ : *Long-term measured mean wind velocity profile, period: 1958-1986.*
○ : *Long-term adjusted mean wind velocity profile, period: 1958-1986.*
◇ : *Short-term measured mean wind velocity profile, period: 1982-1986.*
□ : *Short-term measured mean wind velocity profile, period: 1958-1967.*

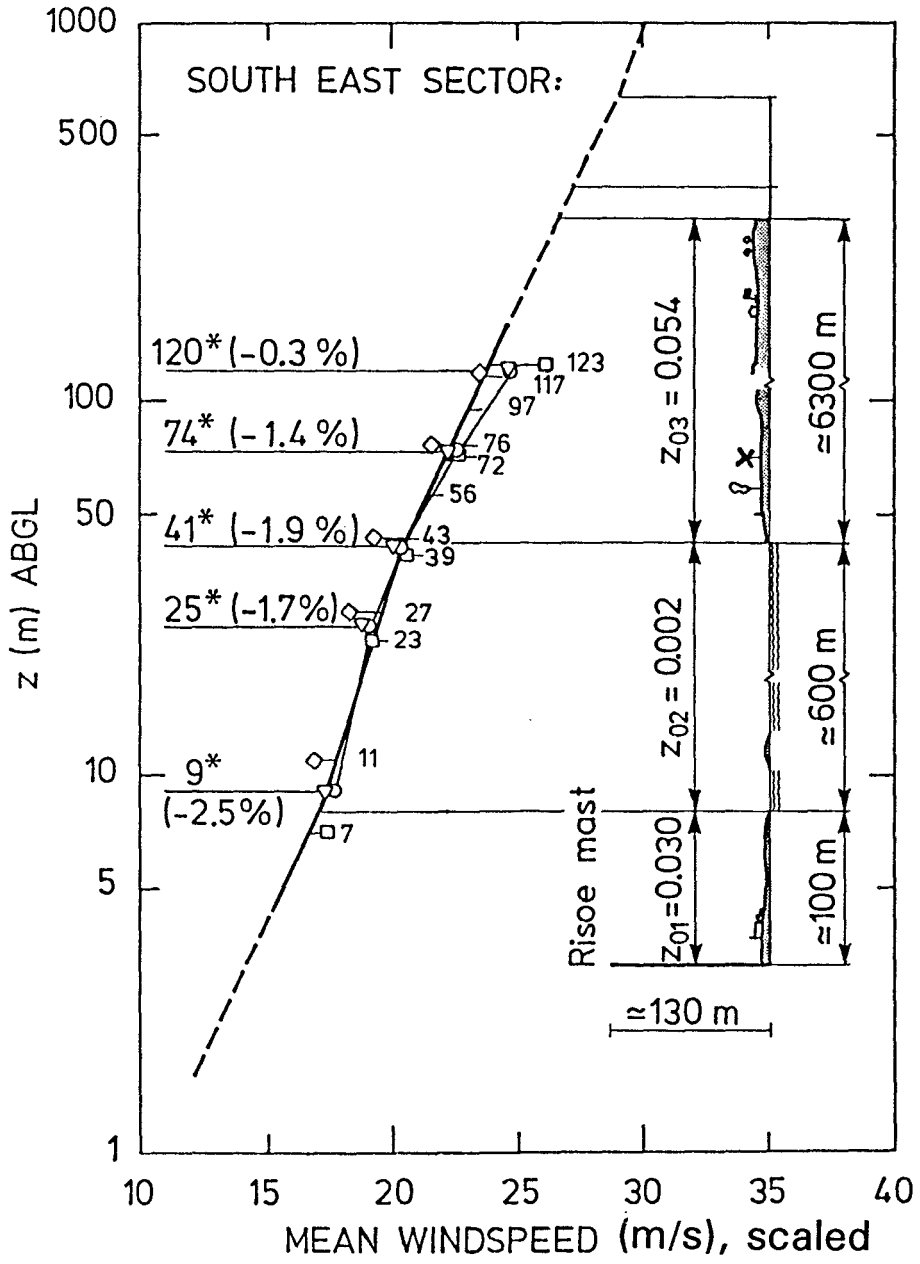

▽ : *Long-term measured mean wind velocity profile, period: 1958-1986.*
○ : *Long-term adjusted mean wind velocity profile, period: 1958-1986.*
◇ : *Short-term measured mean wind velocity profile, period: 1982-1986.*
□ : *Short-term measured mean wind velocity profile, period: 1958-1967.*

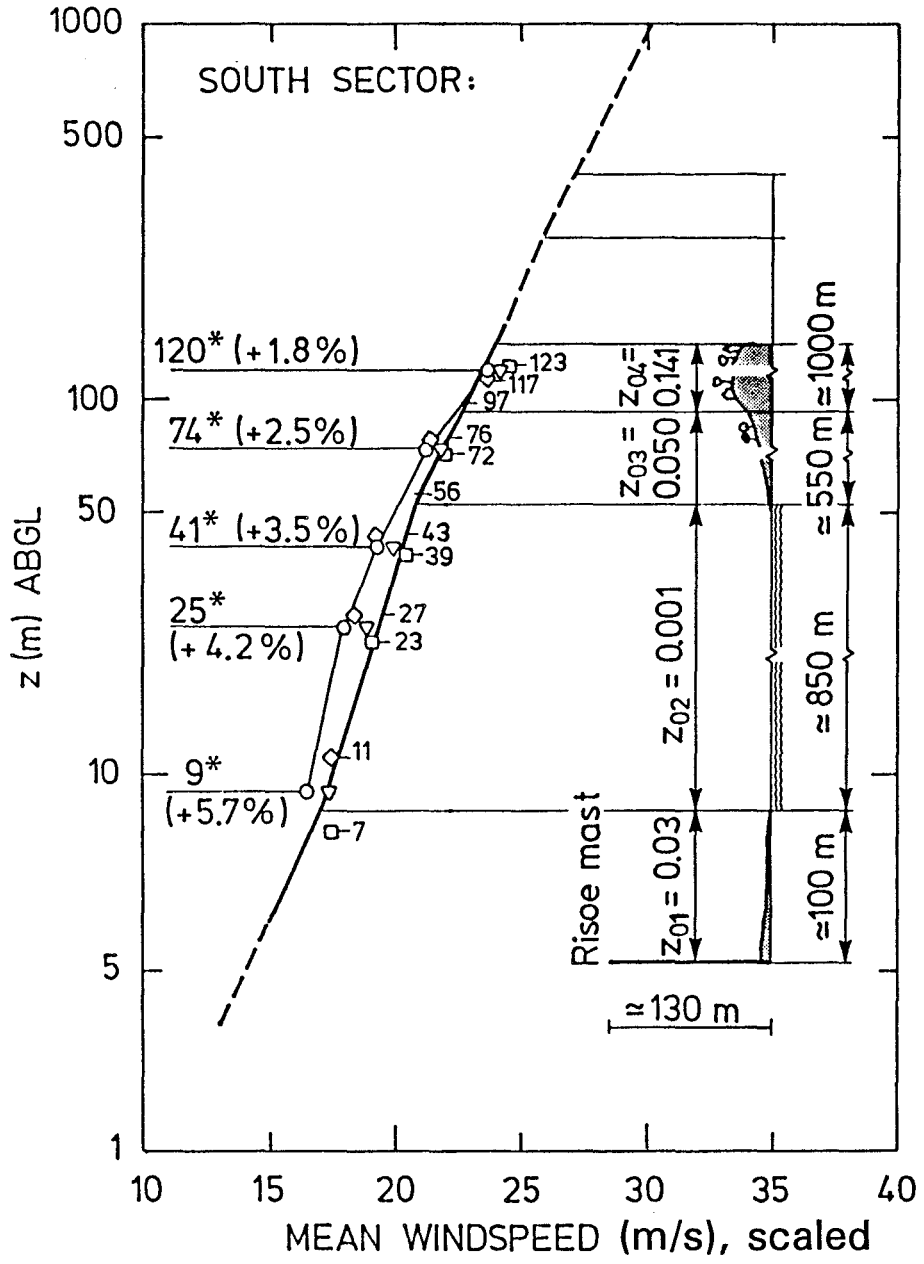

▽ : *Long-term measured mean wind velocity profile, period: 1958-1986.*
○ : *Long-term adjusted mean wind velocity profile, period: 1958-1986.*
◇ : *Short-term measured mean wind velocity profile, period: 1982-1986.*
□ : *Short-term measured mean wind velocity profile, period: 1958-1967.*

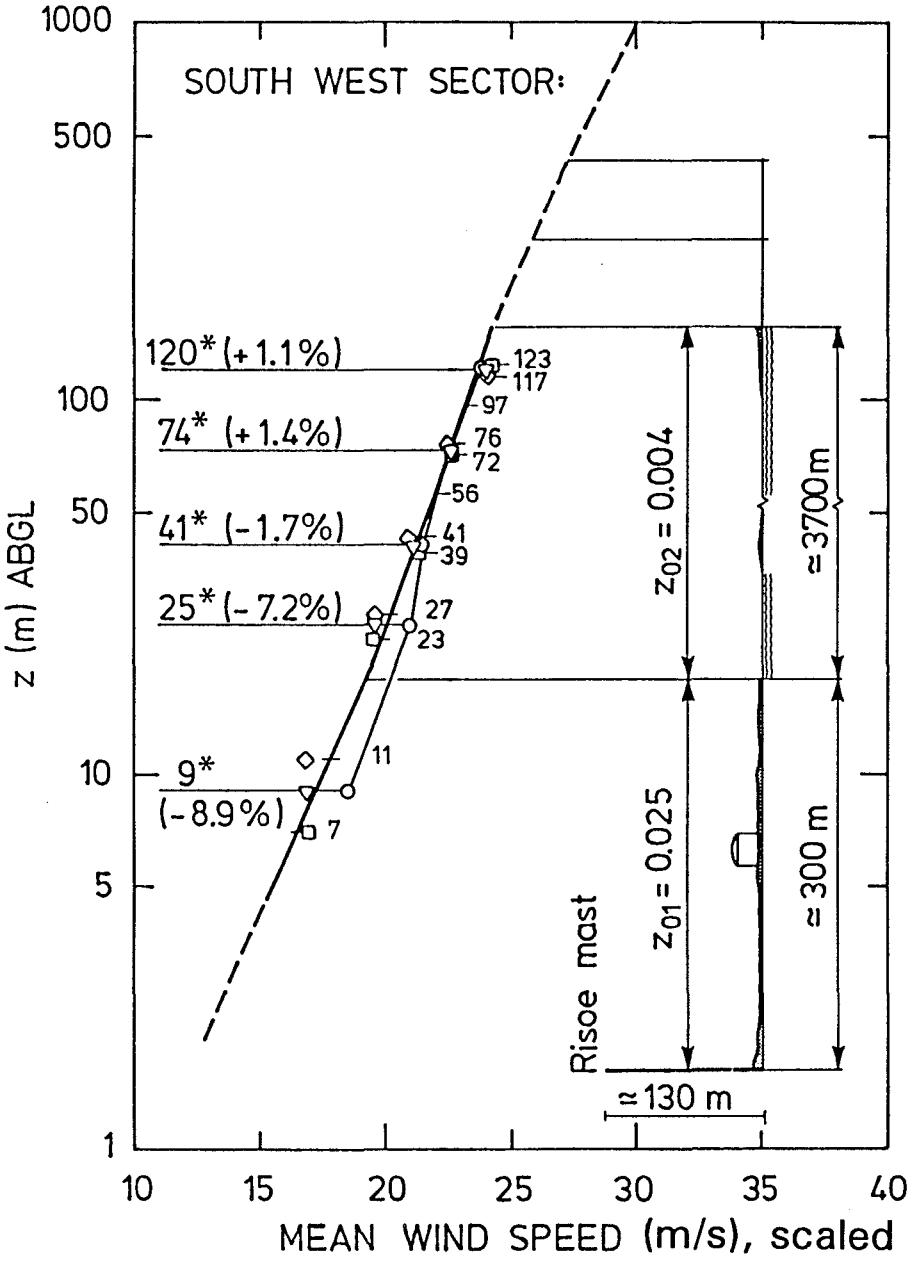

▽ : *Long-term measured mean wind velocity profile, period: 1958-1986.*
○ : *Long-term adjusted mean wind velocity profile, period: 1958-1986.*
◇ : *Short-term measured mean wind velocity profile, period: 1982-1986.*
□ : *Short-term measured mean wind velocity profile, period: 1958-1967.*

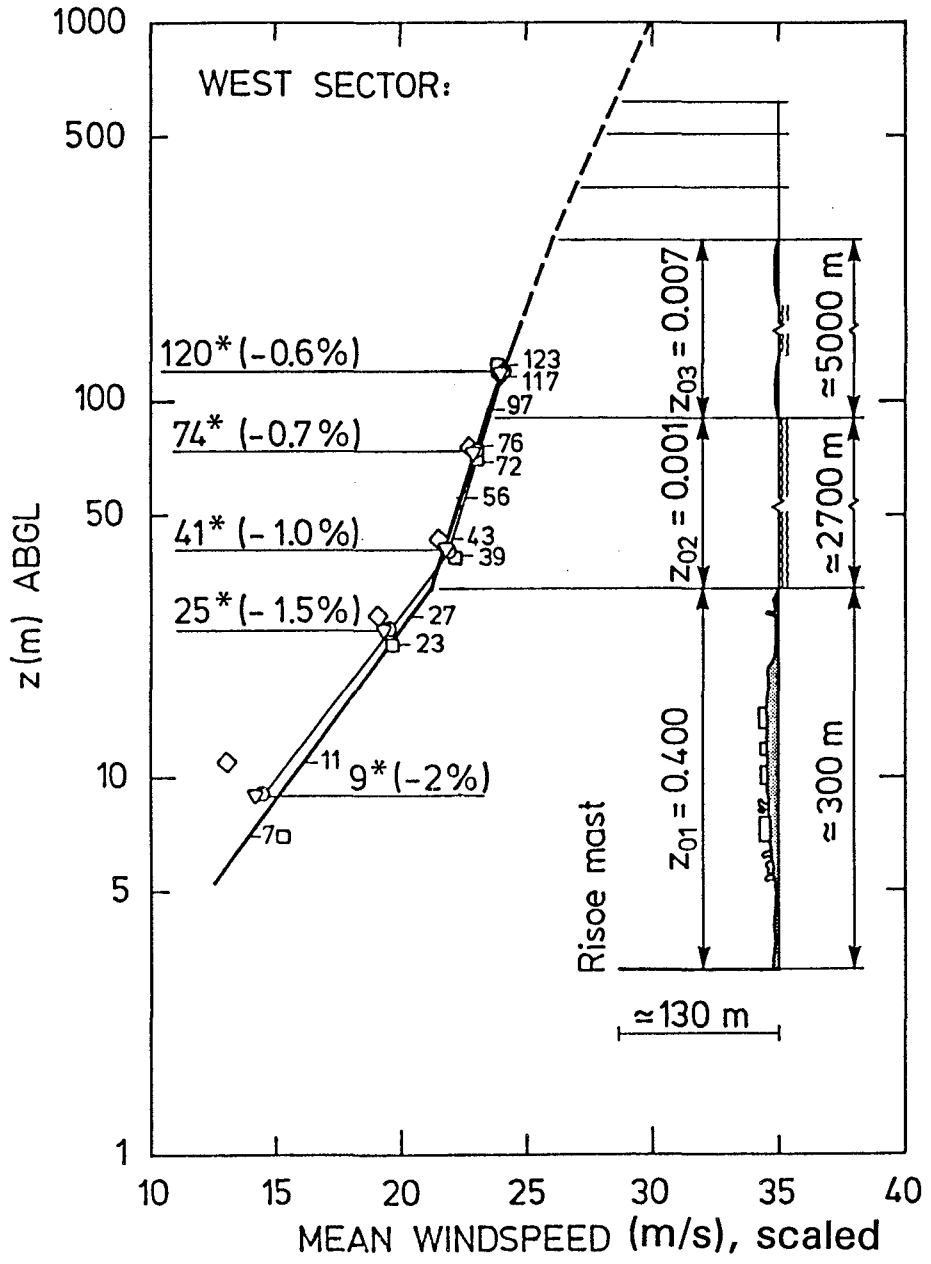

▽ : *Long-term measured mean wind velocity profile, period: 1958-1986.*
○ : *Long-term adjusted mean wind velocity profile, period: 1958-1986.*
◇ : *Short-term measured mean wind velocity profile, period: 1982-1986.*
□ : *Short-term measured mean wind velocity profile, period: 1958-1967.*

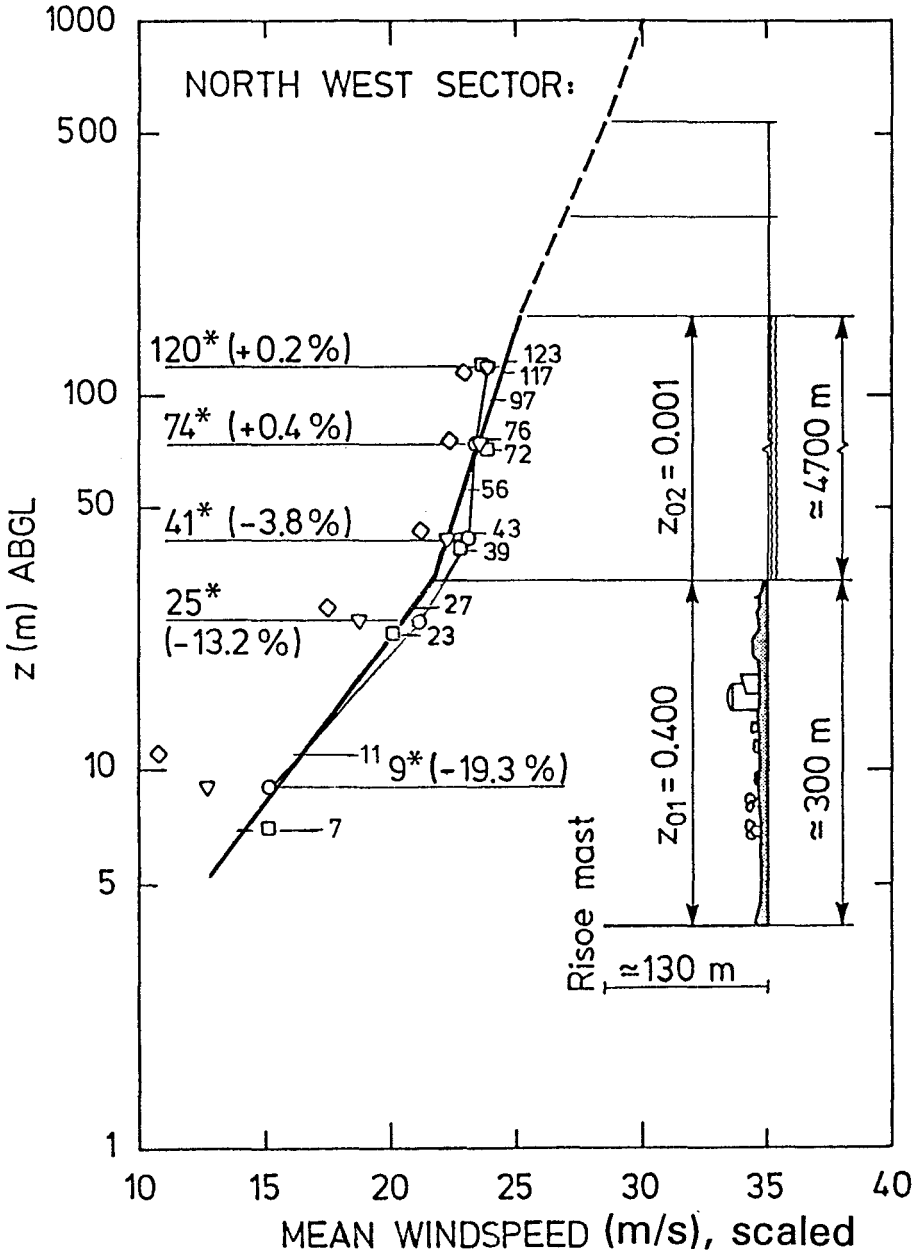

▽ *: Long-term measured mean wind velocity profile, period: 1958-1986.*
○ *: Long-term adjusted mean wind velocity profile, period: 1958-1986.*
◇ *: Short-term measured mean wind velocity profile, period: 1982-1986.*
□ *: Short-term measured mean wind velocity profile, period: 1958-1967.*

Appendix B:

Distributions of wind speed for different azimuth sectors.

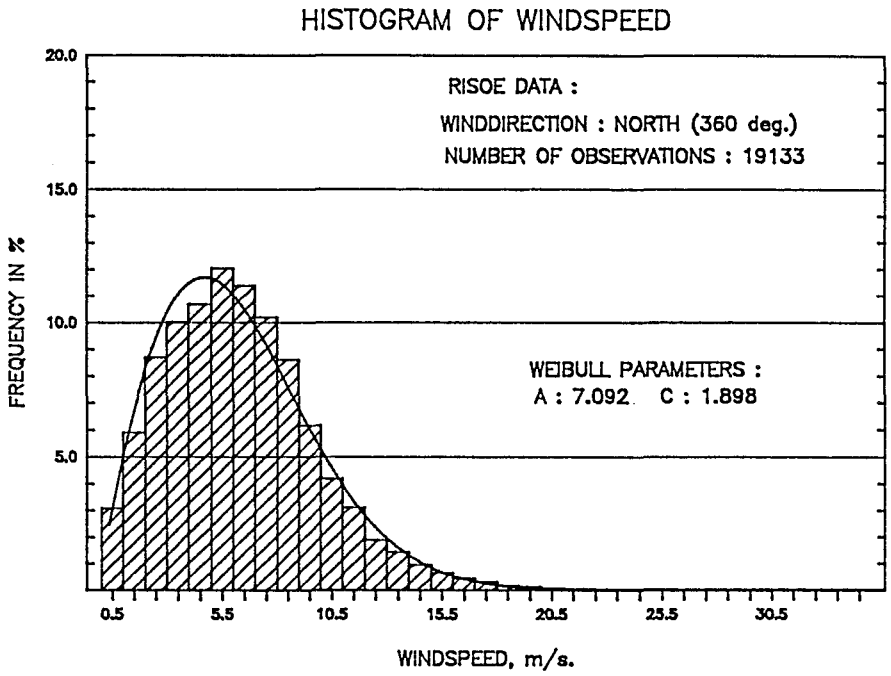
HISTOGRAM OF WINDSPEED
RISOE DATA :
WINDDIRECTION : NORTH (360 deg.)
NUMBER OF OBSERVATIONS : 19133
WEIBULL PARAMETERS :
A : 7.092 C : 1.898
FREQUENCY IN %
20.0
15.0
10.0
5.0
0.5
5.5
10.5
15.5
20.5
25.5
30.5
WINDSPEED, m/s.

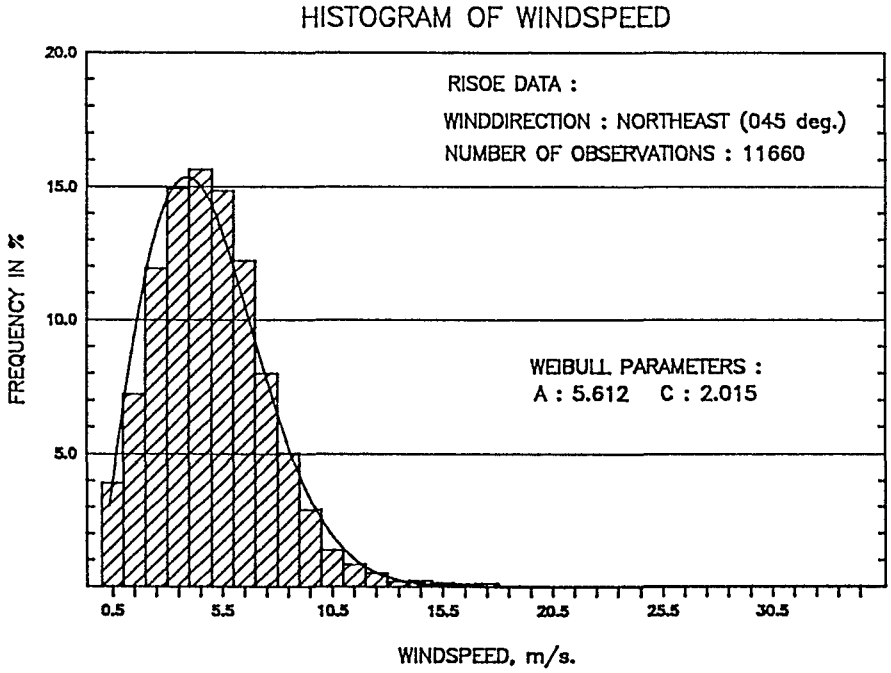
HISTOGRAM OF WINDSPEED
RISOE DATA :
WINDDIRECTION : NORTHEAST (045 deg.)
NUMBER OF OBSERVATIONS : 11660
WEIBULL PARAMETERS :
A : 5.612 C : 2.015
FREQUENCY IN %
20.0
15.0
10.0
5.0
0.5
5.5
10.5
15.5
20.5
25.5
30.5
WINDSPEED, m/s.

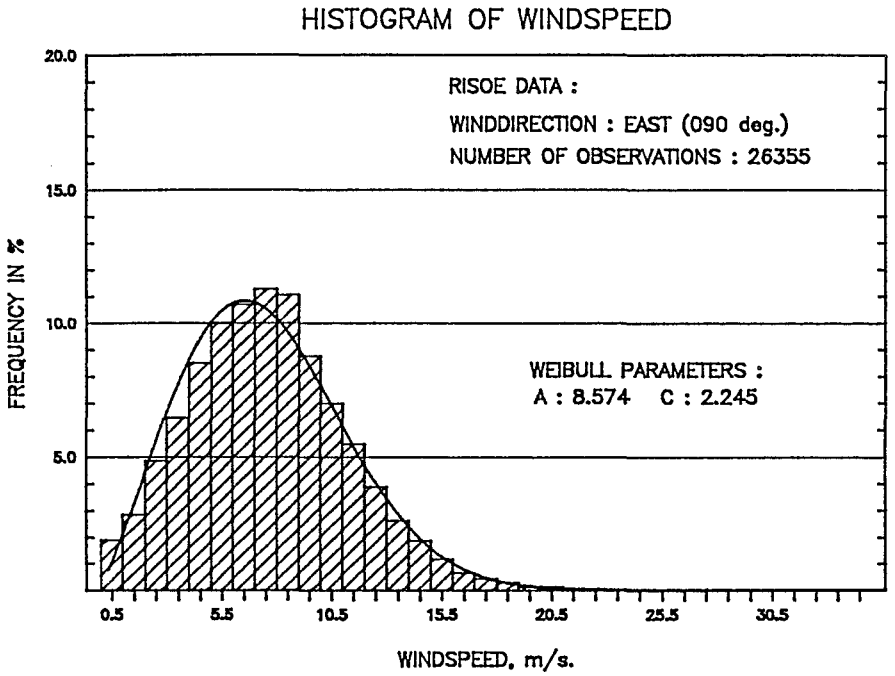
HISTOGRAM OF WINDSPEED
RISOE DATA :
WINDDIRECTION : EAST (090 deg.)
NUMBER OF OBSERVATIONS : 26355
WEIBULL PARAMETERS :
A : 8.574 C : 2.245
FREQUENCY IN %
20.0
15.0
10.0
5.0
0.5
5.5
10.5
15.5
20.5
25.5
30.5
WINDSPEED, m/s.

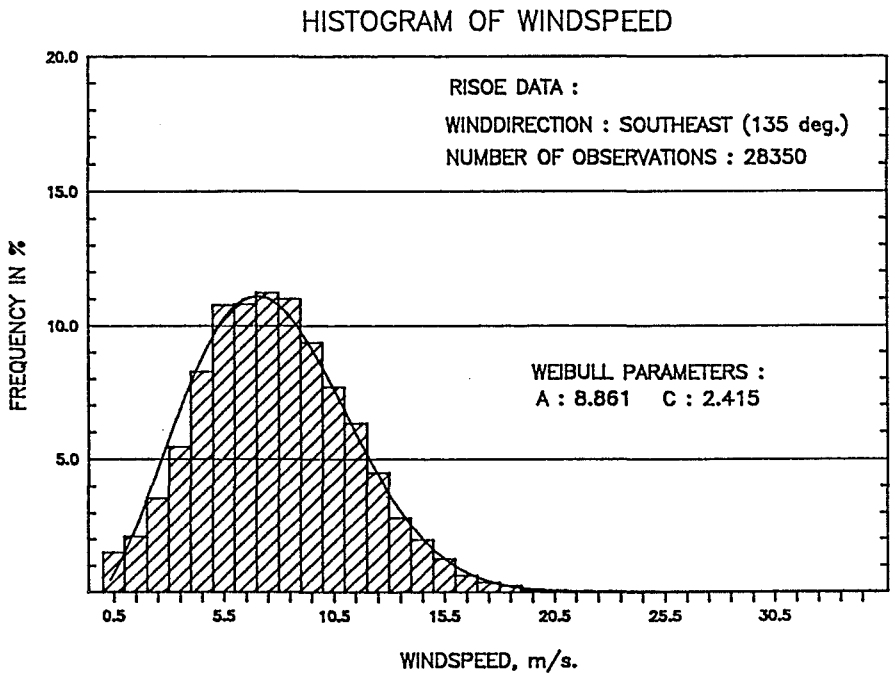
HISTOGRAM OF WINDSPEED
RISOE DATA :
WINDDIRECTION : SOUTHEAST (135 deg.)
NUMBER OF OBSERVATIONS : 28350
WEIBULL PARAMETERS :
A : 8.861 C : 2.415
FREQUENCY IN %
20.0
15.0
10.0
5.0
0.5
5.5
10.5
15.5
20.5
25.5
30.5
WINDSPEED, m/s.

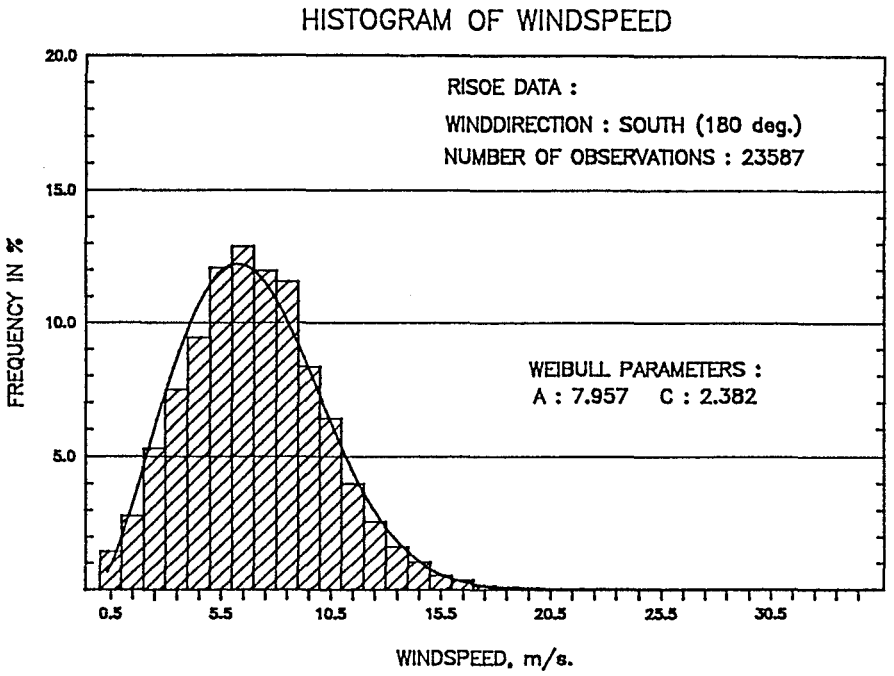
HISTOGRAM OF WINDSPEED
RISOE DATA :
WINDDIRECTION : SOUTH (180 deg.)
NUMBER OF OBSERVATIONS : 23587
WEIBULL PARAMETERS :
A : 7.957 C : 2.382
FREQUENCY IN %
20.0
15.0
10.0
5.0
0.5
5.5
10.5
15.5
20.5
25.5
30.5
WINDSPEED, m/s.

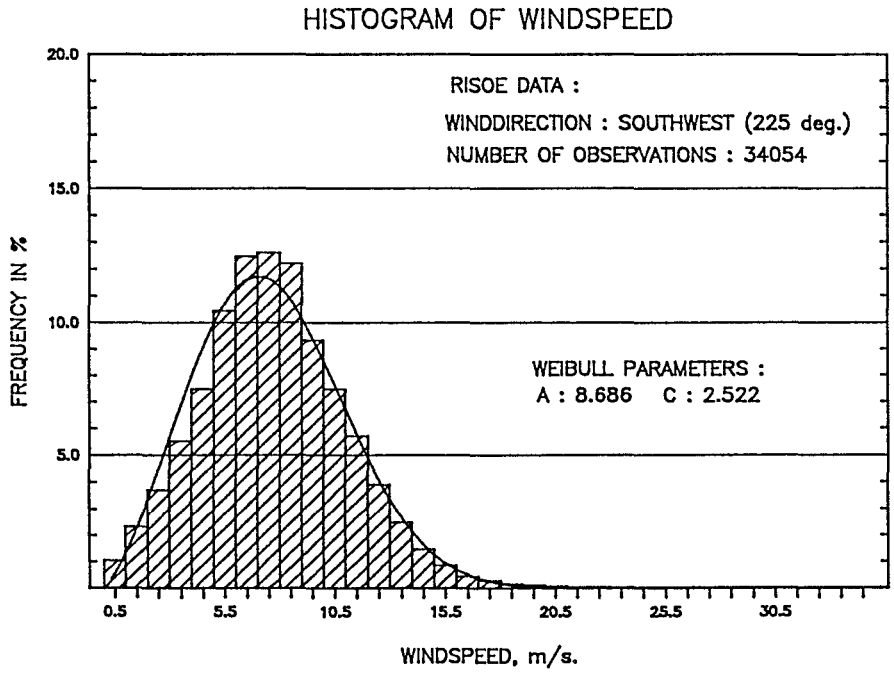
HISTOGRAM OF WINDSPEED
RISOE DATA :
WINDDIRECTION : SOUTHWEST (225 deg.)
NUMBER OF OBSERVATIONS : 34054
WEIBULL PARAMETERS :
A : 8.686 C : 2.522
FREQUENCY IN %
20.0
15.0
10.0
5.0
0.5
5.5
10.5
15.5
20.5
25.5
30.5
WINDSPEED, m/s.

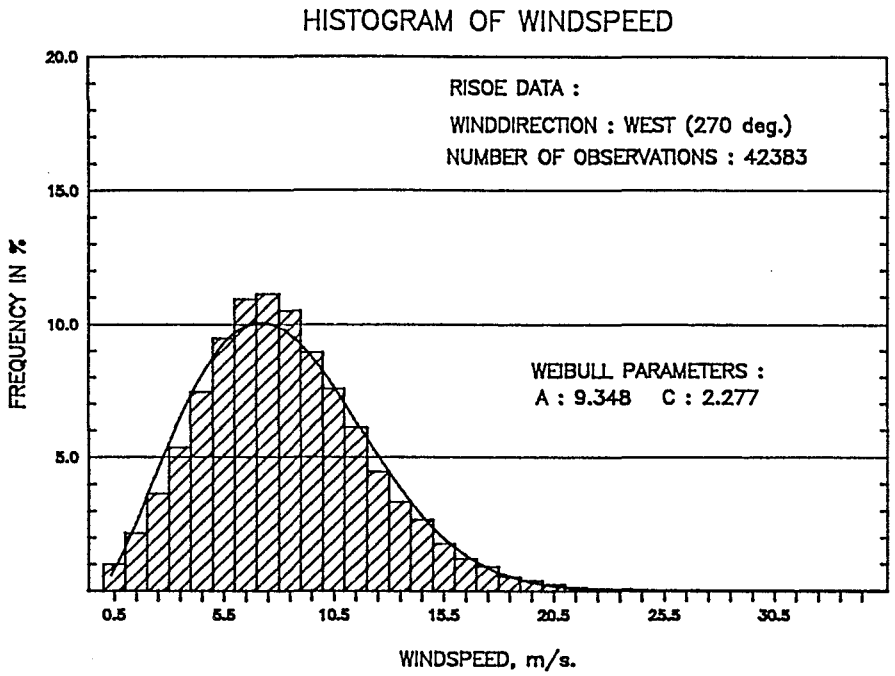
HISTOGRAM OF WINDSPEED
RISOE DATA :
WINDDIRECTION : WEST (270 deg.)
NUMBER OF OBSERVATIONS : 42383
WEIBULL PARAMETERS :
A : 9.348 C : 2.277
FREQUENCY IN %
20.0
15.0
10.0
5.0
0.5
5.5
10.5
15.5
20.5
25.5
30.5
WINDSPEED, m/s.

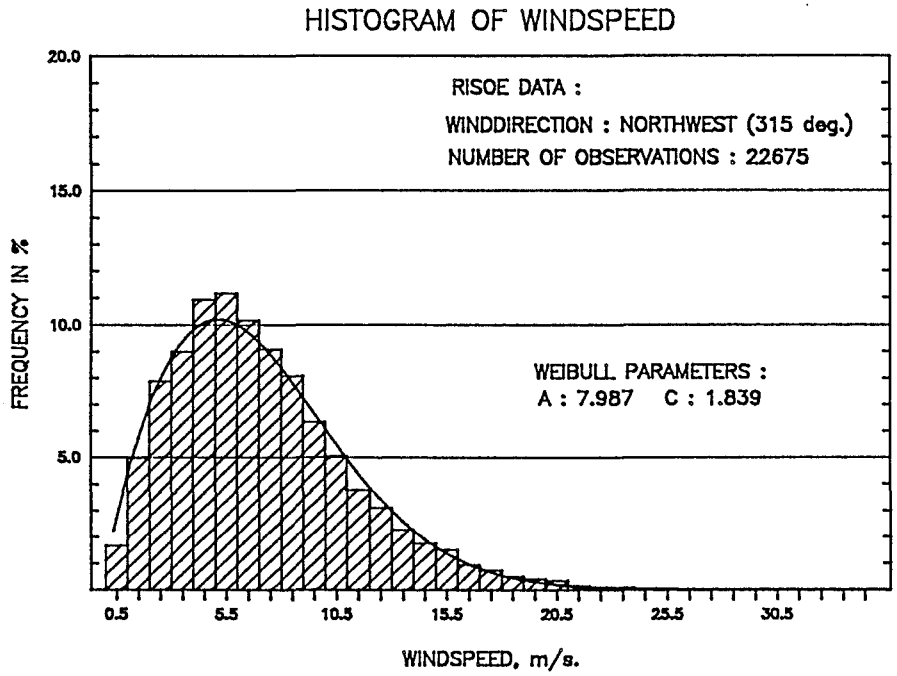
HISTOGRAM OF WINDSPEED
RISOE DATA :
WINDDIRECTION : NORTHWEST (315 deg.)
NUMBER OF OBSERVATIONS : 22675
WEIBULL PARAMETERS :
A : 7.987 C : 1.839
FREQUENCY IN %
20.0
15.0
10.0
5.0
0.5
5.5
10.5
15.5
20.5
25.5
30.5
WINDSPEED, m/s.

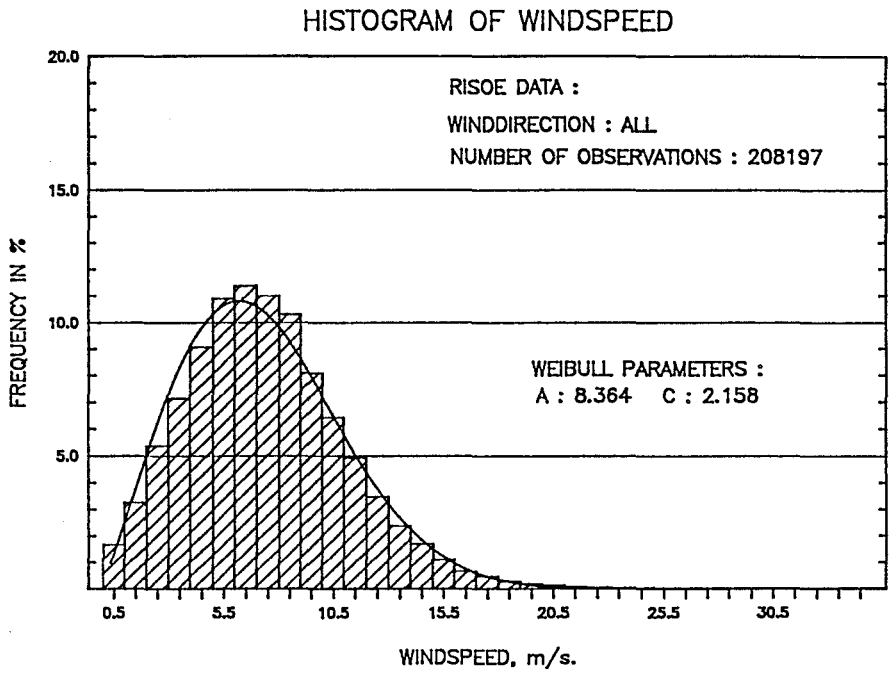
HISTOGRAM OF WINDSPEED
RISOE DATA :
WINDDIRECTION : ALL
NUMBER OF OBSERVATIONS : 208197
WEIBULL PARAMETERS :
A : 8.364 C : 2.158
FREQUENCY IN %
20.0
15.0
10.0
5.0
0.5
5.5
10.5
15.5
20.5
25.5
30.5
WINDSPEED, m/s.

Appendix C:

Tables on extreme AM - and POT series wind speed data and model parameters for different azimuth sectors.

Data from the Annual Maximum (AM) Model.

Obs. Rank R	Plot. Pos. $P_r = \frac{r}{n+1}$	N Sector Date	N Sector u_{max} m/s	N Sector Dir. °)	NE Sector Date	NE Sector u_{max} m/s	NE Sector Dir. °)	E Sector Date	E Sector u_{max} m/s	E Sector Dir. °)
1	0.036	710311^{08}	22.1	355	680111^{07}	25.6	25	591207^{10}	21.8	110
2	0.071	830925^{00}	20.1	351	781231^{15}	19.2	65	661213^{04}	21.4	100
3	0.107	680111^{11}	19.9	16	610321^{09}	18.6	47	791214^{14}	21.3	109
4	0.143	670922^{14}	19.3	346	580226^{02}	16.2	48	601101^{19}	20.4	110
5	0.179	860120^{04}	18.9	359	601210^{19}	16.2	38	720117^{11}	20.1	110
6	0.214	640205^{17}	18.9	346	660414^{07}	15.6	38	690313^{18}	19.7	100
7	0.250	761226^{00}	18.1	359	670612^{10}	15.5	27	620416^{13}	19.6	90
8	0.286	650208^{02}	18.1	16	690216^{08}	14.9	38	670216^{13}	19.5	110
9	0.321	620217^{10}	18.1	346	711124^{00}	14.8	58	841117^{10}	19.5	101
10	0.357	600111^{00}	17.7	6	830208^{00}	14.8	63	650504^{17}	18.8	110
11	0.393	850430^{10}	17.3	354	760103^{22}	14.7	27	710423^{15}	18.7	100
12	0.429	630126^{15}	17.3	6	590419^{15}	13.9	27	781231^{09}	18.6	70
13	0.462	700612^{13}	16.5	346	630126^{19}	13.9	27	850508^{12}	18.6	89
14	0.500	840109^{01}	16.5	14	840109^{02}	13.9	24	701130^{05}	18.5	100
15	0.536	610328^{08}	15.7	341	650208^{14}	13.6	27	831127^{19}	18.4	75
16	0.571	721018^{10}	15.6	7	701229^{07}	13.6	59	761014^{14}	18.1	104
17	0.607	811106^{03}	15.6	360	720129^{22}	13.6	39	630103^{21}	17.8	110
18	0.643	801203^{16}	15.5	2	820614^{04}	13.5	31	640313^{21}	17.8	100
19	0.679	820426^{15}	15.3	352	850214^{20}	13.5	29	771208^{14}	17.8	110
20	0.731	790208^{15}	15.2	351	861021^{00}	12.7	32	860130^{22}	17.0	91
21	0.750	580203^{10}	15.2	347	801014^{18}	12.2	25	611007^{15}	16.9	110
22	0.786	690830^{10}	14.7	7	770328^{16}	12.0	26	581213^{05}	16.0	101
23	0.821	660528^{10}	14.3	357	810223^{07}	11.8	35	680603^{13}	16.0	101
24	0.857	751121^{01}	13.9	1	791211^{18}	11.3	66	810513^{15}	15.7	95
25	0.893	770410^{14}	13.7	357	620221^{11}	11.2	28	800322^{14}	15.3	110
26	0.929	590913^{17}	12.6	347	640212^{12}	10.7	39	821007^{20}	15.2	71
$n = 27$ (No. of years)	0.964	780827^{08}	12.3	349	75.....	10.1	...	751013^{16}	13.8	101

Data from the Annual Maximum (AM) Model continued.

Obs. Rank R	Plot. Pos. $P_r = \frac{r}{n+1}$	SE Sector Date	u_{max} m/s	Dir. °)	S Sector Date	u_{max} m/s	Dir. °)	SW Sector Date	u_{max} m/s	Dir. °)
1	0.036	711121^{20}	22.6	120	840113^{15}	21.5	202	670223^{20}	24.3	236
2	0.071	760103^{04}	21.7	137	711121^{16}	21.1	166	811124^{13}	23.4	244
3	0.107	660101^{13}	21.0	130	661130^{13}	20.1	166	840113^{18}	21.7	246
4	0.143	600204^{06}	19.7	140	670228^{06}	18.6	196	851106^{10}	21.6	233
5	0.179	721120^{12}	19.1	130	601203^{14}	18.3	196	640917^{08}	21.4	237
6	0.214	830406^{12}	19.1	122	750122^{18}	18.0	195	680115^{14}	20.7	237
7	0.250	780223^{16}	18.6	113	760105^{08}	18.0	199	750928^{08}	19.8	239
8	0.286	771211^{12}	18.5	131	641203^{04}	17.5	186	771224^{11}	19.8	240
9	0.321	580209^{01}	18.4	150	821219^{22}	17.2	175	821210^{14}	19.8	221
10	0.357	650504^{13}	18.4	120	791227^{18}	17.1	164	650928^{02}	19.7	206
11	0.393	700109^{17}	18.4	130	610405^{11}	17.0	167	600118^{22}	19.6	206
12	0.429	790325^{15}	17.2	132	620111^{20}	17.0	197	660814^{16}	19.5	237
13	0.462	670226^{08}	17.0	130	650111^{02}	17.0	167	860516^{10}	19.5	246
14	0.500	800313^{11}	16.8	124	591027^{09}	16.5	184	610130^{00}	19.2	217
15	0.536	591115^{07}	16.7	120	801217^{20}	16.4	192	830106^{15}	19.2	243
16	0.571	610103^{11}	16.7	130	681221^{05}	16.2	177	791126^{16}	18.5	232
17	0.607	620309^{12}	16.7	130	630926^{14}	16.1	197	711106^{19}	18.4	237
18	0.643	820926^{13}	16.4	128	700202^{08}	15.8	167	620112^{00}	18.3	227
19	0.679	810228^{12}	16.3	114	830205^{11}	15.6	167	801215^{13}	18.2	238
20	0.731	691222^{05}	16.0	151	721205^{21}	15.5	197	781114^{21}	18.0	247
21	0.750	630315^{15}	15.9	131	580209^{03}	15.2	167	760105^{09}	17.9	204
22	0.786	840325^{11}	15.9	119	691222^{04}	14.9	167	700104^{06}	17.1	238
23	0.821	860324^{21}	15.6	137	860123^{03}	14.8	202	691118^{21}	16.9	218
24	0.857	751116^{13}	15.4	151	771031^{20}	14.3	168	721206^{04}	16.7	228
25	0.893	680928^{05}	15.2	141	780327^{21}	13.8	193	590121^{11}	16.1	228
26	0.929	851201^{20}	14.3	141	851206^{10}	13.5	196	631113^{11}	15.6	218
$n = 27$ (No. of years)	0.964	640226^{10}	14.2	131	81.....	11.3	...	581230^{04}	14.3	238

Data from the Annual Maximum (AM) Model continued.

Obs. Rank R	Plot. Pos. $P_r = \frac{r}{n+1}$	NW Sector Date	NW Sector u_{max} m/s	NW Sector Dir. °)	All Sectors Date	All Sectors u_{max} m/s	All Sectors Dir. °)	All Sectors Sector
1	0.036	811121^{06}	25.0	293	671017^{21}	29.3	274	W
2	0.071	801223^{21}	23.1	296	811124^{20}	26.5	283	W
3	0.107	670224^{09}	22.0	295	830118^{11}	26.3	290	W
4	0.143	760301^{16}	22.0	297	680111^{07}	25.6	25	NE
5	0.179	711022^{22}	21.6	295	750126^{09}	23.7	252	W
6	0.214	680115^{19}	21.5	295	801223^{21}	23.1	296	NW
7	0.250	770305^{03}	21.4	296	771224^{15}	22.8	268	W
8	0.286	830118^{18}	21.4	295	711121^{20}	22.6	120	SE
9	0.321	750104^{13}	21.4	295	691029^{18}	22.4	275	W
10	0.357	850906^{06}	20.9	295	661218^{18}	22.0	265	W
11	0.393	781025^{13}	20.6	298	760301^{16}	22.0	297	NW
12	0.429	590220^{21}	20.5	296	840113^{18}	21.7	246	SW
13	0.462	691029^{19}	20.2	310	851106^{10}	21.6	233	SW
14	0.500	610327^{04}	20.1	296	640917^{08}	21.4	237	SW
15	0.536	620216^{10}	19.3	296	791214^{14}	21.3	109	E
16	0.571	721024^{09}	19.1	296	650105^{04}	21.1	276	W
17	0.607	641118^{08}	18.7	310	781025^{13}	20.6	298	NW
18	0.643	791127^{07}	18.5	297	590220^{21}	20.5	296	NW
19	0.679	580717^{07}	18.4	296	610326^{22}	20.5	276	W
20	0.731	600422^{14}	18.4	296	620212^{10}	20.5	266	W
21	0.750	820130^{13}	18.3	298	601101^{19}	20.4	110	E
22	0.786	840623^{19}	18.1	294	821216^{08}	20.2	272	W
23	0.821	701105^{16}	17.7	300	720117^{11}	20.1	110	E
24	0.857	660322^{02}	17.6	296	860516^{10}	19.5	246	SW
25	0.893	860921^{19}	15.6	294	580209^{14}	19.3	286	W
26	0.929	650330^{04}	14.3	297	700104^{07}	18.8	266	W
$n = 27$ (No. of years)	0.964	631022^{20}	12.5	321	630103^{21}	17.8	110	E

The Annual Maximum (AM) Model

	N Sector	NE Sector	E Sector
$b_0 = \bar{x} = \frac{1}{n} \sum_{i=1}^{n} x_i$	16.607	14.356	18.233
$b_1 = \frac{1}{n} \sum_{R} \frac{(R-1)}{(n-1)} x_R$	8.99	7.97	9.70
$b_2 = \frac{1}{n} \sum_{R} \frac{(R-1)(R-2)}{(n-1)(n-2)} x_R$	6.24	5.64	6.65
$s_x =$	2.393	3.116	2.021
Parameter Estimation, EV1-Distribution			
$\hat{\alpha}_{EV1} = \frac{\ln 2}{2b_1 - b_0}$	0.506	0.439	0.592
$\hat{\beta}_{EV1} = b_0 - \frac{0.577}{\hat{\alpha}}$	15.47	13.05	17.26
Parameter Estimation, GEV-Distribution			
$c = \frac{2b_1 - b_0}{3b_2 - b_0} - \frac{\ln 2}{\ln 3}$	0.018	–0.014	0.049
$\hat{k}_{GEV} = 7.859 \cdot c + 2.9554\, c^2$	0.145	–0.107	0.395
$\hat{\alpha}_{GEV} = \frac{\Gamma(1+\hat{k})(1-2^{-\hat{k}})}{(2b_1 - b_0)\hat{k}}$	0.450	0.490	0.460
$\hat{\beta}_{GEV} = b_0 + \frac{1}{\hat{\alpha} \cdot \hat{k}} (\Gamma(1+\hat{k}) - 1)$	15.61	12.91	17.61

The Annual Maximum (AM) Model continued.

	SE Sector	S Sector	SW Sector
$b_0 = \bar{x} = \frac{1}{n}\sum_{i=1}^{n} x_i$	17.474	16.604	19.081
$b_1 = \frac{1}{n}\sum_{R} \frac{(R-1)}{(n-1)} x_R$	9.34	8.93	10.18
$b_2 = \frac{1}{n}\sum_{R} \frac{(R-1)(R-2)}{(n-1)(n-2)} x_R$	6.46	6.17	7.00
$s_x =$	2.128	2.249	2.259
Parameter Estimation, EV1-Distribution			
$\hat{\alpha}_{EV1} = \frac{\ln 2}{2b_1 - b_0}$	0.573	0.550	0.542
$\hat{\beta}_{EV1} = b_0 - \frac{0.577}{\hat{\alpha}}$	16.46	15.55	18.02
Parameter Estimation, GEV-Distribution			
$c = \frac{2b_1 - b_0}{3b_2 - b_0} - \frac{\ln 2}{\ln 3}$	0.003	0.029	0.036
$\hat{k}_{GEV} = 7.859 \cdot c + 2.9554\, c^2$	0.020	0.228	0.285
$\hat{\alpha}_{GEV} = \frac{\Gamma(1+\hat{k})(1-2^{-\hat{k}})}{(2b_1 - b_0)\hat{k}}$	0.563	0.464	0.442
$\hat{\beta}_{GEV} = b_0 + \frac{1}{\hat{\alpha}\cdot\hat{k}}(\Gamma(1+\hat{k}) - 1)$	16.48	15.76	18.29

The Annual Maximum (AM) Model cont.

	NW Sector	All Sectors
$b_0 = \bar{x} = \frac{1}{n}\sum_{i=1}^{n} x_i$	19.563	21.911
$b_1 = \frac{1}{n}\sum_{R} \frac{(R-1)}{(n-1)} x_R$	10.52	11.65
$b_2 = \frac{1}{n}\sum_{R} \frac{(R-1)(R-2)}{(n-1)(n-2)} x_R$	7.23	8.05
$s_x =$	2.672	2.568
Parameter Estimation, EV1-Distribution		
$\hat{\alpha}_{EV1} = \frac{\ln 2}{2b_1 - b_0}$	0.468	0.499
$\hat{\beta}_{EV1} = b_0 - \frac{0.577}{\hat{\alpha}}$	18.33	20.75
Parameter Estimation, GEV-Distribution		
$c = \frac{2b_1 - b_0}{3b_2 - b_0} - \frac{\ln 2}{\ln 3}$	0.064	−0.010
$\hat{k}_{GEV} = 7.859 \cdot c + 2.9554\, c^2$	0.514	−0.078
$\hat{\alpha}_{GEV} = \frac{\Gamma(1+\hat{k})(1-2^{-\hat{k}})}{(2b_1 - b_0)\hat{k}}$	0.349	0.539
$\hat{\beta}_{GEV} = b_0 + \frac{1}{\hat{\alpha}\cdot\hat{k}}(\Gamma(1+\hat{k}) - 1)$	19.15	20.69

Data from the Peak over Threshold (POT) Model .

Obs. Rank R	Plot. Pos. $P_r = \frac{r}{n+1}$	N Sector Date	u_{max} m/s	Dir. °)	NE Sector Date	u_{max} m/s	Dir. °)	E Sector Date	u_{max} m/s	Dir. °)
1	0.036	710311^{08}	22.1	355	680111^{07}	25.6	25	591207^{10}	21.8	110
2	0.071	830925^{00}	20.1	351	781231^{15}	19.2	65	661213^{04}	21.4	100
3	0.107	680111^{11}	19.9	16	610321^{09}	18.6	47	791214^{14}	21.3	109
4	0.143	670922^{14}	19.3	346	580226^{02}	16.2	48	601101^{19}	20.4	110
5	0.179	680126^{17}	19.1	346	601210^{19}	16.2	38	720117^{11}	20.1	110
6	0.214	640205^{17}	18.9	346	660414^{07}	15.6	38	591116^{13}	20.0	100
7	0.250	860120^{04}	18.9	359	670612^{10}	15.5	27	690313^{18}	19.7	100
8	0.286	761226^{00}	18.1	359	690216^{08}	14.9	38	620416^{13}	19.6	90
9	0.321	650208^{02}	18.1	16	711124^{00}	14.8	58	670216^{13}	19.5	110
10	0.357	620217^{10}	18.1	346	830208^{00}	14.8	63	841117^{10}	19.5	101
11	0.393	670114^{04}	18.1	346	760103^{22}	14.7	27	650504^{17}	18.8	110
12	0.429	670418^{17}	18.1	346	600114^{05}	14.7	38	710423^{15}	18.7	100
13	0.462	711208^{14}	17.8	6	590419^{15}	13.9	27	711122^{04}	18.7	110
14	0.500	600111^{00}	17.7	6	630126^{19}	13.9	27	790217^{12}	18.7	84
15	0.536	671204^{08}	17.4	346	840109^{02}	13.9	24	621109^{18}	18.7	90
16	0.571	630126^{15}	17.3	6	610319^{06}	13.8	38	781231^{09}	18.6	70
17	0.607	850430^{10}	17.3	354	610510^{08}	13.8	38	850508^{12}	18.6	89
18	0.643	680314^{13}	17.1	356	701229^{02}	13.6	59	701130^{05}	18.5	100
19	0.679	711228^{07}	17.1	346	650208^{14}	13.6	27	661011^{00}	18.5	110
20	0.731	850203^{03}	16.6	348	651121^{12}	13.6	59	840521^{14}	18.4	91
21	0.750	840109^{01}	16.5	14	720129^{22}	13.6	39	831127^{19}	18.4	75
22	0.786	710429^{19}	16.5	356	831127^{21}	13.6	64	700507^{14}	18.4	100
23	0.821	700612^{13}	16.5	346	850214^{20}	13.5	29	761014^{14}	18.1	104
24	0.857	680311^{14}	16.4	357	820614^{04}	13.5	31	780223^{17}	17.8	112
25	0.893	630114^{16}	16.4	6	700511^{23}	13.5	49	771208^{14}	17.8	110
26	0.929	631120^{16}	16.4	356	610514^{14}	13.3	39	650903^{08}	17.8	100
n=27	0.964	760427^{10}	16.2	12	580206^{00}	13.3	49	640313^{21}	17.8	100

Data from the Peak over Threshold (POT) Model continued.

Obs. Rank R	Plot. Pos. $P_r = \frac{r}{n+1}$	SE Sector			S Sector			SW Sector		
		Date	u_{max} m/s	Dir. °)	Date	u_{max} m/s	Dir. °)	Date	u_{max} m/s	Dir. °)
1	0.036	711121^{20}	22.6	120	840113^{15}	21.5	202	670223^{20}	24.3	236
2	0.071	760103^{04}	21.7	137	711121^{16}	21.1	166	811124^{13}	23.4	244
3	0.107	660101^{13}	21.0	130	661130^{13}	20.1	166	840113^{18}	21.7	246
4	0.143	600204^{06}	19.7	140	661231^{17}	18.7	176	851106^{10}	21.6	233
5	0.179	721120^{12}	19.1	130	670228^{06}	18.6	196	640917^{08}	21.4	237
6	0.214	830406^{12}	19.1	122	601203^{14}	18.3	196	671017^{17}	21.2	227
7	0.250	600229^{22}	18.9	120	750122^{18}	18.0	195	680115^{14}	20.7	237
8	0.286	780223^{16}	18.6	113	760105^{08}	18.0	199	670420^{13}	20.1	247
9	0.321	771211^{12}	18.5	131	641203^{04}	17.5	186	840103^{12}	20.1	246
10	0.357	700109^{17}	18.4	130	751202^{06}	17.5	170	750928^{08}	19.8	239
11	0.393	650504^{13}	18.4	120	600118^{20}	17.4	196	771224^{11}	19.8	240
12	0.429	580209^{01}	18.4	150	670327^{14}	17.4	187	821210^{14}	19.8	221
13	0.462	580210^{12}	18.0	130	821219^{22}	17.2	175	650928^{02}	19.7	206
14	0.500	650111^{03}	18.0	150	791227^{18}	17.1	164	840117^{15}	19.7	239
15	0.536	600309^{06}	17.6	120	610405^{11}	17.0	167	600118^{22}	19.6	206
16	0.571	601102^{01}	17.6	120	650111^{02}	17.0	167	660814^{16}	19.5	237
17	0.607	600219^{20}	17.2	150	620111^{20}	17.0	197	860516^{10}	19.5	246
18	0.643	790325^{15}	17.2	132	591027^{09}	16.5	187	860328^{16}	19.3	239
19	0.679	720112^{06}	17.1	130	641008^{02}	16.5	177	610130^{00}	19.2	217
20	0.731	670226^{08}	17.0	130	651126^{00}	16.5	167	830106^{15}	19.2	243
21	0.750	651125^{23}	16.9	150	661130^{13}	16.4	167	661218^{12}	19.1	247
22	0.786	670512^{14}	16.8	140	670327^{22}	16.4	167	670326^{16}	18.9	217
23	0.821	710216^{07}	16.8	120	801217^{20}	16.4	192	661224^{07}	18.8	247
24	0.857	720117^{01}	16.8	120	681221^{05}	16.2	177	680404^{14}	18.8	237
25	0.893	770212^{07}	16.8	113	670905^{14}	16.2	167	750122^{23}	18.8	208
26	0.929	800313^{11}	16.8	124	661208^{20}	16.2	187	651102^{06}	18.7	237
$n = 27$	0.964	620309^{12}	16.7	130	641208^{08}	16.2	187	771112^{09}	18.6	245

Data from the Peak over Threshold (POT) Model continued.

Obs. Rank R	Plot. Pos. $P_r = \frac{r}{n+1}$	NW Sector Date	u_{max} m/s	Dir. °)	All Sectors Date	u_{max} m/s	Dir. °)	Sector
1	0.036	811121^{06}	25.0	293	671017^{21}	29.3	274	W
2	0.071	811102^{14}	24.1	293	811124^{20}	26.5	283	W
3	0.107	801223^{21}	23.1	296	830118^{11}	26.3	290	W
4	0.143	670224^{09}	22.0	295	680111^{07}	25.6	25	NE
5	0.179	671205^{23}	22.0	295	811121^{06}	25.0	293	NW
6	0.214	760301^{16}	22.0	297	811102^{12}	24.6	286	W
7	0.250	670418^{00}	21.8	300	670223^{20}	24.3	236	SW
8	0.286	800419^{07}	21.7	297	810101^{14}	24.2	292	W
9	0.321	711022^{22}	21.6	295	750126^{09}	23.7	252	W
10	0.357	680115^{19}	21.5	295	801223^{21}	23.1	296	NW
11	0.393	810208^{15}	21.5	296	771224^{15}	22.8	268	W
12	0.429	750104^{13}	21.4	295	670420^{15}	22.8	265	W
13	0.462	770305^{03}	21.4	296	711121^{20}	22.6	120	SE
14	0.500	830118^{18}	21.4	295	680115^{18}	22.5	275	W
15	0.536	850906^{06}	20.9	295	691029^{18}	22.4	275	W
16	0.571	800822^{01}	20.8	297	810208^{12}	22.3	290	W
17	0.607	851011^{23}	20.8	293	690922^{12}	22.2	275	W
18	0.643	781025^{13}	20.6	298	710311^{08}	22.1	355	N
19	0.679	590220^{21}	20.5	296	661218^{18}	22.0	265	W
20	0.731	801002^{13}	20.3	296	671205^{23}	22.0	295	NW
21	0.750	670316^{14}	20.2	300	760301^{16}	22.0	297	NW
22	0.786	691029^{19}	20.2	310	591207^{10}	21.8	110	E
23	0.821	751007^{11}	20.2	297	670418^{00}	21.8	300	NW
24	0.857	810101^{15}	20.2	298	760103^{04}	21.7	137	SE
25	0.893	610327^{04}	20.1	296	800419^{07}	21.7	297	NW
26	0.929	760121^{11}	20.1	297	840113^{18}	21.7	246	SW
$n = 27$	0.964	810203^{12}	20.1	299	711022^{22}	21.6	295	NW

Peak over Threshold (POT) Model

		N Sector	NE Sector	E Sector
Threshold level:	w':	12.5 m/s	10.5 m/s	14.5 m/s
No. of obs.	N:	120	115	110
Mean:	$\bar{x} =$	14.82	12.37	16.51
Stand. dev.	$s_x =$	2.40	2.33	2.35
Parameter est. in the Poisson model				
Intensity:	$\hat{\lambda} = \frac{N}{n}$, $n = 27$	4.44	4.26	4.07
Mean above w':	$\hat{\alpha} = \bar{x} - w'$	2.32	1.87	2.01

Peak over Threshold (POT) Model continued.

		SE Sector	S Sector	SW Sector
Threshold level:	w'	14.5 m/s	13.5 m/s	15.5 m/s
No. of obs.:	N	104	122	106
Mean:	$\bar{x} =$	16.14	15.18	17.56
Stand. dev.:	$s_x =$	2.23	2.07	2.49
Parameter est. in the Poisson model:				
Intensity:	$\hat{\lambda} = \frac{N}{n}$, $n = 27$	3.85	4.52	3.93
Mean above w' :	$\hat{\alpha} = \bar{x} - w'$	1.64	1.68	2.06

Peak over Threshold (POT) Model continued.

		W Sector	NW Sector	All Sectors
Threshold level:	w'	17.5 m/s	16.5 m/s	18.5 m/s
No. of obs.:	N	107	114	142
Mean:	$\bar{x} =$	19.74	18.59	20.31
Stand. dev.:	$s_x =$	2.88	2.54	2.50
Parameter est. in the Poisson model:				
Intensity:	$\hat{\lambda} = \frac{N}{n}$, $n = 27$	3.96	4.22	5.26
Mean above w' :	$\hat{\alpha} = \bar{x} - w'$	2.24	2.09	1.81

Appendix D:

Histograms of POT-data from different azimuth sectors with fitted exponential frequency distributions.

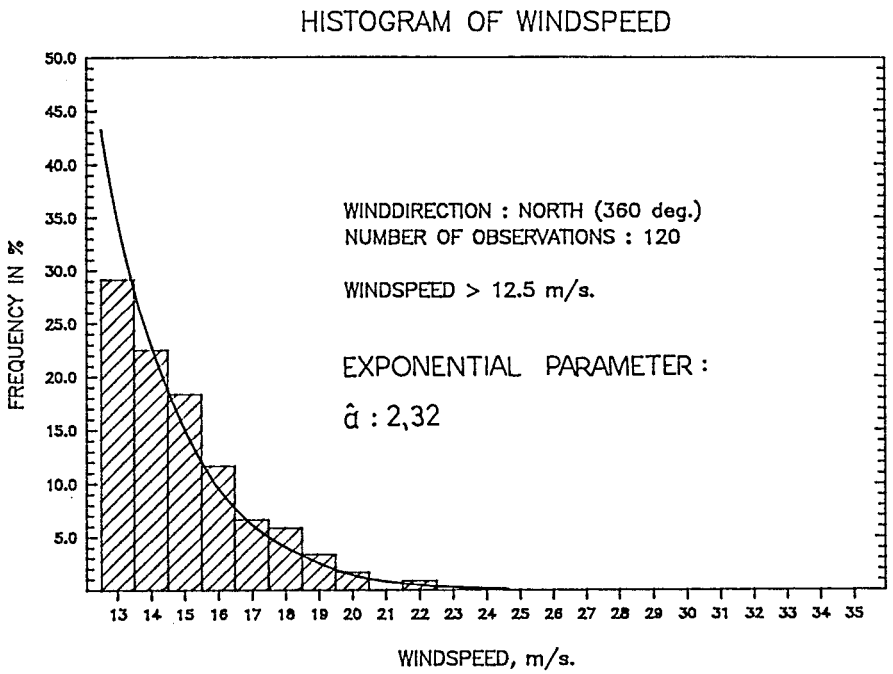
HISTOGRAM OF WINDSPEED
FREQUENCY IN %
50.0
45.0
40.0
35.0
30.0
25.0
20.0
15.0
10.0
5.0
WINDDIRECTION : NORTH (360 deg.)
NUMBER OF OBSERVATIONS : 120
WINDSPEED > 12.5 m/s.
EXPONENTIAL PARAMETER :
â : 2,32
13 14 15 16 17 18 19 20 21 22 23 24 25 26 27 28 29 30 31 32 33 34 35
WINDSPEED, m/s.

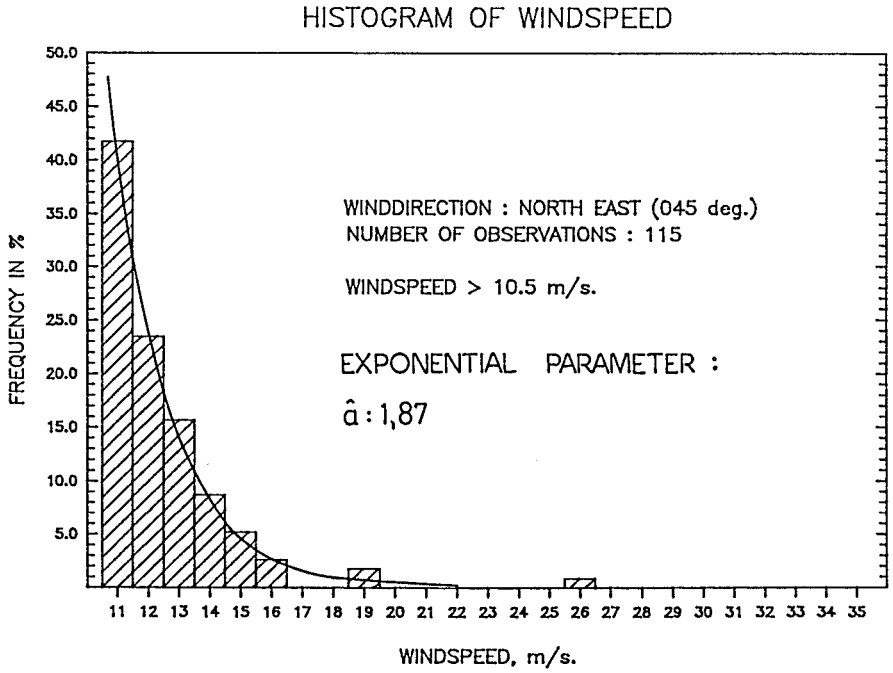
HISTOGRAM OF WINDSPEED
FREQUENCY IN %
50.0
45.0
40.0
35.0
30.0
25.0
20.0
15.0
10.0
5.0
WINDDIRECTION : NORTH EAST (045 deg.)
NUMBER OF OBSERVATIONS : 115
WINDSPEED > 10.5 m/s.
EXPONENTIAL PARAMETER :
â : 1,87
11 12 13 14 15 16 17 18 19 20 21 22 23 24 25 26 27 28 29 30 31 32 33 34 35
WINDSPEED, m/s.

HISTOGRAM OF WINDSPEED

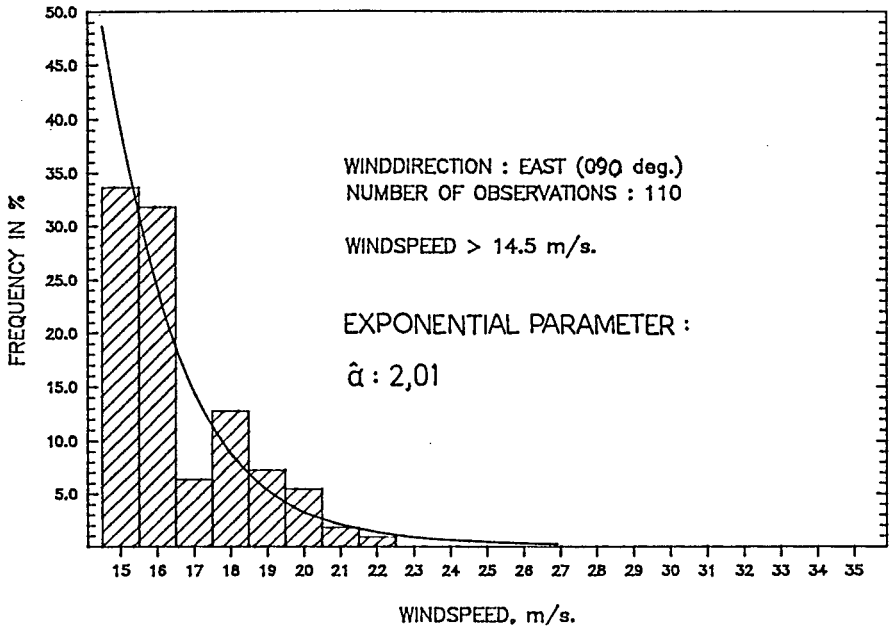

HISTOGRAM OF WINDSPEED

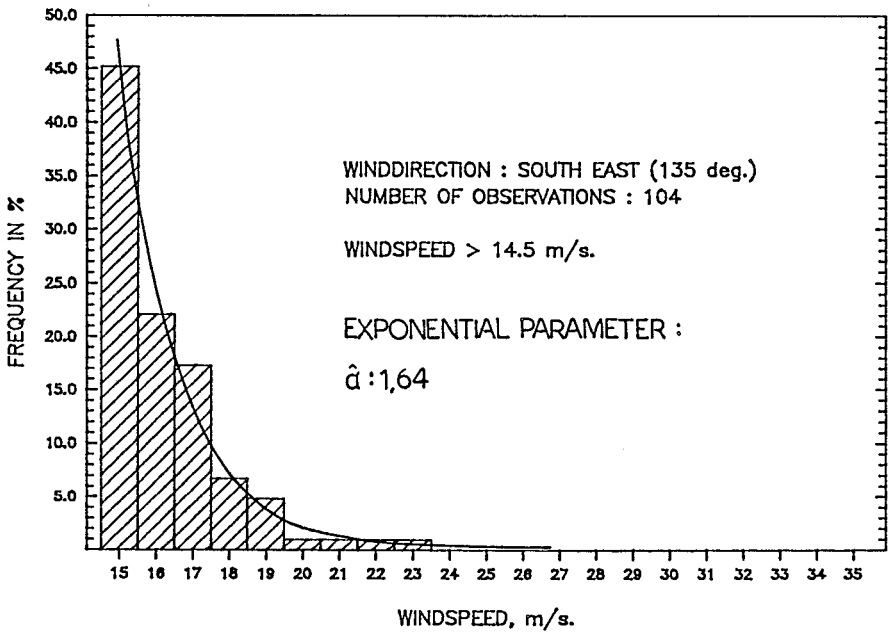

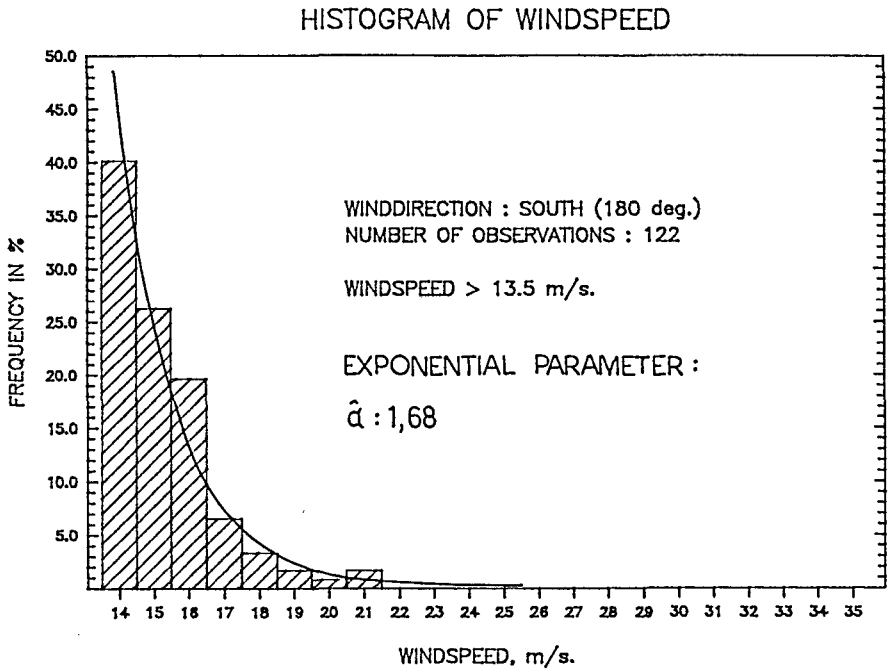
HISTOGRAM OF WINDSPEED
FREQUENCY IN %
50.0
45.0
40.0
35.0
30.0
25.0
20.0
15.0
10.0
5.0
WINDDIRECTION : SOUTH (180 deg.)
NUMBER OF OBSERVATIONS : 122
WINDSPEED > 13.5 m/s.
EXPONENTIAL PARAMETER :
â : 1,68
14 15 16 17 18 19 20 21 22 23 24 25 26 27 28 29 30 31 32 33 34 35
WINDSPEED, m/s.

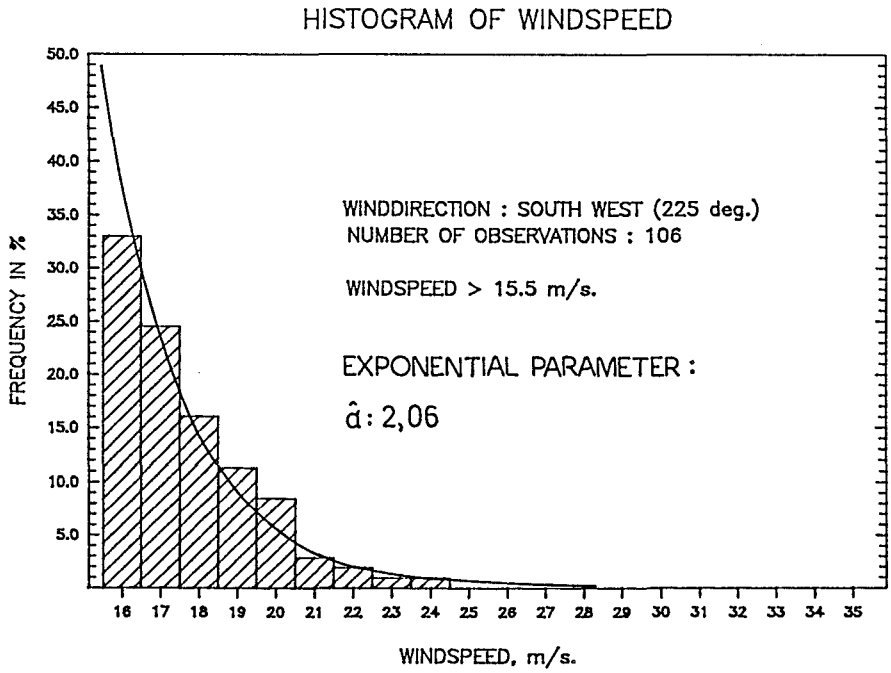
HISTOGRAM OF WINDSPEED
FREQUENCY IN %
50.0
45.0
40.0
35.0
30.0
25.0
20.0
15.0
10.0
5.0
WINDDIRECTION : SOUTH WEST (225 deg.)
NUMBER OF OBSERVATIONS : 106
WINDSPEED > 15.5 m/s.
EXPONENTIAL PARAMETER :
â : 2,06
16 17 18 19 20 21 22 23 24 25 26 27 28 29 30 31 32 33 34 35
WINDSPEED, m/s.

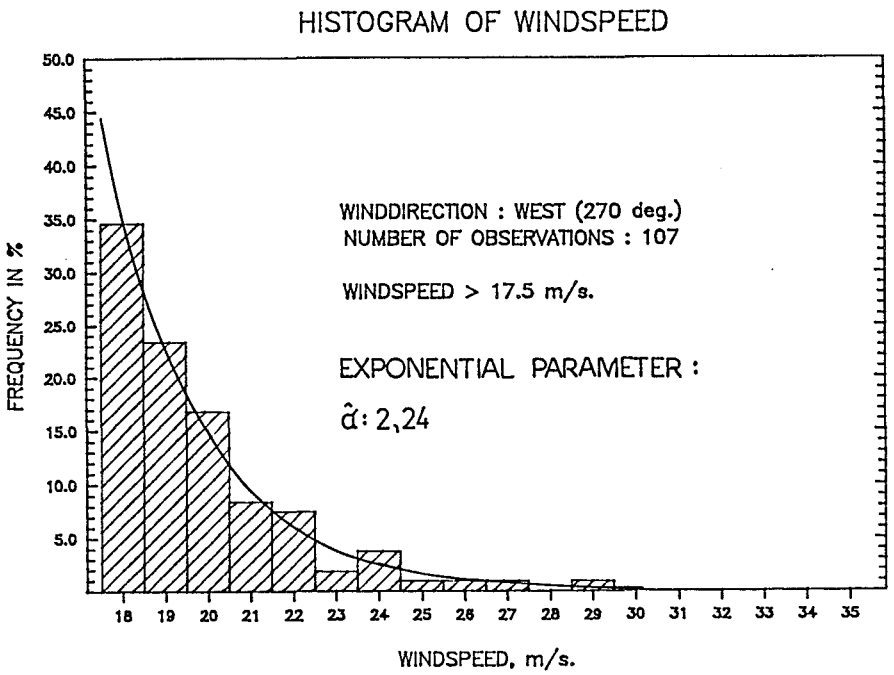
HISTOGRAM OF WINDSPEED
FREQUENCY IN %
50.0
45.0
40.0
35.0
30.0
25.0
20.0
15.0
10.0
5.0
WINDDIRECTION : WEST (270 deg.)
NUMBER OF OBSERVATIONS : 107
WINDSPEED > 17.5 m/s.
EXPONENTIAL PARAMETER :
α̂: 2,24
18 19 20 21 22 23 24 25 26 27 28 29 30 31 32 33 34 35
WINDSPEED, m/s.

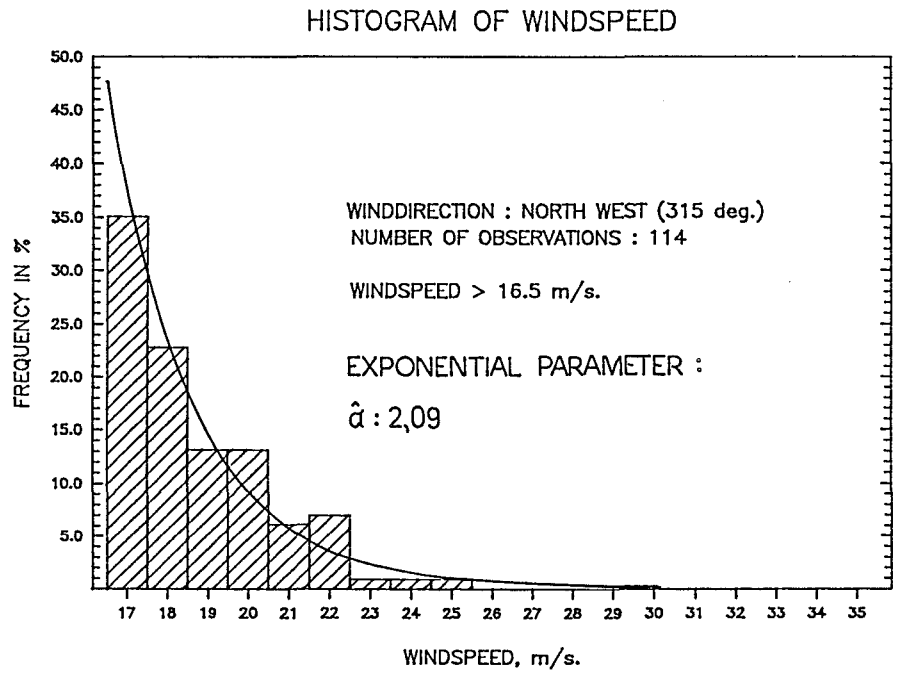
HISTOGRAM OF WINDSPEED
FREQUENCY IN %
50.0
45.0
40.0
35.0
30.0
25.0
20.0
15.0
10.0
5.0
WINDDIRECTION : NORTH WEST (315 deg.)
NUMBER OF OBSERVATIONS : 114
WINDSPEED > 16.5 m/s.
EXPONENTIAL PARAMETER :
α̂ : 2,09
17 18 19 20 21 22 23 24 25 26 27 28 29 30 31 32 33 34 35
WINDSPEED, m/s.

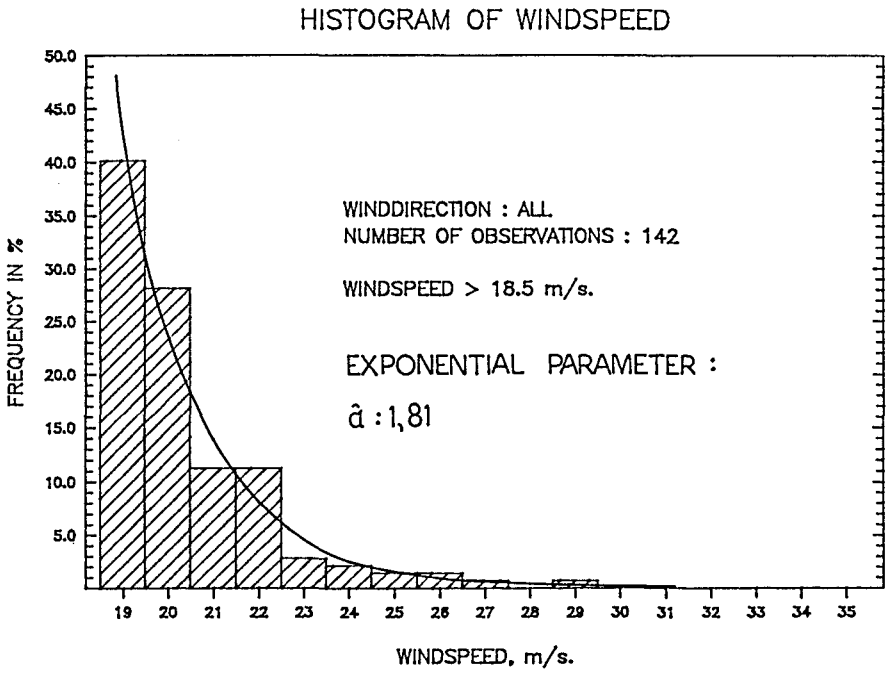
HISTOGRAM OF WINDSPEED
FREQUENCY IN %
50.0
45.0
40.0
35.0
30.0
25.0
20.0
15.0
10.0
5.0
WINDDIRECTION : ALL.
NUMBER OF OBSERVATIONS : 142
WINDSPEED > 18.5 m/s.
EXPONENTIAL PARAMETER :
â : 1,81
19 20 21 22 23 24 25 26 27 28 29 30 31 32 33 34 35
WINDSPEED, m/s.

Appendix E:

Extreme value models versus data for different azimuth sectors.

North sector

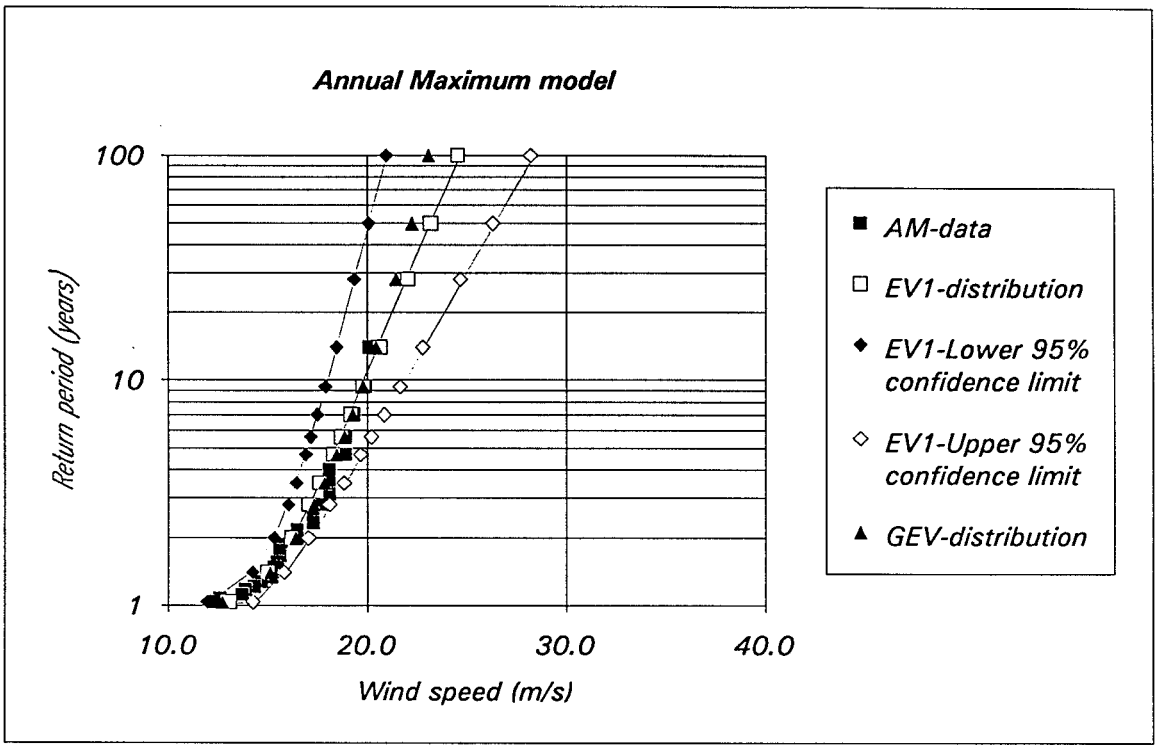

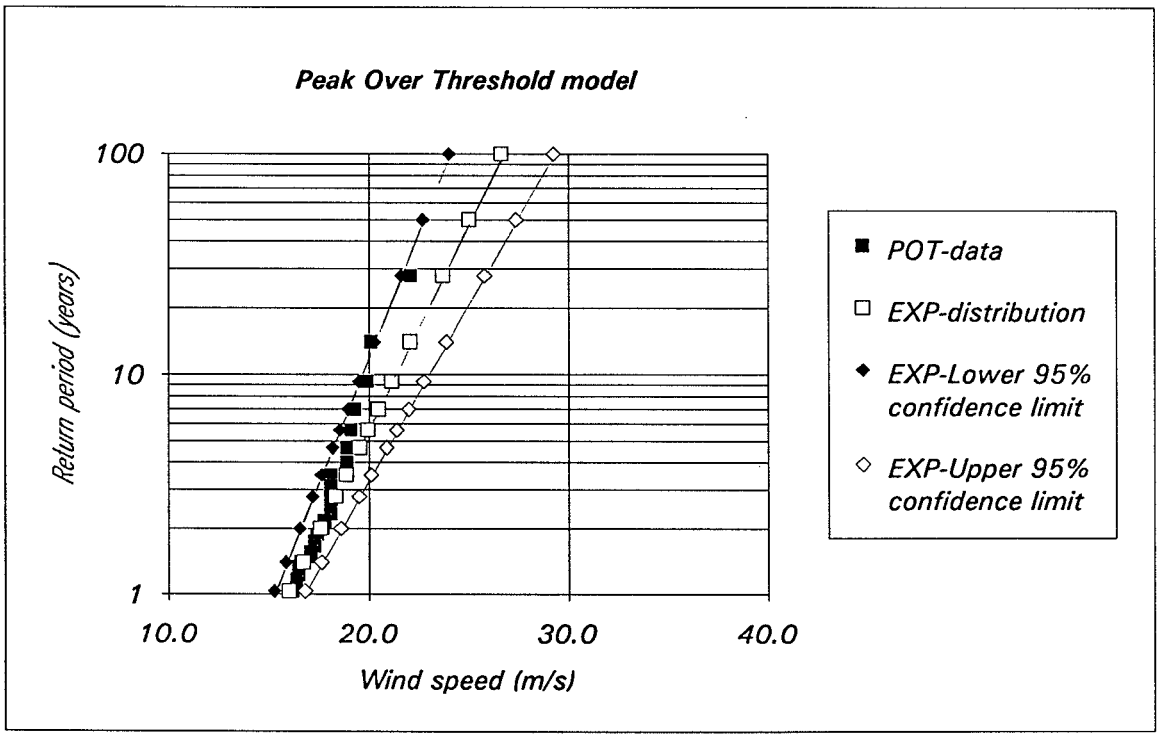

North-east sector

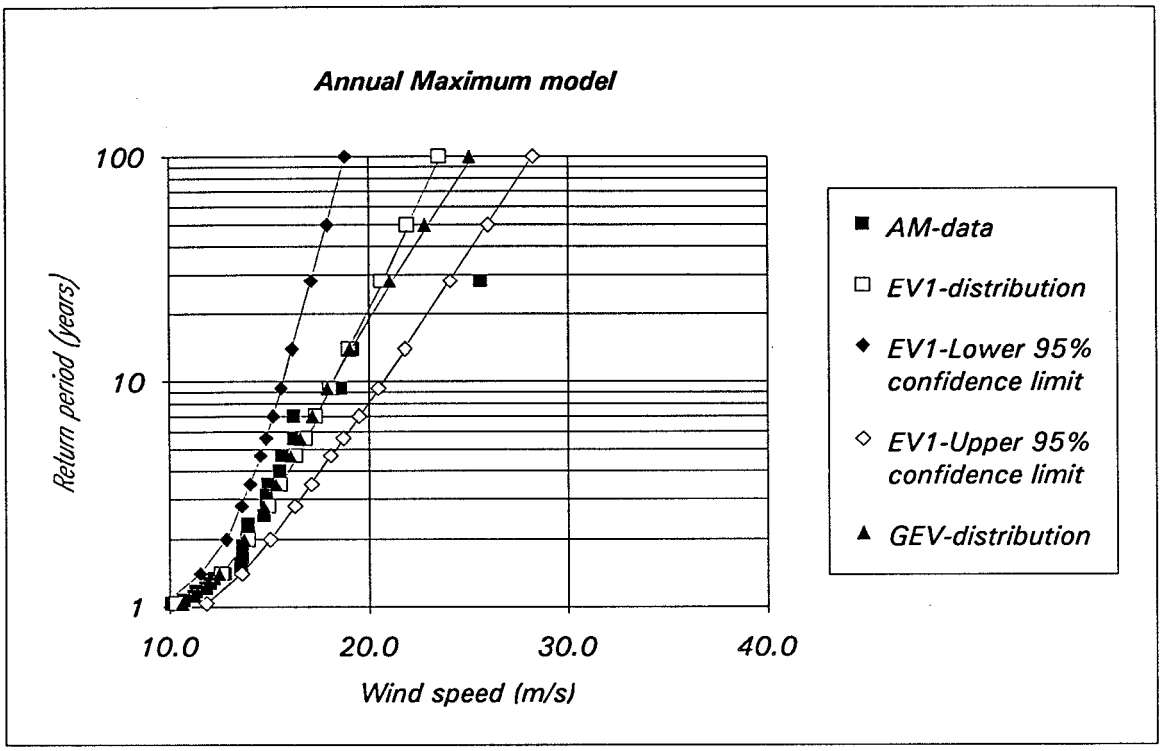

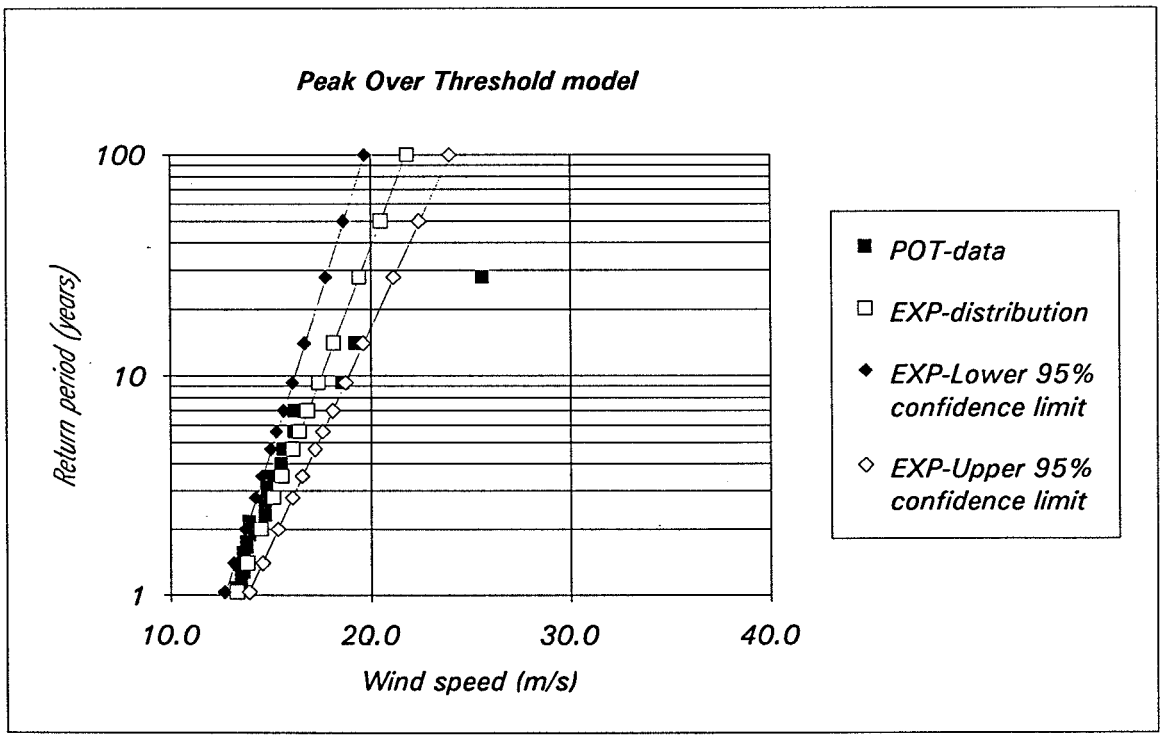

Note: Data from the North-east sector should be regarded with caution due to a considerable tower shadow effect, see figs. 16 - 21 and comments in Appendix A.

East sector

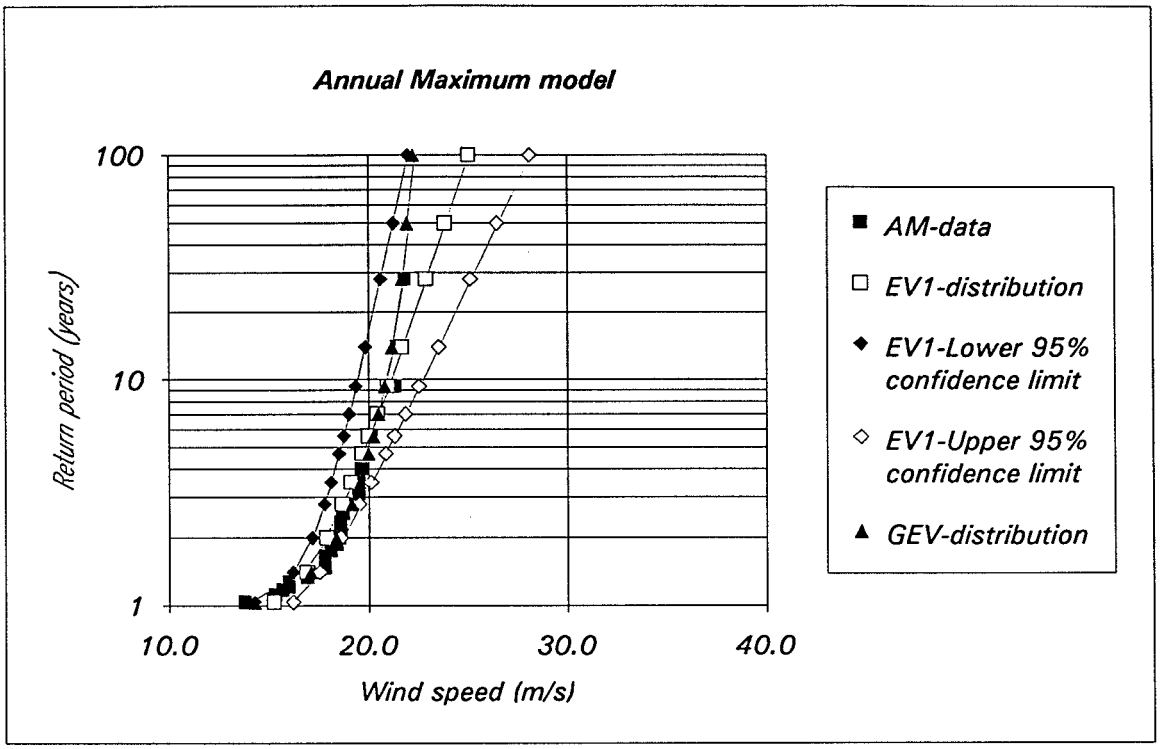
Annual Maximum model
100
10
1
Return period (years)
10.0
20.0
30.0
40.0
Wind speed (m/s)
AM-data
EV1-distribution
EV1-Lower 95% confidence limit
EV1-Upper 95% confidence limit
GEV-distribution

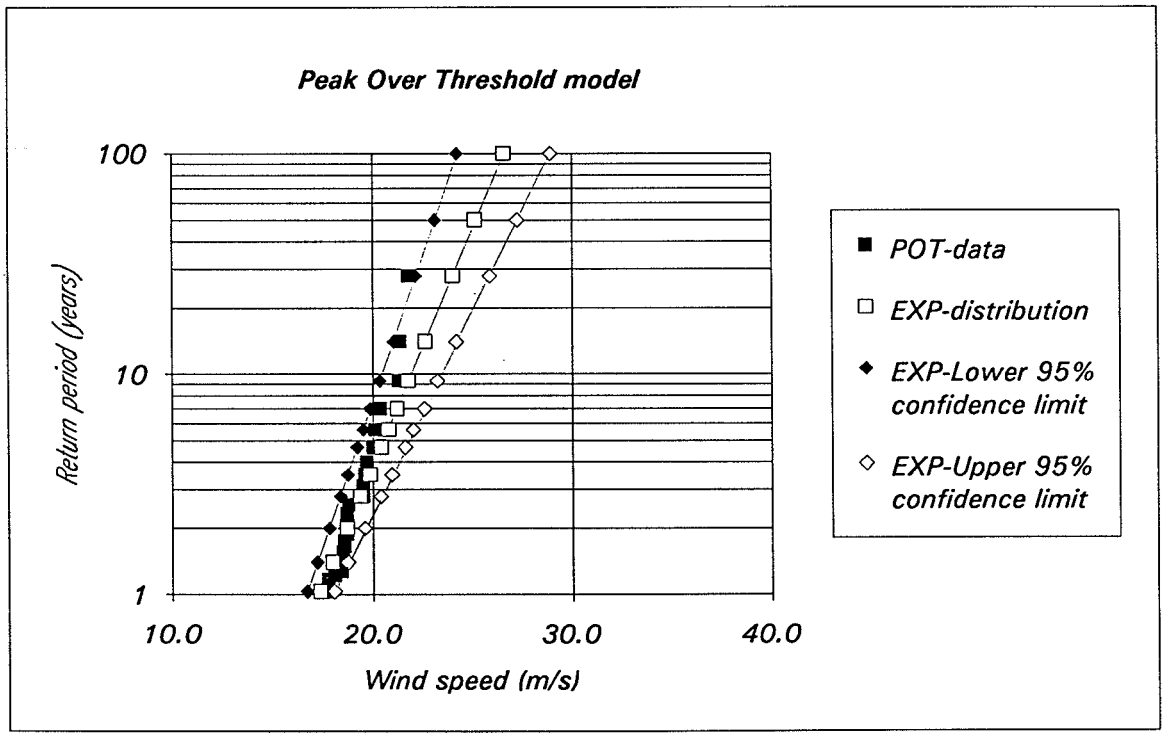
Peak Over Threshold model
100
10
1
Return period (years)
10.0
20.0
30.0
40.0
Wind speed (m/s)
POT-data
EXP-distribution
EXP-Lower 95% confidence limit
EXP-Upper 95% confidence limit

South-east sector

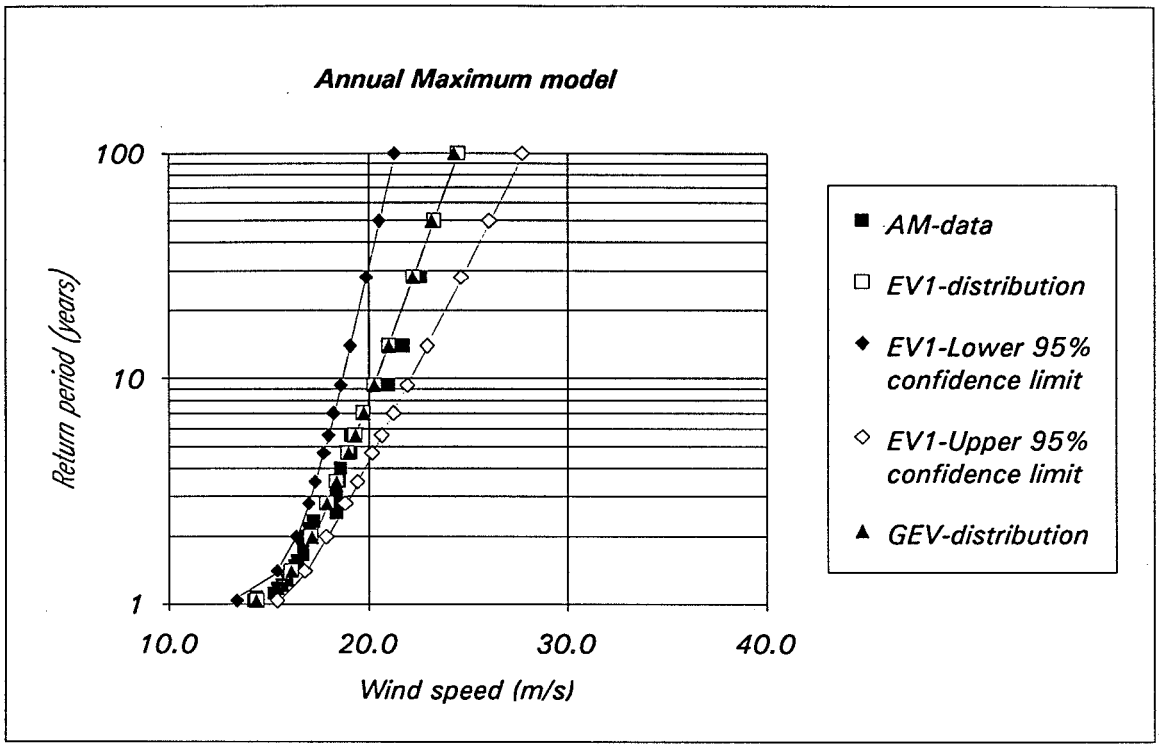

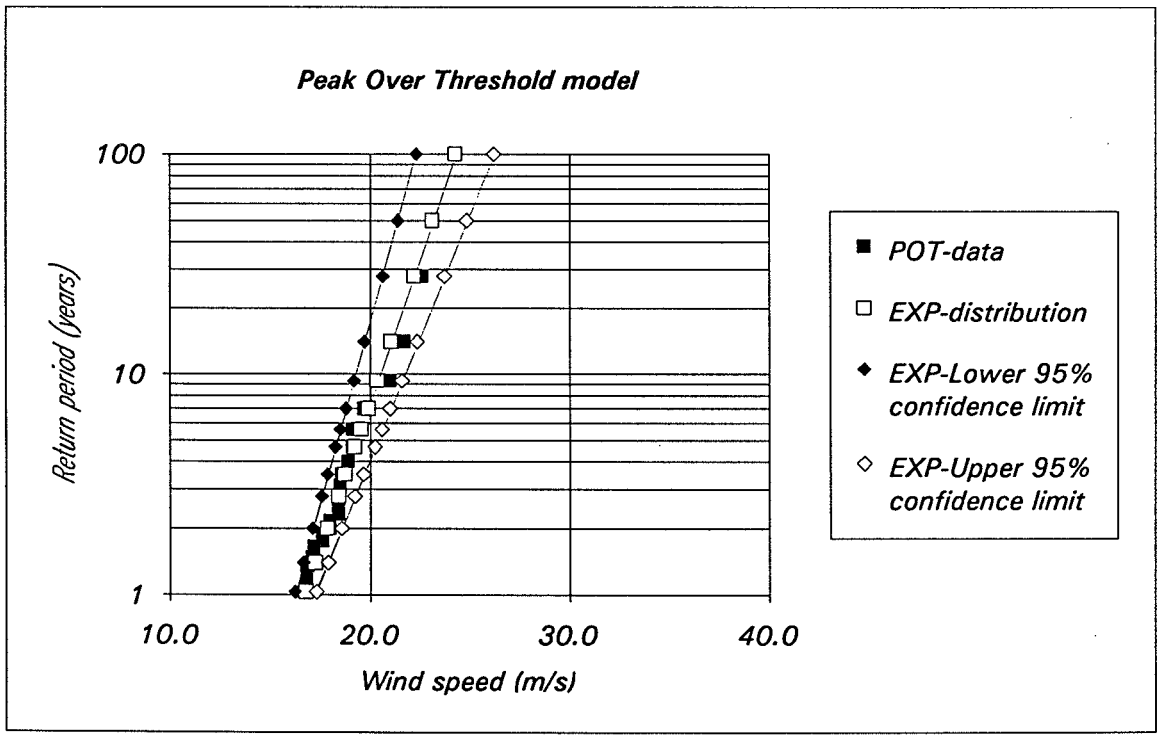

South sector

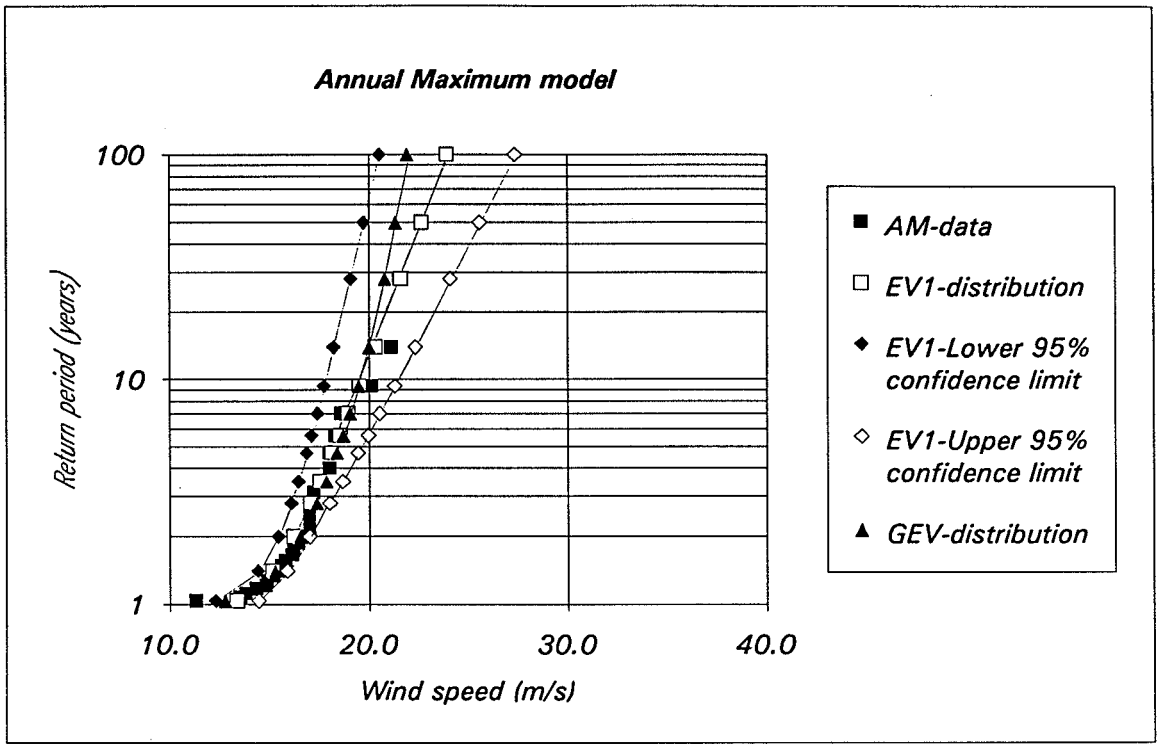

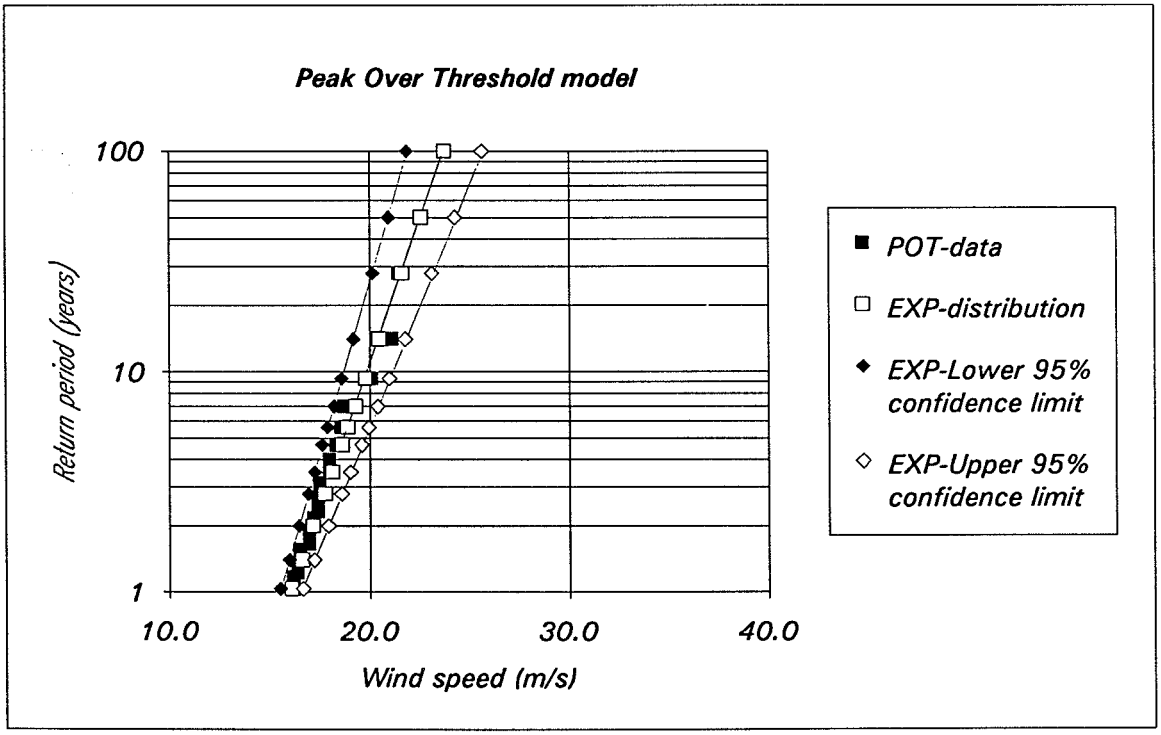

South-west sector

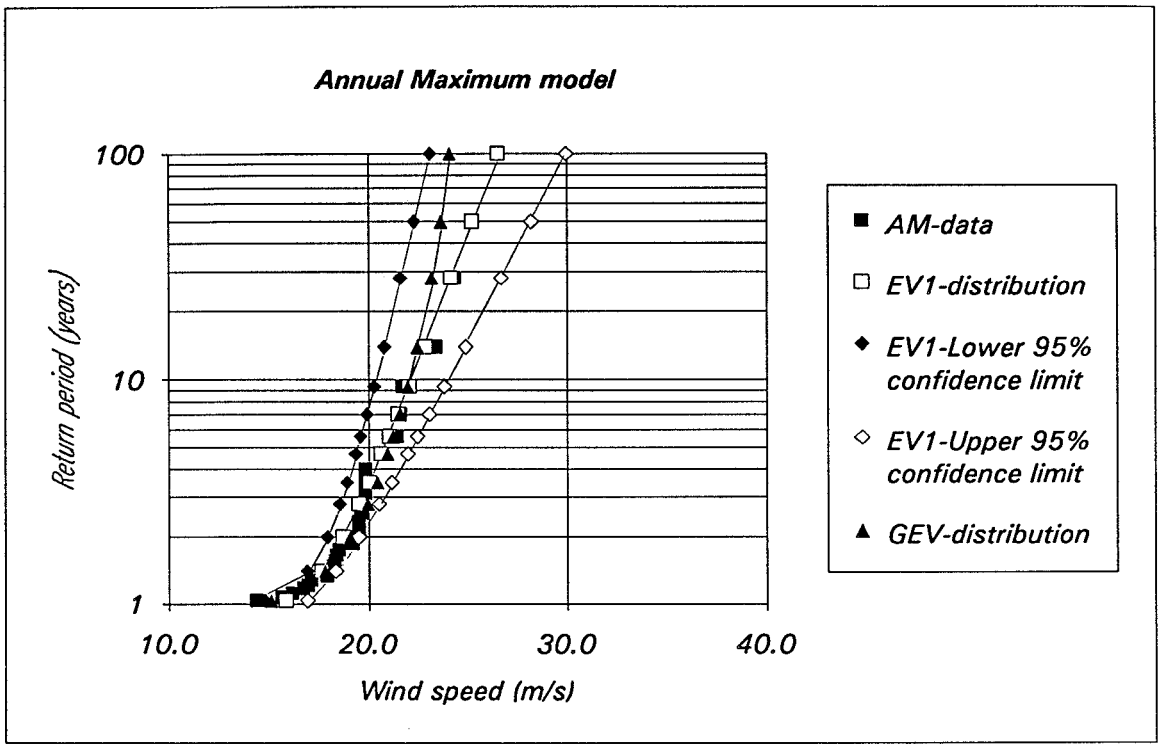

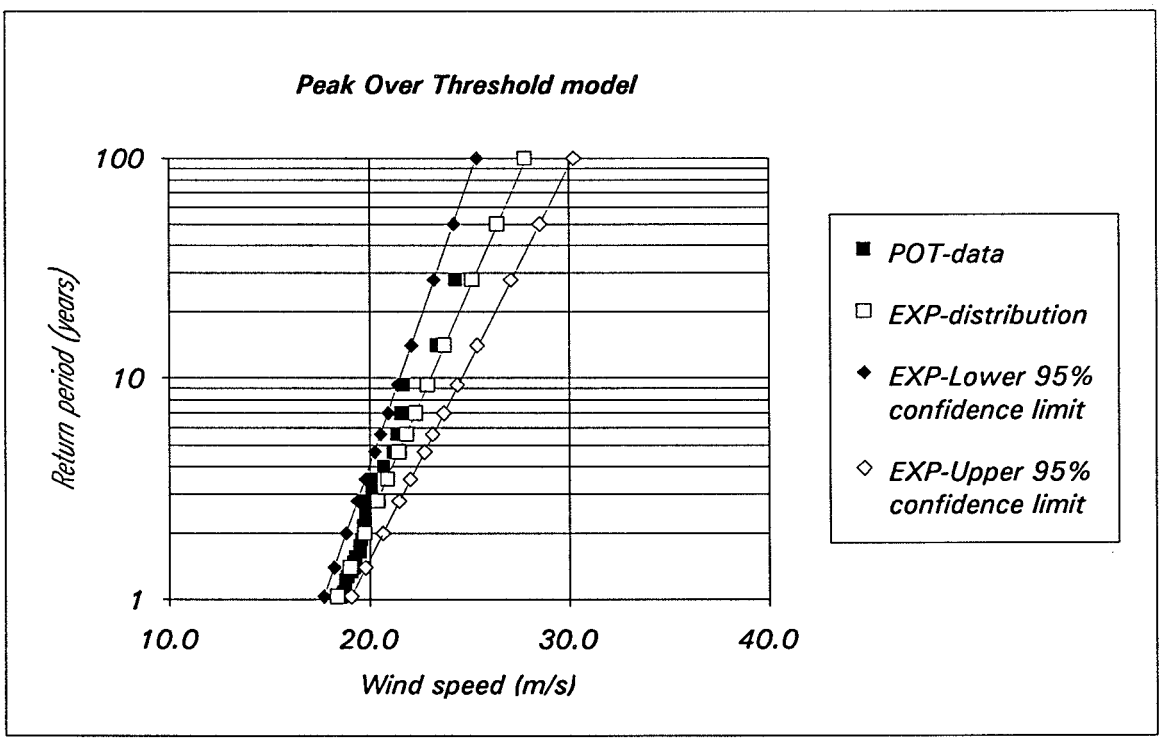

West sector

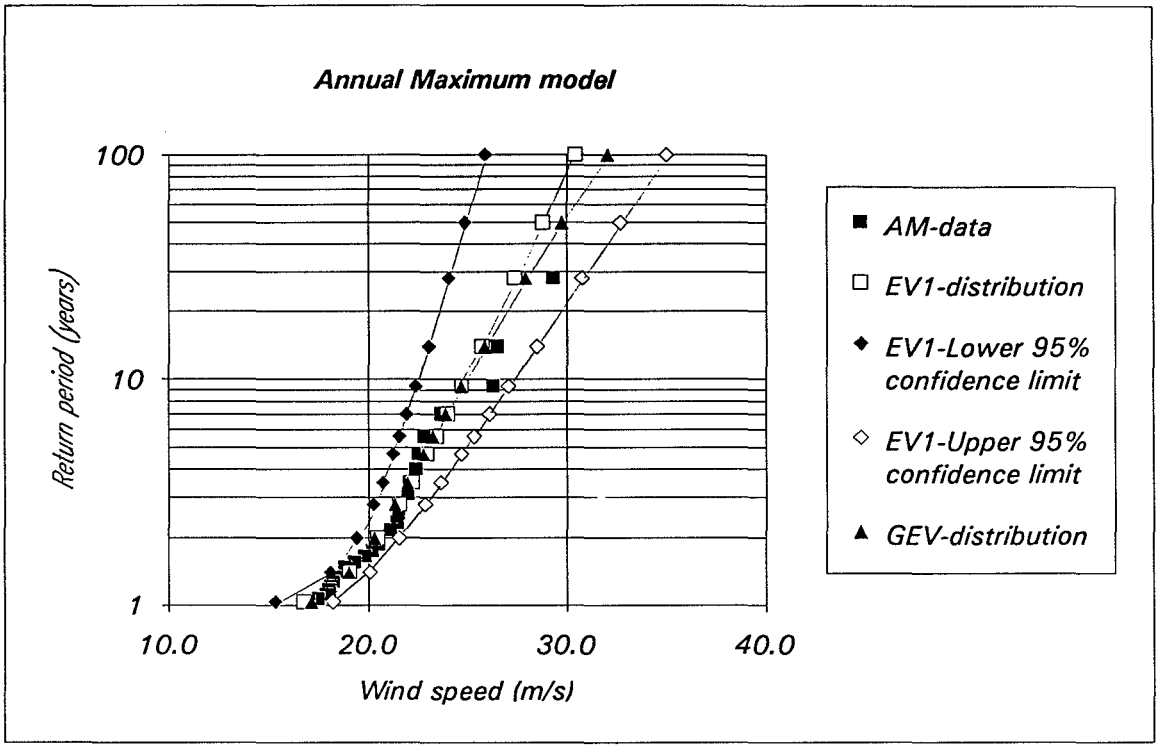
Annual Maximum model
100
10
1
Return period (years)
10.0
20.0
30.0
40.0
Wind speed (m/s)
AM-data
EV1-distribution
EV1-Lower 95% confidence limit
EV1-Upper 95% confidence limit
GEV-distribution

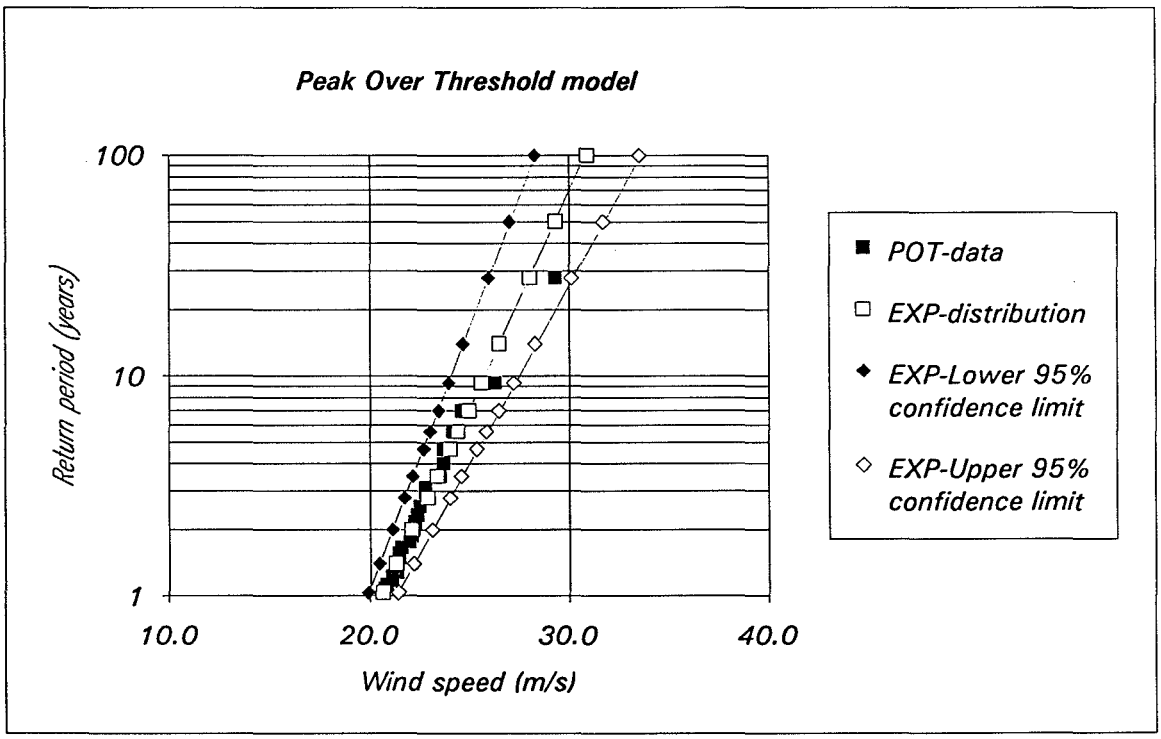
Peak Over Threshold model
100
10
1
Return period (years)
10.0
20.0
30.0
40.0
Wind speed (m/s)
POT-data
EXP-distribution
EXP-Lower 95% confidence limit
EXP-Upper 95% confidence limit

North-west sector

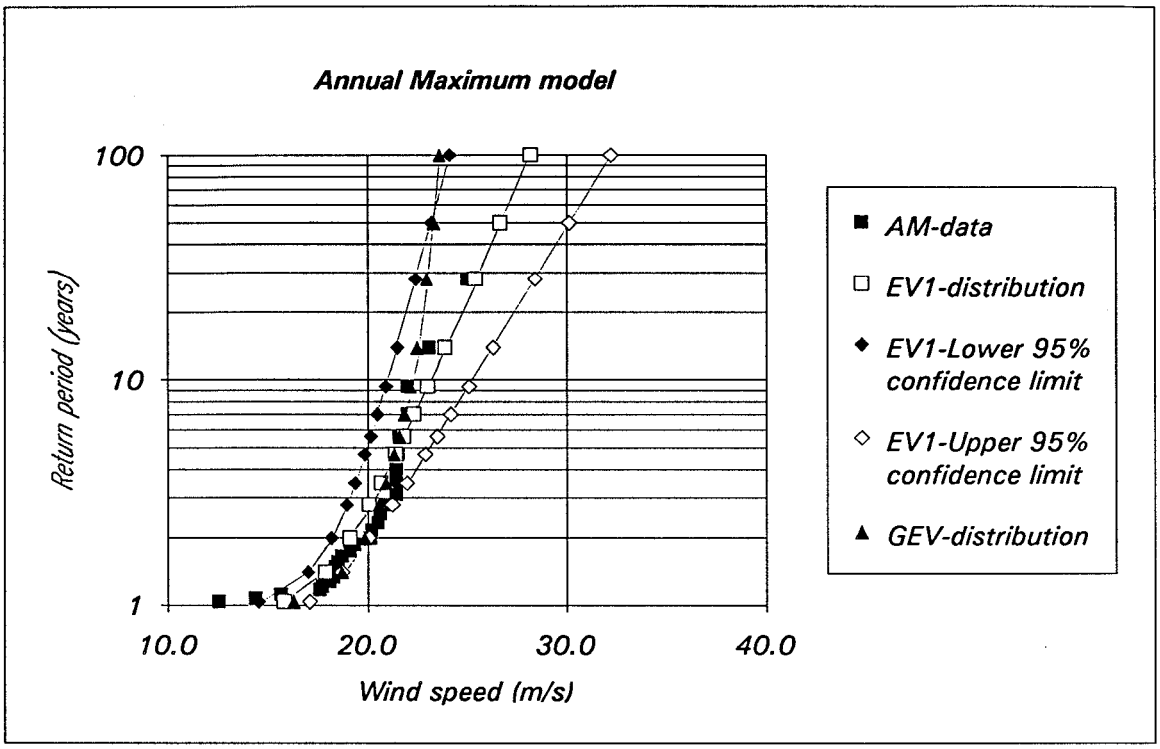

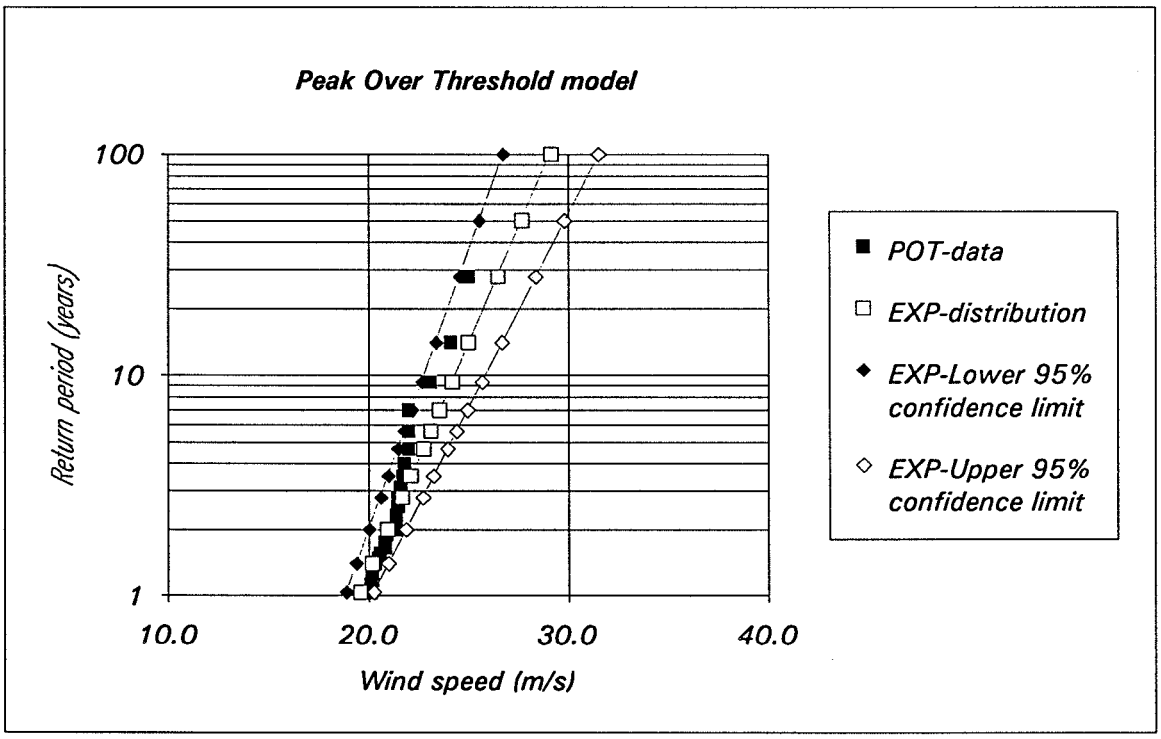

All sectors

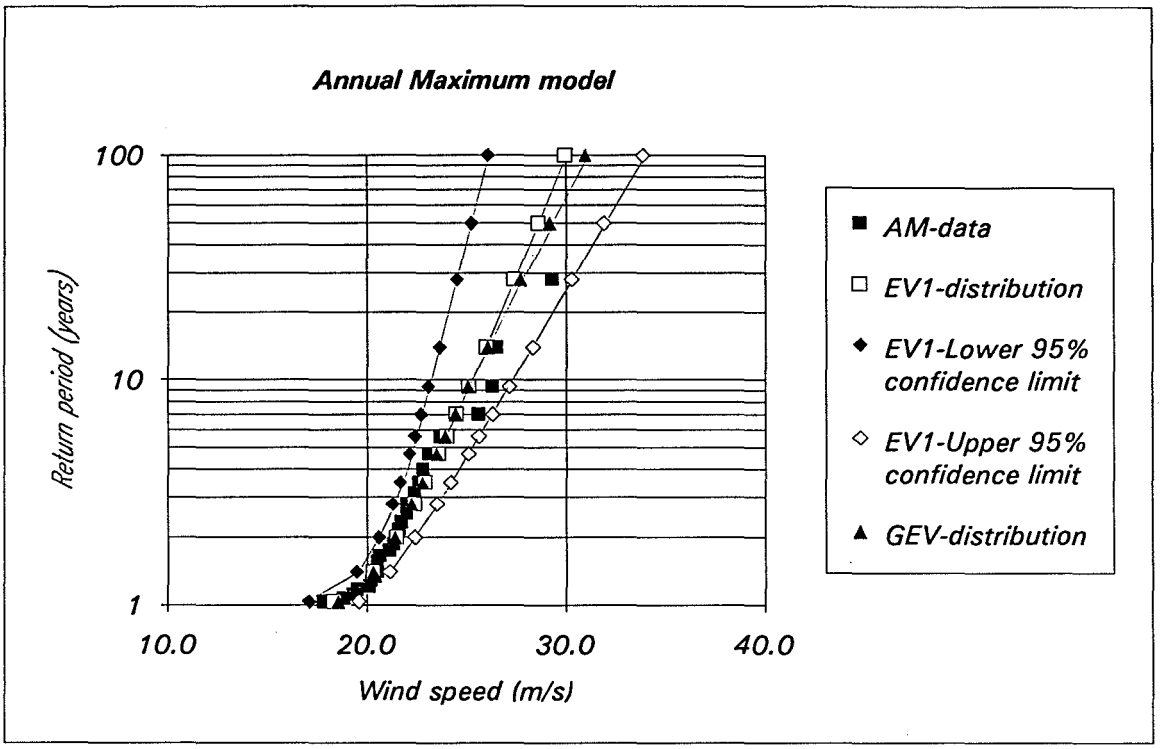
Annual Maximum model
100
10
1
Return period (years)
10.0
20.0
30.0
40.0
Wind speed (m/s)
AM-data
EV1-distribution
EV1-Lower 95% confidence limit
EV1-Upper 95% confidence limit
GEV-distribution

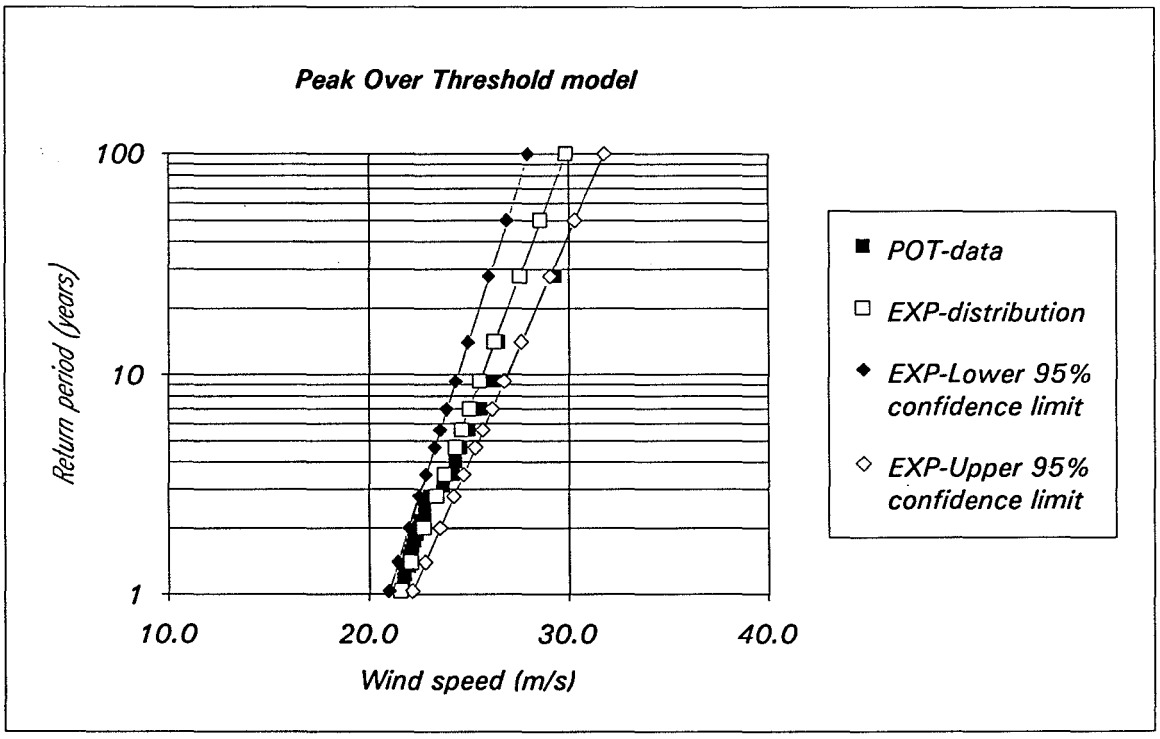
Peak Over Threshold model
100
10
1
Return period (years)
10.0
20.0
30.0
40.0
Wind speed (m/s)
POT-data
EXP-distribution
EXP-Lower 95% confidence limit
EXP-Upper 95% confidence limit

Bibliographic Data Sheet **Risø–R–722(EN)**

Title and author(s)

Application of the Wind Atlas Method to
Extremes of Wind Climatology

J. Abild

ISBN	ISSN
87–550–1438–0	0106–2840

Dept. or group	Date
Meteorology and Wind Energy	January 1994

Groups own reg. number(s) Project/contract No.

Pages	Tables	Illustrations	References
174	29	29	59

Abstract (Max. 2000 char.)

A terrain description model is established for the Risø site through a WASP computation. Mean wind profiles for eight wind direction sectors are compared with the model boundary profiles. Wind data from the 72/76 m recording level of the Risø mast are updated, including identification of missing and erroneous data. The wind atlas procedure ("the double extrapolation method") is applied to extrapolate Risø data to open-water conditions 10 m above mean sea level. Three different extreme value distributions are applied to the extrapolated storm data – two of which are based on the annual maximum (AM) method, and one on the peak-over-threshold (POT) method. T-year estimates including standard error estimates are provided. Finally, a verification is performed by comparing extrapolated storm data with corresponding measured wind data from the Dan and Gorm fields in the North Sea. A high correlation is found for severe storms from the west. A significantly lower correlation is found for moderate and easterly storms.

Descriptors INIS/EDB

BOUNDARY CONDITIONS; CALCULATION METHODS; CLIMATES; COMPLEX TERRAIN; DENMARK; EXPERIMENTAL DATA; EXTRAPOLATION; METEOROLOGY; RISØ NATIONAL LABORATORY; ROUGHNESS; SITE CHARACTERIZATION; STATISTICAL DATA; STORMS; TOPOGRAPHY; VELOCITY; W CODES; WIND

Available on request from:
Risø Library, Risø National Laboratory (Risø Bibliotek, Forskningscenter Risø)
P.O. Box 49, DK–4000 Roskilde, Denmark
Phone (+45) 46 77 46 77, ext. 4004/4005 · Telex 43 116 · Telefax (+45) 46 75 56 27

RISØ

OBJECTIVE

The objective of Risø National Laboratory is to further technological development in three main areas: energy, environment and materials.

USERS

Risø's scientific results are widely applied in industry, agriculture and public services. Risø contributes its share of new knowledge to the global research community.

RESEARCH PROFILE

Risø emphasises long-term and strategic research providing a solid scientific foundation for the technological development of society.

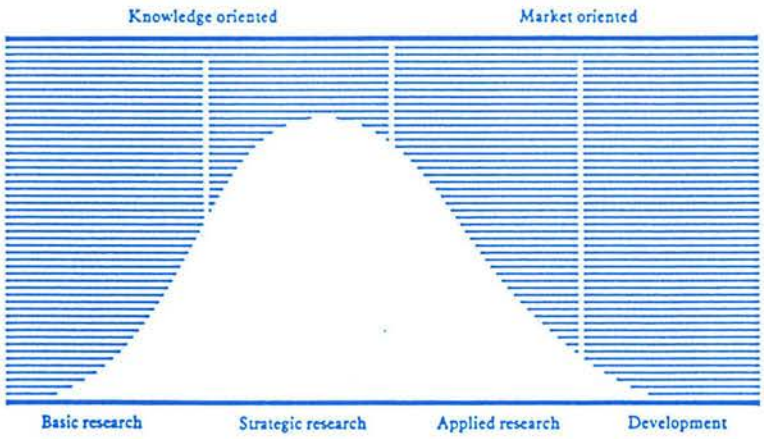

PRIORITY AREAS

- **Combustion and gasification**
- **Wind energy**
- **Energy materials**
- **Energy and environmental planning**
- **Assessment of environmental loads**
- **Reduction of environmental loads**
- **Safety and reliability of technical systems**
- **Nuclear safety**
- **Atomic structure and properties of materials**
- **Advanced materials and materials technologies**
- **Optics and fluid dynamics**

Risø-R-722(EN)
ISBN 87-550-1438-0
ISSN 0106-2840

Available on request from:
Risø Library
Risø National Laboratory
P.O. Box 49, DK-4000 Roskilde, Denmark
Phone +45 46 77 46 77, ext. 4004/4005
Telex 43116, Telefax 46 75 56 27